COMBUSTION STUDIES OF FUEL-RICH PROPELLANTS

Merrill K. King

August, 1976

FINAL REPORT

Kinetics and Combustion Group
Atlantic Research Corporation
5390 Cherokee Avenue
Alexandria, Virginia 22314

TR-PL-5520

Contract No. F44620-71-C-0124

Air Force Office of Scientific Research
Building 410
Bolling AFB, DC 20332

ATLANTIC RESEARCH CORPORATION
ALEXANDRIA, VIRGINIA · 22314

COMBUSTION STUDIES OF FUEL-RICH PROPELLANTS

Merrill K. King

August, 1976

FINAL REPORT

Kinetics and Combustion Group
Atlantic Research Corporation
5390 Cherokee Avenue
Alexandria, Virginia 22314

TR-PL-5520

Contract No. F44620-71-C-0124

Approved for Public Release; Distribution Unlimited

Air Force Office of Scientific Research
Building 410
Bolling AFB, DC 20332

UNCLASSIFIED

SECURITY CLASSIFICATION OF THIS PAGE (When Data Entered)

REPORT DOCUMENTATION PAGE	READ INSTRUCTIONS BEFORE COMPLETING FORM
1 REPORT NUMBER: AFOSR-TR-76-1079	2. GOVT ACCESSION NO. / 3. RECIPIENT'S CATALOG NUMBER
4 TITLE (and Subtitle): Combustion Studies of Fuel-Rich Propellants.	5 TYPE OF REPORT & PERIOD COVERED: Final rept. 1 July 1971 - 30 June 1976
	6. PERFORMING ORG. REPORT NUMBER: TR-PL-5520
7 AUTHOR(s): Merrill K. King	8. CONTRACT OR GRANT NUMBER(s): F44620-71-C-0124
9 PERFORMING ORGANIZATION NAME AND ADDRESS: Atlantic Research Corporation, 5390 Cherokee Avenue, Alexandria, Virginia 22314	10. PROGRAM ELEMENT, PROJECT, TASK AREA & WORK UNIT NUMBERS: 681308, 9711-01, 61102F
11 CONTROLLING OFFICE NAME AND ADDRESS: Air Force Office of Scientific Research/NA, Building 410, Bolling AFB, DC 20332	12. REPORT DATE: August 1976 / 13. NUMBER OF PAGES: 146
14 MONITORING AGENCY NAME & ADDRESS (if different from Controlling Office): 155p.	15. SECURITY CLASS. (of this report): UNCLASSIFIED / 15a. DECLASSIFICATION DOWNGRADING SCHEDULE

16 DISTRIBUTION STATEMENT (of this Report)

Approved for public release, distribution unlimited.

AF-9711 9711-01

17 DISTRIBUTION STATEMENT (of the abstract entered in Block 20, if different from Report)

18 SUPPLEMENTARY NOTES

19 KEY WORDS (Continue on reverse side if necessary and identify by block number)

Boron	Air-augmented rockets
Magnesium	Fuel generator
Ignition	Ramburner
Combustion	Flame speed
Fuel-rich propellants	Dust Cloud

20 ABSTRACT (Continue on reverse side if necessary and identify by block number)

This report presents the results of several tasks aimed at identifying the ignition and combustion ~~characteristics~~ of boron, and ~~at identifying and characterizing~~ promising highly magnesium-loaded formulations for air-augmented rocket applications. Studies are reported.

In the boron work, ignition and combustion characteristics of pure boron and of boron-containing particulate ejecta from highly-boron-loaded fuel-rich primary motor formulations were studied. Physical and chemical characteristics

DD FORM 1 JAN 73 1473 EDITION OF 1 NOV 65 IS OBSOLETE

UNCLASSIFIED 400 016

SECURITY CLASSIFICATION OF THIS PAGE (When Data Entered)

LB

20. of the motor ejecta were studied. ~~In addition~~, their ignition/combustion characteristics were compared to those for pure boron. The minimum surrounding temperature for ignition for the two materials was nearly identical but the ignition delay time was considerably lower for the motor ejecta material. Burning times for comparable size particles of each type were equal within experimental error. In the size range of interest (2 to 10 micron diameter), the burning was observed to be characterized by a d^1-law (kinetics-limited combustion), rather than the d^2-law (diffusion-limited combustion) observed with larger particles. A model of boron ignition treating the inhibiting effect of a boric oxide coating was developed and found to give good agreement with boron particle ignition data in dry gases. A detailed model of boron-oxygen-nitrogen dust cloud flames including this boron particle ignition model was developed and used for prediction of flame speeds in such clouds as a function of numerous parameters; again, good agreement was found with the limited available experimental data.

Thermodynamic screening of possible highly-magnesium-loaded fuel-rich propellants was carried out and ~~several~~ candidate castable and pressed formulations for air-augmented rocket applications were defined. Several of these candidates were ~~successfully~~ formulated ~~and~~ characterized in terms of their safety and ballistic properties. Experiments were performed to identify the characteristics of the exhaust products ~~resulting~~ from combustion ~~of these propellants~~ in the absence of air. These experiments indicated that considerable magnesium, with a significant fraction of it in the gas phase is produced. ~~Analytical studies indicate that~~ the presence of such quantities of magnesium gas should result in excellent combustion of the product streams emanating from these propellants with air in a ramburner. Motor tests were conducted with four of these formulations, with identification of nozzle plugging and residue formation ~~as~~ possible problem areas; however, these tests did indicate likely approaches to resolution of these problems. Connected-pipe afterburning tests were conducted with the three most promising formulations. These tests indicate that very high afterburning efficiencies may be achieved under extremely adverse operating conditions where state-of-the-art high-boron-loaded formulations ~~suffer from~~ inefficient afterburning.

TABLE OF CONTENTS

LIST OF TABLES

LIST OF TABLES (Continued)

LIST OF FIGURES

LIST OF FIGURES (Continued)

LIST OF FIGURES (Continued)

SECTION I

INTRODUCTION

Recent years have witnessed a large development of fuel-rich propellant technology to produce formulations for primary rockets in air-breathing propulsion systems. Two types of systems have been especially prominent, air-augmented rockets and external-burning missiles or projectiles. In an air-augmented rocket, the incompletely combusted products of a fuel-rich primary motor formulation are mixed and burned with ram air inside a secondary chamber at a pressure equal to or less than the air inlet recovery pressure. In external burning, the fuel-rich primary motor exhaust is injected directly into the free-stream around the missile and burns at atmospheric pressure (sea level or altitude). Both types of systems primarily utilize composite solid propellants with ammonium perchlorate oxidizer: thus non-metalized formulations typically produce compounds consisting of C, H, O, N, Cl, and possibly F, while metalized systems also produce B, Al, Mg, or combinations of these metals.

An essential prerequisite of success in air-breathing applications is rapid and efficient combustion of the primary exhaust in air. It is of interest to spell out here the conditions for this combustion. In ducted propulsion, the pressures in the secondary range from 15 or 20 atm down to perhaps half an atmosphere depending upon the flying altitude and Mach number, and the residence times typically are a few milliseconds. In external burning, the pressures range from 1 to 0.1 atm, and the residence times are a fraction of a millisecond. Thus it is easily seen that these air-breathing systems often place stringent demands upon preignition and combustion times of the primary exhaust fuel products with air.

Boron is a particularly attractive ingredient for propellants for air-breathing rocket applications due to its high heating value. Generally, it is desirable that the amount of boron in the fuel-rich

propellant be maximized, subject to processability and primary motor ejection efficiency constraints. The practical upper limit of boron loading is approximately 50 to 60 percent by weight. At these loading levels, very little boron is burned in the primary motor, due to lack of sufficient oxidizer. Thus, most of the boron must be burned in particulate form with air in the secondary combustor for its heating value to be utilized. In addition, at these high loadings, primary motor flame temperatures tend to be low. These factors, combined with the low residence times available for mixing, ignition, and combustion processes in the secondary chamber had led to afterburning efficiency problems, particularly under operating conditions which result in afterburner pressures of 50 psia or less.

The objective of the first two-and-one-half years of this work was to characterize the nature of the primary exhaust condensed-phase material from fuel-rich motors containing boron, and to study its ignition and combustion characteristics, especially as compared to the known information for pure boron. Results of this phase of the program were presented in detail in an Interim Scientific Report[1] entitled "Studies of the Ignition and Combustion of Boron Particles for Air-Augmented Rocket Applications" (AFOSR-TR-75-0043, October, 1974) and will be covered only relatively briefly in this report.

During the final two-and-one-half years of the program, emphasis was placed on magnesium-containing fuel-rich propellant systems. Theoretical screening calculations were performed to identify promising compositions, both pressed and castable, several of which were subsequently formulated. These formulations were then characterized in terms of combustion of the basic propellants themselves, as well as in terms of the combustibility of their fuel-rich products with air in a ramburner. In addition, basic studies of the composition of the exhaust products were carried out along with single particle combustion studies of magnesium and magnesium nitride (two of the more important exhaust products). The magnesium propellant work will be described in somewhat more detail than the boron work in this report.

SECTION II

BORON COMBUSTION STUDIES

A. COLLECTION AND ANALYSIS OF CONDENSED-PHASE EXHAUSTS OF BORON-LOADED FUEL-RICH PROPELLANTS

In this phase of the program, condensed-phase exhaust products from two different highly-boron-loaded fuel-rich propellants were collected and analyzed in terms of both physical and chemical characteristics. In addition, combustion of the condensed-phase exhaust products (CE) was studied in a flat-flame burner. Finally, modeling studies describing the ignition of single boron particles in hot gas streams and propagation of flames in boron-oxygen-nitrogen dust clouds were performed.

Two propellants were studied. Both were composite ammonium perchlorate-binder formulations containing large amounts (almost 50%) of boron and a few percent of magnesium and aluminum. ARCADENE (Atlantic Research Corporation trade name) 256A is a carboxy-terminated polybutadiene formulation and ARCADENE 280, a polyester formulation. The boron used in both formulations was Kawecki Company material with nominal average particle diameters of 3 μm. However, the diameters range widely from about 1 to 20 μm or more. Thus both formulations are made up of the following elements: C, H, O, N, Cl, B, Mg, Al. In addition to these, the 256A formulation contains a small amount of iron, because it is catalyzed by n-butyl ferrocene.

Two motors were fired with each formulation into a large cylindrical tank (5.2 m long, 2.9 m in diameter) which was first evacuated and then filled with argon to 0.35 atm pressure prior to each run. The rocket chamber pressure and the tank pressure were measured continuously throughout each run.

Data pertaining to the four motor tests are given in Table 1. Each propellant grain was weighed before the test; as was the residue remaining inside the motor after the test. Comparison of the third and fourth columns of Table 1, in which the respective weights are listed,

TABLE 1. MOTOR FIRING CONDITIONS

Run No.	Propellant	Propellant Weight (gm)	Residue Weight (gm)	Tank Pressure (atm) Initial	Tank Pressure (atm) Final	Nominal Chamber Pressure (atm)
1	280*	805	10.5	0.35	0.71	6-15
2	256A**	746	4.4	0.35	0.46	2
3	280	743	18.1	0.35	0.77	65
4	256A	760	47.4	0.35	0.54	40

*Polyester binder

**CTPB Binder

shows that the ejection efficiency ranged from 93.8% in Run 4 to 99.4% in Run 2. During all the tests, the tank pressure rose continuously from the initial to the final value. The low final value recorded in Run 2 can be ascribed to the fact that the burning time was about twice that of other runs, thus allowing more cooling and condensation during the run. As shown, each propellant was tested at a high and a low pressure.

After each test, the tank filled with argon was kept closed for about one hour so the CE would settle in a large (5.4 m^2 surface area) metal trough at the bottom of the tank. The trough was then emptied into a bottle by remote action without opening the tank. Thus, the CE samples were not exposed to air while hot. Thereafter, ordinary precautions were observed to avoid undue exposure to air and humidity (e.g., the samples were stored in corked vials in desiccators), but no attempt was made at absolute exclusion of atmospheric oxidants.

A set of two thermodynamic equilibrium computations, "A" and "B", was made, corresponding to each experimental motor run. The results are given in Table 2. Computations "A" took into account most species which can reasonably be expected to appear in the products. Computations "B" omitted B_4C and BN, two species which are very important thermodynamically, but which are generally suspected not to appear in reality for kinetic reasons.

The theoretical characterization of the CE relevant to this report can by summarized as follows: (a) All of the boron will be found in the CE. The fraction of the CE which is boron (any form) is about 50% for either propellant regardless of the type of computation ("A" or "B"). (b) Most of the boron (roughly 90%) is found in three solid species: B, B_4C, and BN. The question of the realistic distribution of boron among these three, i.e., the relative merits of computations "A" and "B", must be resolved by experiment. (When full equilibrium is assumed ["A"], most of the boron in the exhaust is predicted to be solid B_4C and a significant fraction solid BN.) (c) The remainder of

TABLE 2. THERMODYNAMIC EQUILIBRIUM COMPUTATIONS

Run No.	Pressure (atm)		Temperature (°K)				Weight % CE	
			Chamber		Exhaust			
	Chamber	Exhaust	A	B*	A	B*	A	B*
1	10.2	0.5	2186	2001	1872	1696	83.7	77.5
2	2.0	0.5	1888	1762	1740	1635	84.9	87.2
3	65.3	0.5	2409	2208	1858	1677	86.6	81.8
4	40.1	0.5	2071	1975	1618	1552	88.9	92.0

*B_4C and BN omitted in computations.

the boron is in the CE in the form of boron-oxygen-hydrogen species. While some of these are rather volatile, all will be condensed at the room temperature. (d) The remainder of the CE consists largely of $MgAl_2O_4$ and $MgCl_2$ in computations "A", and $MgAl_2O_4$, $MgCl_2$, and C(s) in computations "B".

The collected condensed exhaust was examined under an optical microscope with magnifications up to 500X. The untreated CE consists of very large, but only loosely agglomerated clusters. The tumbling of the clusters with soft (plastic) balls breaks up the mass of the CE into smaller particles, ranging from about 3 to 50 microns in diameter. Several distinctive features were observed under the microscope. The bulk of the CE is dark and apparently amorphous, but quite a few crytals are also visible. The crystals are either white or colorless. The dark material could be carbon and carbonous material, elemental boron, or possibly B_4C. The light material could be any and all of the following: B_2O_3 (colorless), $B_2O_3 \cdot H_2O$ (triclinic crystals, white), $MgCl_2$ (colorless hexagonal), $MgCl_2 \cdot H_2O$ (white), $MgAl_2O_4$ (colorless), and BN (white hexagonal).

Densities of the CE samples were determined by suspension in inert liquids having several different specific gravities. For CE collected from Sample 1, all particles were found to have specific gravities of less than 2.2, with some being even less than 1.8, but with most having a specific gravity of about 2.0. After washing in a hot mixture of methyl and ethyl alcohol, a standard procedure for removal of B_2O_3 from boron powder, the residue was found to have a specific gravity greater than 2.3. For the purpose of comparison, two suspensions made with the "off-the-shelf" boron powder (Kawecki Co. material used in all ARC propellants), were checked for specific gravity; virtually all of the powder has the specific gravity of about 2.3, i.e., distinctly higher than the unwashed CE, but perhaps slightly lower than the washed CE. The handbook value for the specific gravity of pure boron is 2.32 - 2.35. Thus the 2.3 value for the commercial powder is very reasonable, especially since the material is known to contain about 2% B_2O_3, which has a lower specific gravity.

Our conclusion is that in the CE, low-density substances either coat or are firmly attached to solid B (and B_4C, if any). The washing removes these substances and leaves a residue consisting largely of B (sp. gr. 2.32 - 2.35), and possibly graphite (sp. gr. 2.26), B_4C (sp. gr. 2.54) or BN (sp. gr. 2.25). The possible low-density species are: B_2O_3 (sp. gr. 1.85), $B_2O_3 \cdot 3H_2O$ (sp. gr. 1.49), and $MgCl_2 \cdot 6H_2O$ (sp. gr. 1.56): the $MgCl_2$ without any crystalline water has the specific gravity of 2.33. Since carbon is insoluble in alcohol, the fact that the washed CE contains little low-density material suggests that the untreated CE contained little or no amorphous carbon (sp. gr. 1.8 to 2.1). This has to be interpreted in the light of the thermodynamic computations: the full computation on Run 1 including B_4C and BN in the products, predicts no solid carbon; if B_4C and BN are "suppressed," the thermodynamic computations predicts the CE to contain about 7% carbon. This comparison suggests that computations "A" may be somewhat more realistic.

The CE samples from all four motor runs were analyzed chemically for boron. The analysis was performed by Ledoux and Company, Teaneck, New Jersey, on a subcontract from Atlantic Research. The CE samples were first separated into the soluble and the insoluble portions by boiling water, and then each of the two portions was analyzed for total boron.

The results of the chemical analysis are summarized in Table 3, which lists (a) fraction of the CE which is boron (any form), (b) division of the CE into soluble and insoluble portions, and (c) fraction of the total boron in each of these portions. In each case, we have listed the thermodynamically predicted values along with the experimentally determined ones. The species assumed insoluble for the purpose of comparison of the computation with the experiment are listed in Table 3. Detailed discussion of Table 3 is presented in the Interim Scientific Report[1] referred to in Section I of this report. It is concluded that according to both the experimental data and either one of the two computations, only about 50% of the total CE is boron. Beyond that, one can see

TABLE 3. CHEMICAL ANALYSIS OF THE CE (WEIGHT PERCENT)

Run No.	Fraction of the CE which is Boron (in any form)			Insoluble Portion** (% of CE)			% B in insoluble portion			% B in soluble portion		
	Comput. A	Comput. B*	Experim.	Comput. A	Comput. B*	Experim.	Comput. A	Comput. B*	Experim.	Comput. A	Comput. B*	Experim.
1	51.6	56.5	46.6	70.0	71.0	73.1	64.1	70.8	57.3	22.6	21.8	17.8
2	52.7	51.3	38.5	80.0	75.5	84.8	62.5	62.4	64.2	13.9	17.0	27.0
3	50.6	53.5	44.3	68.5	68.3	74.5	62.3	67.7	51.0	25.0	23.2	24.7
4	50.2	48.6	35.6	77.5	72.5	53.4	60.3	59.9	55.4	15.9	18.9	8.6

* B_4C and BN omitted in computations

** Species assumed insoluble: B, C, MgO, $MgAl_2O_4$, B_4C, BN, Fe, Mg. All others assumed soluble.

that three out of four questions which can be answered by the results of the chemical analysis, namely the amount of boron in the CE, the fraction of the CE which is insoluble, and the amount of boron in the insoluble portion, are predicted reasonably well (order of 10%) by the full thermodynamic computation (column "A" in Table 3). Computations "B" are somewhat less successful, but it appears that they also give a rough idea of the composition of the CE. Indeed, it is possible that the assumptions inherent in the theoretical comparison, e.g., the freezing of the exhaust equilibrium, introduce more of an uncertainty than the difference between the two sets of computations. Only an extensive chemical analysis of several species (Mg, B_4C, C, and others) could resolve the problem of the detailed composition of the CE.

B. COMBUSTION OF THE CONDENSED EXHAUST

As described earlier, the ball-milled CE consists of many small particles with sizable agglomerates interspersed. Prolonged ball-milling and sieving through a 20 μm mesh screen produced a fine powder consisting of particles having a fairly uniform size distribution with average diameters of 3 to 4 μm. By careful screening between 30 and 35 μm, it was also found possible to separate coarse powder samples consisting of firm agglomerates which could be treated as single particles.

Combustion of the coarse CE samples was studied by a single-particle technique, utilizing a gas burner, which was previously developed and extensively used at Atlantic Research for combustion studies of aluminum,[2-4] beryllium,[5-6] and boron.[7] Since particles smaller than 10 or 20 μm in diameter are difficult to handle and observe singly, the gasburner technique was adapted for a study of particle clouds. The newly developed technique was used to study ignition and combustion of the fine CE powder. Details of the experimental procedures were presented in the aforementioned Interim Scientific Report,[1] and will not be repeated here.

The single-particle technique was used for a study of both the ignition and the subsequent combustion of a 30 - 40 μm sample collected

in Run 4. The gas burner was run on propane-oxygen-nitrogen mixtures. The burner gases consisted of 1.4 - 20% O_2, most observations having been made with about 20% O_2, 15 - 20% H_2O, and 10 - 12% CO_2; the remainder was mostly N_2. Gas temperatures were varied from 1850 to 2300°K. Velocities of burner gases were about 1000 cm/sec, and those of the carrier (helium) about 100 cm/sec.

Quantitative ignition and combustion parameters of neat boron powder in the 30 to 40 μm range are well-known from our previously published work.[7] Since it is of obvious interest to compare the combustion characteristics of the CE to those of boron, the relevant results of that work shall now be briefly stated. The entire history of the boron particles ($\bar{d}$ = 35 μm) in the burner gases (2240°K, 19% O_2, 16% H_2O) can be divided into three phases: a dark pre-ignition period (ca. 8 msec), followed by a peculiar two stage combustion, the durations of the two periods being t_1 = 4 msec and t_2 = 11 msec. The first combustion stage begins when the particle temperature is about 1850°K. The first stage is generally believed to correspond to slow combustion, impeded by a layer of liquid B_2O_3. Most of the mass of boron is consumed during the rapid second stage, controlled by the gas-phase diffusion of oxidants toward the particle; thus t_2 approximates the total diffusion-combustion time of the particle, $t_2 \lesssim t_b$. The minimum temperature of the burner gases necessary for ignition of particles was found to be 1880 $\pm$ 20°K.

The CE agglomerates, 30 μm < d < 40 μm, were found to burn as single particles: there is no separation of particle trajectories. Thus, we can make a quantitative comparison of the CE combustion to combustion of boron. When the CE, 30 μm < d < 40 μm, is burned in the same burner gases as the 35 μm boron (T_g = 2240°K, 19%O_2, 16%H_2O; see previous paragraph), the following differences are observed:

1. The CE "particles" give well-defined burning times, but there is no sign of two-stage combustion.
2. The average burning time of the CE is t_b = 10 $\pm$ 1.5 msec.

3. The CE ignites substantially lower in the burner gases than the boron: it is estimated that the preignition delay of the CE is 30 to 50% lower than for boron particles.

In addition to the test at constant gas temperature and constant mole fraction of O_2, two series of experiments were run in which these two parameters were varied. Variation of temperature at constant mole fraction of O_2 (ca. 0.2) showed that the minimum gas temperature necessary for ignition of the CE is 1850 $\pm$ 25°K. Variation of O_2 content at the approximately constant gas temperature of 2200 to 2300°K shows that the CE continues to burn, although very slowly, even at the lowest mole fraction of O_2 which we tried, 0.014.

Since the burning time of a particle is a strong function of its diameter, and since we have no accurate value for the average diameter of the CE, the two values, t_b = 10 msec for the CE and $t_b \sim t_2$ = 11 msec for boron, must be considered the same within the experimental error.

The cloud technique for combustion of small particles, described in detail in the Interim Scientific Report,[1] yields average preignition delays (t_i) and burning times (t_b). Both t_i and t_b are approximate because in a burning cloud one cannot define clear points of onset and cessation of combustion. Furthermore, since the preignition delay necessarily overlaps the carrier-gas mixing time, one cannot obtain cloud ignition temperatures from measured preignition delays as in single-particle work; one can only determine relative ignitabilities of two clouds by comparing the preignition distances in two replicate experiments.

Two CE samples, from Runs 1 and 4, have been studied by this technique. The results obtained with these two samples are indistinguishable from each other.

The CE samples used in the cloud experiments consisted of the material which had passed through a 20 μm mesh screen. However, since the gas burner operates in such a way that the material is subjected to prolonged swirling with plastic balls, there is no assurance that the

particle size distribution injected into the burner gases is the same as in the original (sieved) sample. Therefore, the unburned material was sampled after injection into the burner gases, i.e., at a point between the injection orifice but below the point of ignition. Microscopic examination of the sampled material revealed that the particle diameters were in the range between 2 and 7 μm. The average diameter was about 3.5 μm.

In addition to the CE, two other samples were studied by the cloud-combustion technique for the purpose of comparison: an amorphous boron sample, supplied by U. S. Borax, Inc., stated to be 98% pure; and the material supplied by Kawecki, Inc. The Borax powder particle diameters are in the narrow range of 1.0 ± 0.2 μm. The Kawecki powder has a wide distribution of particle diameters, ca. 1 to 20 μm, with the number average of 3 μm. The Kawecki boron is used both in ARCADENE 256A and 280 propellants.

The minimum gas temperature necessary for ignition of the particle cloud was found to be the same, within experimental error for the Borax sample and for the CE: 1980 ± 20°K. (This is approximately 100 to 150°C higher than the analogous limiting temperature for 30 to 40 micron particles of either the CE or crystalline boron, as mentioned earlier.)

Measurements of the minimum gas temperatures necessary for ignition of powders, which we shall refer to as "temperature limits" from here on, have thus resulted in two conclusions: (a) temperature limits for clouds of small (< 10 μm) particles are 100 to 150°K higher than for large 30 to 40 μm particles; (b) regardless of the particle size, temperature limits are the same for the CE and for boron.

The cloud combustion technique has also been used for burning time measurements of the CE, of the Borax boron, and of the Kawecki boron. The burning time t_b was taken to be equal to the length of the burning cloud divided by the linear velocity of the burner gases. Since the luminosity of the cloud both develops and fades out gradually, an approximate visual judgement concerning the length of combustion must be made. The velocity of the burner gases can be calculated from known (metered) input gas flow and known flame temperature; it can also be obtained by measurement

of single-particle velocities. The calculated and the measured values usually agree within about 25%. It is estimated that the combined uncertainties of the cloud length and particle velocity may conceivably lead to an error in determination of t_b of up to a factor of two, but most t_b values are probably more closely defined than that.

The average results of three cloud-combustion measurements are shown in Figure 1. The burner gas properties in all three experiments were: T = 2240°K, $X(O_2)$ = 0.19, $X(H_2O)$ = 0.16. A single point for the t_b of a spherical boron particle, d = 37 μm, is given in the same plot. The single-particle point is a small extrapolation of an accurate measurement (see Table VI of Ref. 8) in a somewhat different burner gas: T = 2280°K, $X(O_2)$ = 0.23, $X(H_2O)$ = 0. Even with the extrapolation, the values of both t_b and of d are no doubt much more accurate for the single-particle point than for the cloud measurements. In view of the uncertainties in the cloud measurements, one should be careful about assigning a specific numerical value to the slope, n, in Figure 1. However, an inspection of the figure shows that even if the cloud data are in error by a factor of 2, n will still be closer to unity than to a value of 2, predicted by single-particle diffusion theories.[9,10]

In addition to experiments run with burner gases having a constant, relatively high mole fraction of oxygen, $X(O_2)$ = 0.2, cloud experiments were made with decreasing values of $X(O_2)$, both with the CE and with the Borax boron powder. Gas temperatures in all the tests were kept at about 2300°K. Only visual observations were made. It was found that both powders burned about equally vigorously down to $X(O_2)$ = 0.14. The combustion brightness decreased rather sharply between $X(O_2)$ = 0.14 and 0.12, and then very gradually down to about $X(O_2)$ = 0.05 with both powders. At very low mole fractions of oxygen, 0.015 to 0.05, the CE powder burned very weakly, and the boron powder hardly at all.

The single-particle experiments indicate that the burning times t_b of the CE are about the same as for boron. This appears a priori reasonable, particularly if the combustion is diffusion-limited, but even if it is kinetics-limited, provided the limiting reaction is the same,

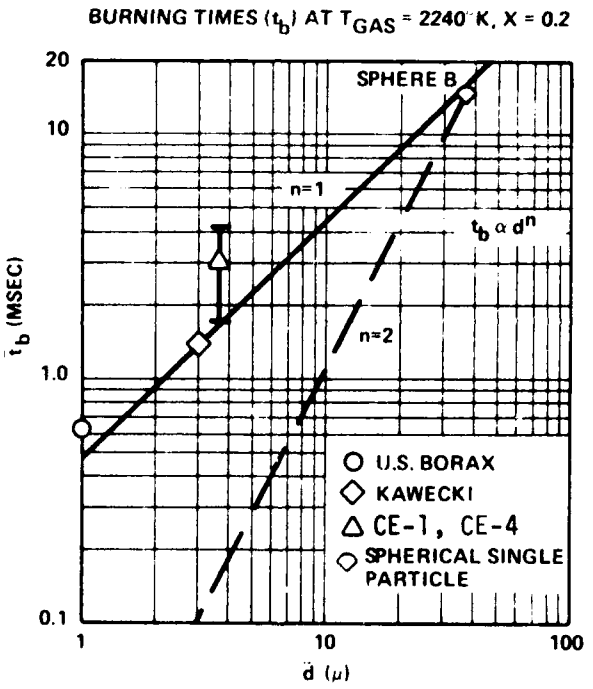

Figure 1. Burning Times (t_b) of Various Particles

as seems likely. Higher volatility of some expected CE ingredients should accelerate the burning rate of particles. Thus, if the CE is rich in species such as Mg, $MgCl_2$, and Fe, one should expect it to burn somewhat faster than boron. On the other hand, if it contains large amounts of B_4C (and possibly BN), it may burn more slowly: B_4C is known to burn more slowly than boron, and BN has been observed to ignite only with difficulty. In either case, the change in t_b of boron caused by adulteration is probably not sufficient to be clearly demonstrated by our experiments.

C. ANALYTICAL MODELING OF BORON SINGLE-PARTICLE COMBUSTION AND BORON CLOUD FLAME SPEEDS

The model[11] (originally developed under Internal Research and Development funding) of the ignition of boron particles treating the removal of a boron oxide layer from the surface of the boron particle through numerical integration of difference equations describing the generation and removal rate of boric oxide has been revised to more accurately treat the various processes involved. This new model yields predicted ignition times and minimum ambient temperature requirements for particles studied by Macek[7] in dry gas streams which are in good agreement with his measured data. An attempt to treat the effect of water gas on boron particle ignition as being a diffusion-limited reaction of the water with the boric oxide coating to form gaseous HBO_2 was unsuccessful. Effects of various parameters on boron particle ignition were studied with this model. Oxide thickness was found to moderately affect predicted ignition times, this effect decreasing with increasing particle size. The effects of total pressure and oxygen mole fraction on minimum ambient temperature required for ignition and on ignition time were found to be fairly complex. At low oxygen mole fractions, increasing total pressure leads to more difficult ignition, while at high oxygen mole fractions, the reverse is true. At low total pressure, ignition was found to be independent of oxygen mole fraction: at high pressure, increasing oxygen mole fractions led to easier, faster ignition.

Initial particle radius effects are also somewhat complex. For the case of surrounding radiation temperature equal to the gas temperature, minimum ambient gas temperature required for ignition increases with decreasing particle size for particle radii below 10 to 15 microns. Ignition time generally decreases with decreasing particle size, except where affected by the ignition limit dependency on particle size. Ignition time is predicted to increase strongly with decreasing gas temperature. The same type of dependency on surroundings radiation temperature is predicted in the region of ambient gas temperatures which are marginal for ignition.

The same equations used in the numerical analysis have also been used in a stability analysis to define conditions (e.g., ambient temperature) required for ignition. Excellent agreement was found between results obtained with the numerical analysis and the stability analysis. A copy of a technical paper[12] generated from this effort is included as part of the earlier referenced Interim Scientific Report.[1]

A model for prediction of boron-oxygen-nitrogen dust clouds treating the boron particle ignition and combustion processes in detail, as described immediately above, was subsequently developed. The problem was formulated as a double-eigenvalue problem with numerical integration of mass, species and energy difference equations in combination with difference equations describing the ignition and combustion processes through ignition and combustion zones. This model was found to yield predicted flame speeds in reasonable agreement with the limited boron-oxygen-nitrogen dust cloud flame speed data available.

In addition, a vastly simplified closed-form flame speed expression was developed. Predicted flame speeds from this model were found to exceed those predicted from the detailed model by 0 to 130% over the range of parameters examined. It was shown that two of the major error-producing approximations associated with the simplified model tend to drive predicted flame speeds down, while a third tends to drive them up, leading to a large degree of cancellation of these errors. Over the range of conditions examined, it appears that the simple closed-form model can

be used with a correction factor dependent upon Nusselt Number and pressure to obtain reasonable estimates of boron-oxygen-nitrogen dust cloud flame speeds.

Effects of various parameters on predicted flame speed were studied. Predicted flame speeds were found to increase with increasing initial temperature, decreasing initial particle radius, increasing initial oxygen mole fraction, decreasing pressure, increasing particle loading (on fuel-lean side of stoichiometric), increasing post-flame emissivity, decreasing initial oxide coating thickness, and decreasing Nusselt Number. A copy of a paper[13] generated from this modeling effort is also included as part of the Interim Scientific Report.[1]

SECTION III

MAGNESIUM PROPELLANT STUDIES

A. BACKGROUND AND PURPOSE

The potential performance advantages of air-augmented rocket systems over conventional rocket systems, resulting from using "free" air as an oxidizer replacing a large fraction of the relatively low energy oxidizer which must be carried along in a conventional propellant (displacing fuel) have long been recognized. In the past, fuel-rich propellants centered around carbon, aluminum, and boron have been considered as fuels for such systems, while magnesium has been neglected. There have been two major reasons for this neglect. First, magnesium has a lower theoretical heating value (an important parameter for air-augmented rocket applications) than the other three materials. Second, castable magnesium formulations present practical curing problems: the art of preparing Mg-containing propellants with satisfactory physical properties was, therefore, not well-developed at the inception of this program.

Closer examination of the situation, however, indicates that there are other factors dictating further evaluation of magnesium as an ingredient in fuel-rich air-augmented rockets. First, consider in more detail the question of theoretical performance. Listed in Table 4, are theoretical performance parameters for typical highly-boron-loaded fuel-rich formulations, aluminized formulations, carbon-loaded formulations, formulations containing no metal fuel additive, and magnesium-loaded formulations. For operation under conditions where the air-to-fuel ratio is high (20/1 or greater), the mass and volumetric heating values are important parameters in ranking theoretical performance. As may be seen from Table 4, the state-of-the-art boron systems have significantly higher theoretical heating values than any of the other systems. Although the 50% carbon formulation gives higher theoretical heating value than any of the other non-boron formulations, attempts to develop good afterburning propellants with that carbon loading have been unsuccessful, 30% carbon-loaded systems

TABLE 4. HEATING VALUES FOR VARIOUS TYPES OF PRACTICAL FUEL-RICH PROPELLANTS

TYPE OF PROPELLANTS	HEATING VALUE (Btu/lb)	(Btu/in^3)
50% BORON-LOADED CTPB PROPELLANTS	15500-16000	950-1000
50% CARBON-LOADED CTPB PROPELLANTS	12000	630
30% CARBON-LOADED CTPB PROPELLANTS	9800-10100	515-550
35% ALUMINUM-LOADED CTPB PROPELLANTS	7100	480
AP - CTPB PROPELLANTS	4000-7200	225-350
50/10/40 MAGNESIUM/HTPB/HMX	8660	516
65/10/25 MAGNESIUM/HTPB/HMX	9640	567
50/10/40 MAGNESIUM/HTPB/AP	7290	437
65/10/25 MAGNESIUM/HTPB/AP	8790	520

representing the highest successful loadings to date. These may be seen to compare closely in heating value with the potential magnesium systems listed at the bottom of the table. Aluminized fuel-rich propellants and non-metalized formulations within practical composition limits are seen to be inferior in performance. Thus, in terms of theoretical heating value among practical formulations, only the boron systems clearly outrank the listed magnesium systems.

In addition, magnesium offers some important advantages over even boron for air-augmented rockets under certain conditions. For very low air/fuel ratio applications, it may be shown that magnesium-loaded systems will provide higher theoretical performance than systems containing the higher-heating-value additives due to a lower oxygen requirement (per unit heat release) of the magnesium metal. This is demonstrated in Figure 2, via a comparison of a magnesium-loaded formulation designated MK1 (developed in the course of this program) with a state-of-the-art boron-containing formulation. In development of this plot, various air-augmented rocket design conditions (configuration, Mach Number, altitude, drag coefficient) are chosen, which, with the use of the boron formulation, would require operation at the air/fuel ratios plotted on the abscissa of this figure. The required fuel flow rate for each of these conditions is then calculated. The MK1 formulation is then substituted for the state-of-the-art boron formulation and the required fuel flow with the MK1 fuel for operation at the same design condition calculated. The calculational procedure employed is a very simplified one, with a number of approximations and assumptions, basically involving setting the air flow equal for the two cases, and calculating the air/fuel ratios for each fuel which will yield equal values of vacuum sonic gross thrust/air flow rate (S_A). The ratio of the required MK1 fuel flow rate to the required state-of-the-art boron formulation fuel flow rate is then plotted against the operating air/fuel ratio for the boron formulations. (This somewhat involved method of presentation is used to avoid security classification problems.) This ratio is calculated both on a mass basis and a volume basis. As may be seen, as the operating air/fuel ratio decreases, the ratio of required flow rate of

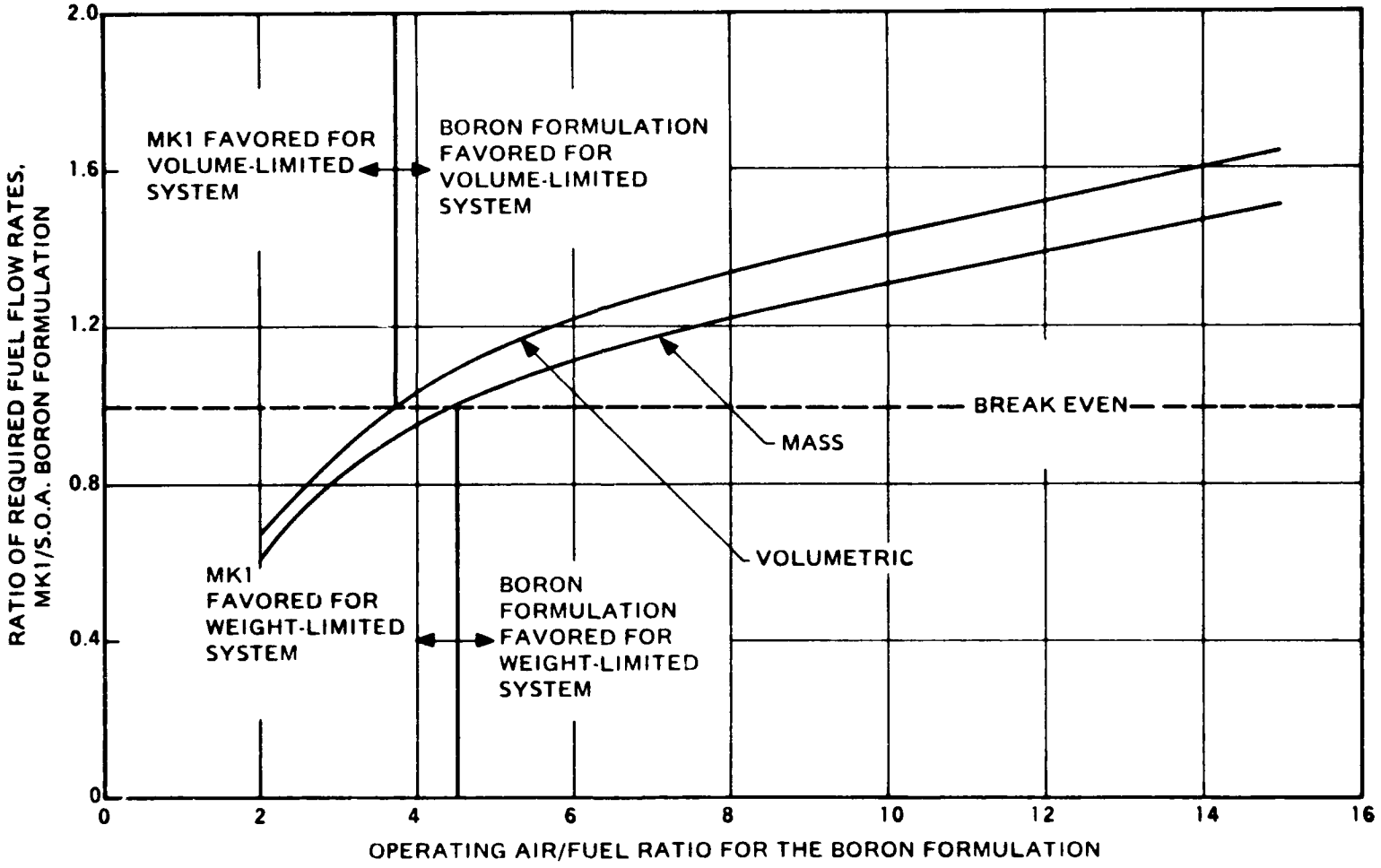

Figure 2. Comparison of Fuel Flow Requirements for Given Operating Design Point for MK1 versus State-of-the-Art Boron Formulation

MK1 to state-of-the-art boron formulation also decreases. A value of 1.0 for this ratio signifies a break-even point between use of these fuels (on theoretical thermodynamic performance considerations alone), with the MK1 magnesium system being superior at lower air/fuel ratios (which tend to be associated with high thrust coefficient requirements). As shown, the MK1 formulation is favored for volume-limited systems in applications where the state-of-the-art boron formulation would be required to operate at air/fuel <3.7, while it is favored for weight-limited system for boron air/fuel <4.4.

In choosing fuel-rich propellants for air-augmented rocket systems, parameters other than theoretical performance must also be considered. For instance, with the aluminum formulations, there are severe (thus far, intractable) nozzle deposition problems caused by formation of Al_2O_3 slag in the primary motor (fuel generator). With boron formulations, materials cost and requirements for elaborate pretreatment of the boron raise considerable difficulty regarding large scale production. Most important, however, is the question of efficiency of combustion of the fuel-rich products exhausting from the primary motor into the afterburner chamber. High theoretical heating value is of little use if the heat cannot be released through combustion of this fuel-rich stream with air in the limited confines of the afterburner. Boron and carbon have been found to be quite difficult to afterburn, leading to severe degradation of delivered performance under conditions of low afterburner pressure, high air/fuel ratio, low air temperature, or low afterburner residence time (small combustor or large throat-to-chamber diameter ratio), particularly if a flame-holding aid cannot be used. This problem should not be encountered with magnesium. In this regard, two positive trends become apparent upon inspection of thermodynamic data presented later in this report. First, even high magnesium loadings, 50 to 60%, give high primary chamber temperatures, well in excess of 2000°K, suggesting that these formulations would burn well and give good primary ejection. Second, very substantial fractions of total magnesium are predicted to appear as the metal vapor in the primary

products, so secondary combustion should present no problems; indeed, it should be exceptionally vigorous at all pressures. Thus, it appears that magnesium-loaded fuel-rich propellants will be advantageous in terms of combustion efficiency under conditions of low afterburner pressure, high air/fuel ratio, low air temperature, low afterburner residence time (small combustor or large throat-to-chamber diameter ratio), particularly if a flame-holding aid cannot be used. In addition, the high degree of reactivity of primary motor exhausts from fuel-rich magnesium propellants should make them attractive for external burning rocket applications, where the burning pressure is, of course, low; available residence time for useful heat release is short; and use of a flame-holding aid is impossible.

Accordingly, the objective of this phase of the program was the identification, formulation, and testing of promising highly-magnesium-loaded fuel-rich propellants suitable for use as air-augmented rocket propellants. Major tasks included: (a) thermodynamic computations to identify promising candidate formulations; (b) experimental formulation and ballistic evaluation of selected compositions; (c) characterization of the combustion products of these formulations; (d) single-particle combustion studies of condensed-phase fuel products produced by burning of these formulations in the absence of air; (e) theoretical study of the effects of magnesium vapor on plume ignition; (f) testing of these formulations in motor configurations to characterize their motor ballistics and ejection properties; and (g) connected-pipe afterburning tests quantifying the afterburning properties of the products of combustion of the selected formulations.

B. THERMODYNAMIC SCREENING

1. General Criteria

There are several characteristics of highly-magnesium-loaded propellants important to their selection as promising candidates which can be quantified through thermodynamic calculations. First, it is generally desirable to maximize the propellant heating value (per unit mass for use in weight-limited systems or per unit volume in volume-limited systems). Next, in order to insure high efficiency of ejection of the fuel stream from

the primary motor to the afterburner and to improve ignitability of this fuel stream as it mixes with air, it is desirable that the primary motor flame temperature be high. (With boron systems, it has been found that primary motor flame temperatures of at least 2000 to 2200°K are necessary for even marginal performance.) Finally, it is obviously desirable that the reaction of combustibles leaving the primary motor which are in the gas phase rather than a condensed phase be maximized in order to minimize particle ignition difficulties and burning time. A useful figure of merit for comparison of potential formulations which contains the first and last parameters is the "reduced volumetric heating value" defined as the product of the total volumetric heating value and the fraction of the heating value not contained in condensed-phase primary motor products. Screening calculations to select promising candidate castable and pressed compositions have been carried out during the course of this program.

2. Castable Compositions

The following classes of castable propellant systems have been considered in this thermodynamic screening effort:

(1) Nitrocellulose (NC)/TEGDN/Polyethylene Glycol (PEG400)/ Magnesium
(2) Nitrocellulose/Nitroglycerin(NG)/Adiponitrile (ADN)/ Magnesium
(3) Nitrocellulose/Dioctyl Adipate (DOA)/Ammonium Perchlorate (AP)/ Magnesium
(4) Polyester Resin (HX 730)/TEGDN/HMX-AP/Magnesium
(5) HTPB/HMX-AP/Magnesium
(6) HTPB/HMX/Magnesium/Aluminum
(7) HTPB/HMX-AP/Magnesium/Boron

(HTPB refers to a standard hydroxy terminated polybutadiene binder system.) The first two systems are double-base systems, the next is a composite-modified double-base the fourth is a nitro-plasticized composite propellant system,

and the last three are composite propellant systems utilizing a hydroxy terminated polybutadiene binder. In the first five systems, the only metal fuel is magnesium, while mixed metal systems are considered as the sixth and seventh systems. Results of thermodynamic computations for these systems are presented in various forms in Figures 3 - 13. The parameters of interest plotted in these figures are:

(1) Volumetric Heating Value of the Formulation (assuming complete combustion with excess air to H_2O (gas), CO_2 (gas) and the condensed-phase metal oxides)

(2) Primary Motor Flame Temperature

(3) Percent heating value contained in Condensed-Phase Combustibles Leaving the Primary Motor

(4) (Volumetric Heating Value) x (1 - Fraction Tied Up in Condensed-Phase Combustibles Leaving the Primary Motor) [Referred to subsequently as Reduced Volumetric Heating Value]

With the first type of system (NC/TEGDN/PEG/Mg), it appears that volumetric heating values up to 520 BTU/in^3 can be obtained at primary motor flame temperatures in the range of 2300 to 2400°K. Heating values are maximized by elimination of TEGDN from the system, with only slight accompanying degradation of primary motor flame temperature. Results of thermodynamic calculations for the NC/PEG/Mg system are shown in Figures 3 - 5, for PEG/NC ratios of 1.0 to 2.0 (covering the practical formulation range) and magnesium loadings of 30 to 75 percent by weight. In Figures 3 and 4, volumetric heating value is plotted against primary motor flame temperature and against the percent heating value contained in condensed-phase combustibles leaving the primary motor. (For these cases, the condensed-phase combustibles are all carbon, with all unburned magnesium existing as an extremely combustible vapor.) As may be seen, increasing magnesium loading at a fixed PEG/NC ratio increases heating value and primary motor flame temperature up to about 50-55% magnesium level - at higher magnesium levels, flame temperature drops rapidly. At a fixed magnesium level, increasing PEG/NC ratio increases heating value,

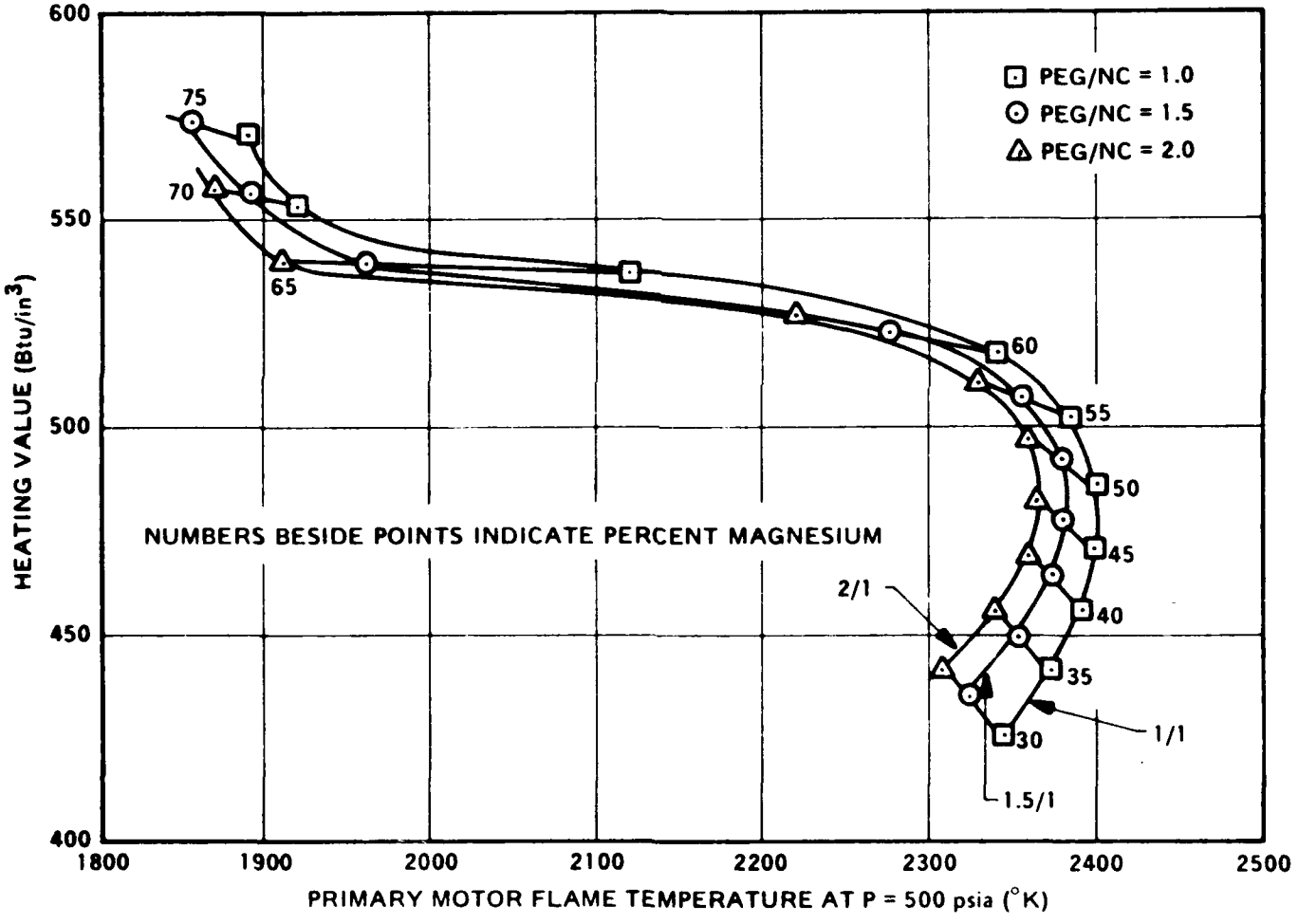

74-612-3

Figure 3. VOLUMETRIC HEATING VALUE VERSUS PRIMARY MOTOR FLAME TEMPERATURE FOR NC/PEG400/MAGNESIUM SYSTEM.

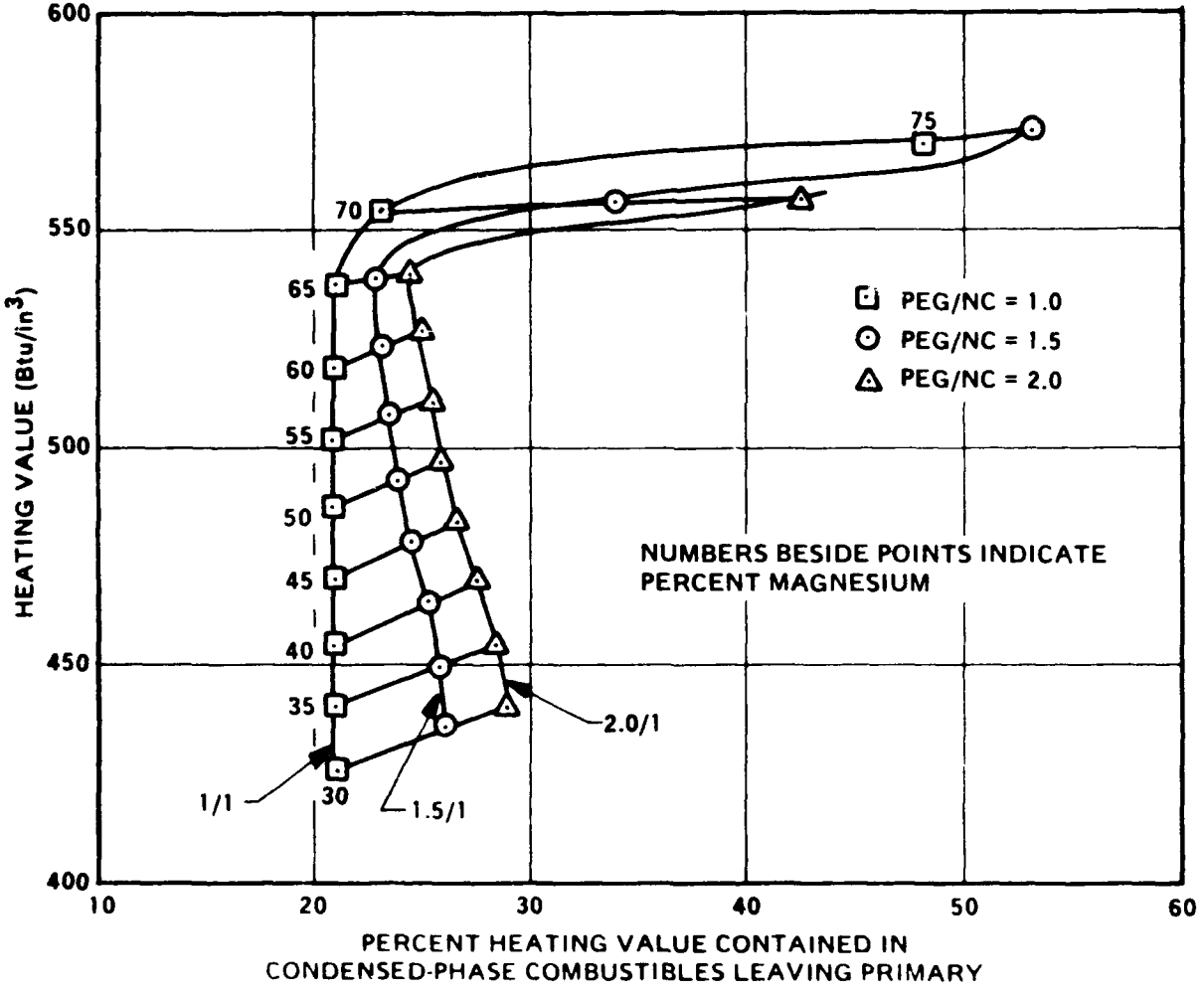

74-612-4

Figure 5. VOLUMETRIC HEATING VALUE VERSUS FRACTION IN CONDENSED-PHASE-COMBUSTIBLES FOR NC/PEG400/MAGNESIUM SYSTEM.

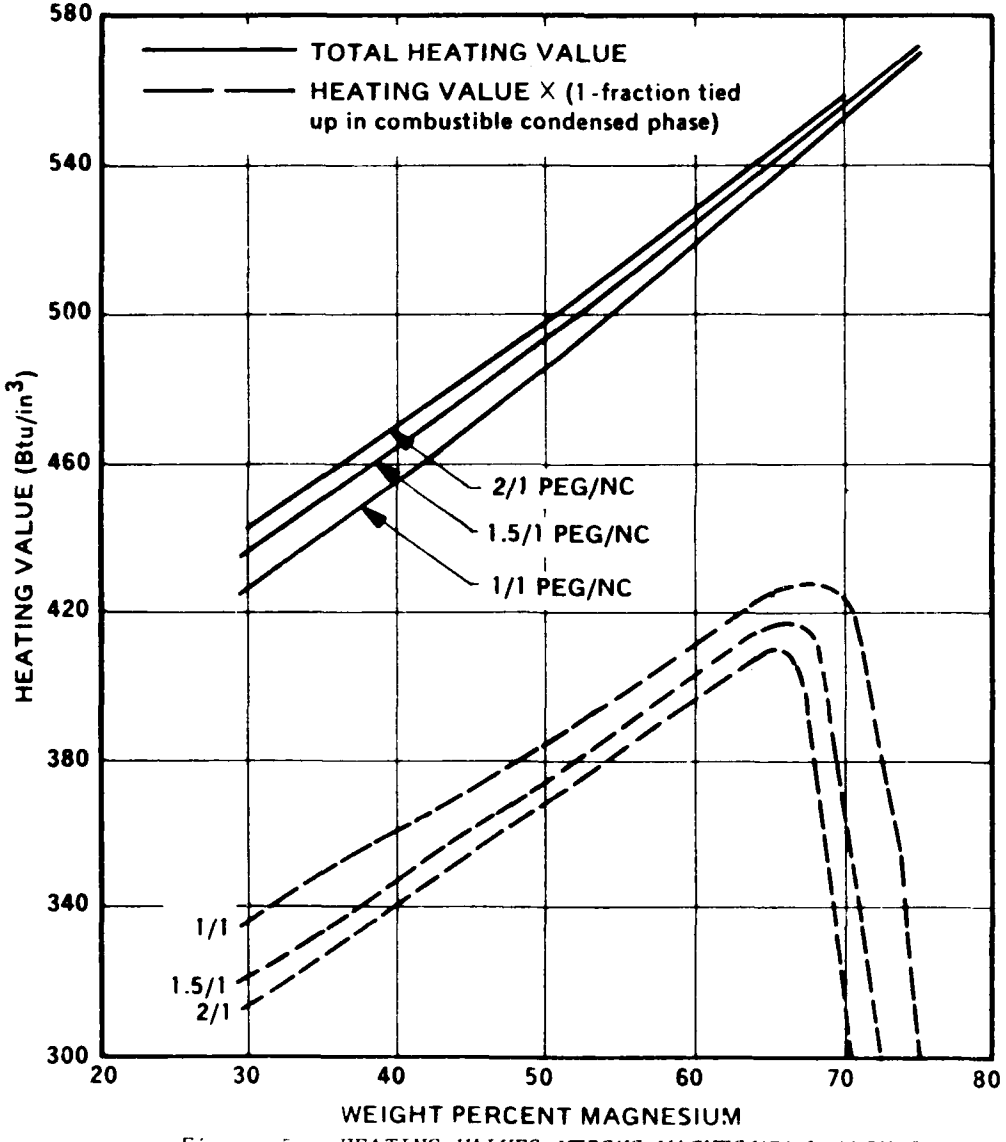

Figure 5. HEATING VALUES VERSUS MAGNESIUM LOADINGS FOR NC/PEG400/MAGNESIUM SYSTEMS

74-612-5

but decreases primary motor flame temperature. Figure 4 shows that the percentage of heating value tied up in condensed-phase combustibles (relatively difficult to afterburn) is independent of magnesium loading for a 1/1 PEG/NC ratio, and actually decreases with increasing magnesium loading for PEG/NC ratios of 1.5 and 2.0, up to approximately 65-70 percent magnesium loading. For a fixed volumetric heating value, the percentage tied up in condensed phase combustibles increases with increasing PEG/NC ratio. It may be concluded from these calculations that theoretical heating value may be maximized without increase of heating value tied up in condensed-phase primary motor exhaust products and with maintenance of adequate primary motor temperatures by increasing magnesium loading up to approximately 65 weight percent, with the optimum relative amounts of nitrocellulose and polyethylene glycol being determined by tradeoffs between heating value and percent heating value in condensed-phase combustibles emanating from the fuel generator. In Figure 5, total volumetric heating value and volumetric heating value reduced by the fraction of that value in condensed-phase combustibles leaving the primary motor are plotted against magnesium loading for the three PEG/NC ratios examined. Total heating value increases monotonically with magnesium loading up to 75 percent magnesium (the highest level examined) while the reduced heating value maximizes at approximately 65-70 percent magnesium loading. Figures 3 to 5 indicate that a heating value of approximately 520 - 540 BTU/in^3 can be obtained in an NC/PEG/Magnesium system with approximately 60 - 65 percent magnesium, which should afterburn well (primary motor flame temperature in excess of 2200°K, approximately 20 percent of potential heating value in condensed phase combustibles entering the afterburner).

Theoretical volumetric heating values and reduced heating values are plotted against magnesium loading for the Nitrocellulose/Nitroglycerin/Adiponitrile/Magnesium system (30/63/7 ratio for the first three ingredients) in Figure 6. This is a very hot system, with a theoretical primary motor flame temperature of 2460°K even at 70 percent magnesium loading. As a result there are no condensed-phase combustibles predicted in the primary exhaust stream at magnesium loadings of less than 50 percent, and only 3.9

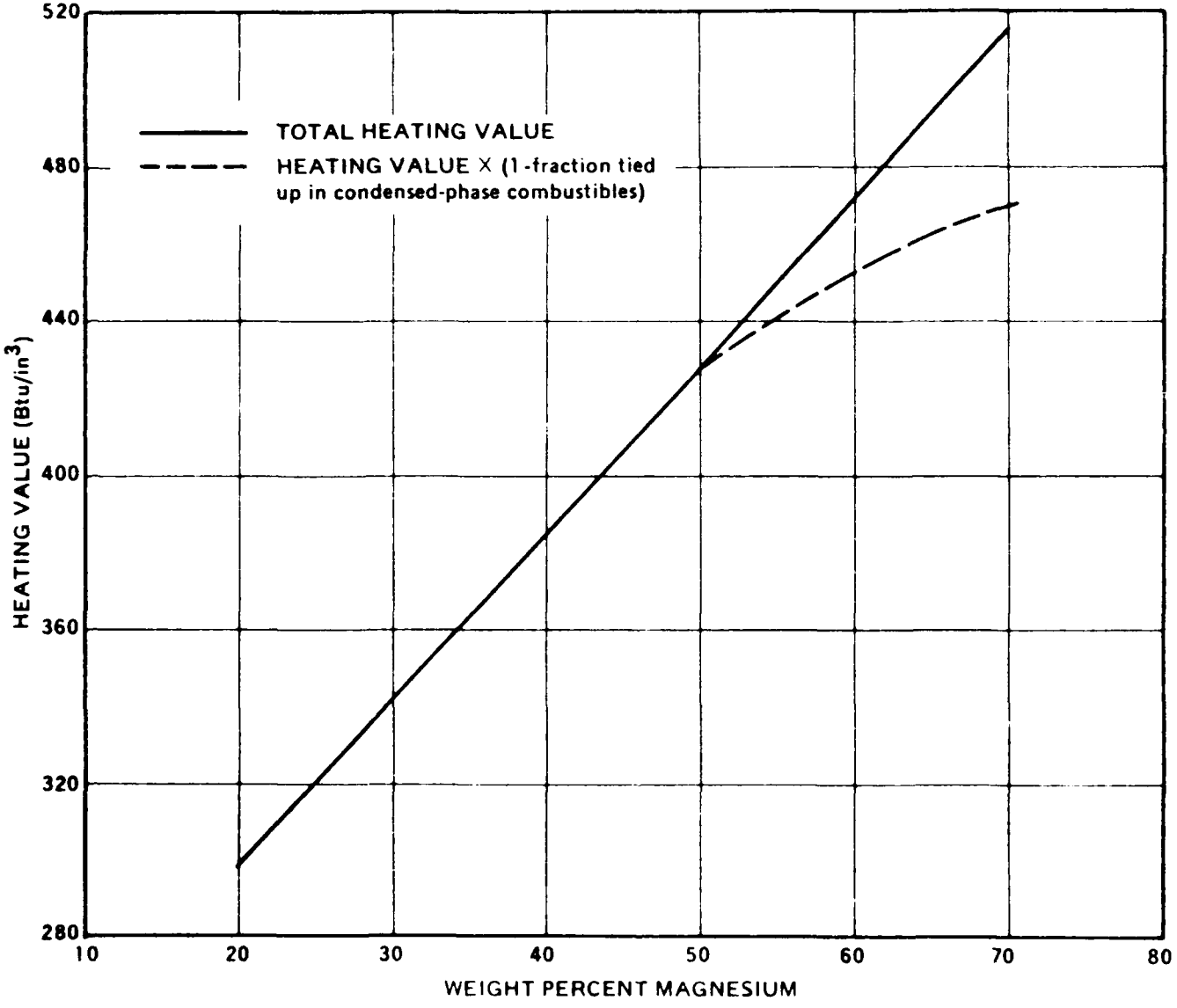

FIGURE 6. HEATING VALUES VERSUS MAGNESIUM LOADINGS FOR NC/NG/ADN/ MAGNESIUM SYSTEMS

and 8.9 percent of the total heating value appears in such products at 60 and 70 percent magnesium loading. Thus, although the total heating value potential of this system is less than the preceding system (470 -495 BTU/in^3 at 60 - 65 percent magnesium loading) the reduced heating value is somewhat higher (460 versus 420 BTU/in^3).

With the third type of system considered (NC/DOA/AP/Mg), it was found that theoretical volumetric heating values of 500 to 520 BTU/in^3 can be achieved at flame temperatures of 2200°K or less for a wide range of compositions, with these values dropping off to 440 to 480 BTU/in^3 as the flame temperature requirement is raised to 2400°K. The fraction of combustibles leaving the primary motor as condensed phases (mostly carbon) is strongly influenced by the ammonium perchlorate level, increasing with decreasing AP level. Results of thermodynamic calculations for a series of practical formulations in which the nitrocellulose and dioctyl adipate content were held at 8 and 12 percent respectively, and the relative amounts of ammonium perchlorate and magnesium were varied are shown in Figures 7 and 8. As the percentage of magnesium is increased (and AP correspondingly decreased), heating value increases, primary motor flame temperature decreases, and percent heating value tied up in condensed-phase combustibles leaving the fuel generator increases. It appears that a heating value of 500-520 BTU/in^3 is attainable at a flame temperature of 2200-2300°K, with about 15 percent of that value in condensed phase combustibles, not markedly different from the NC/PEG/Mg system potential.

Results of thermodynamic calculations for HX730/TEGDN/HMX-AP/Magnesium systems are presented in Figure 9. In all of these calculations, the ratio of HX730 to TEGDN was held at one-to-one. Three binder levels were considered. In addition, cases where all of the oxidizer was HMX and cases where part of the HMX was replaced by ammonium perchlorate were considered. As may be seen, the total heating value increases monotonically with increasing magnesium level, is essentially independent of binder level, and decreases with substitution of AP for HMX. The reduced volumetric heating value (total

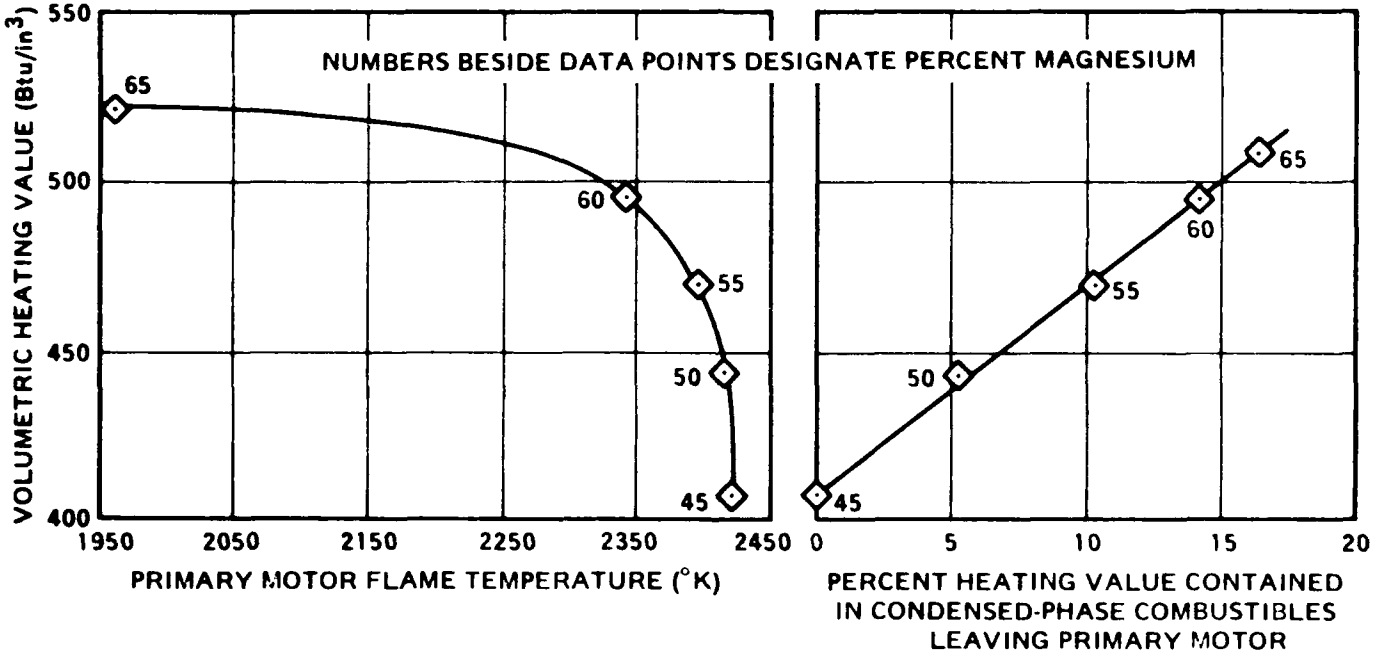

FIGURE 7. THERMODYNAMIC CALCULATIONS FOR NC/DOA/AP/Mg SYSTEMS (8% NC/12% DOA)

74-612-7

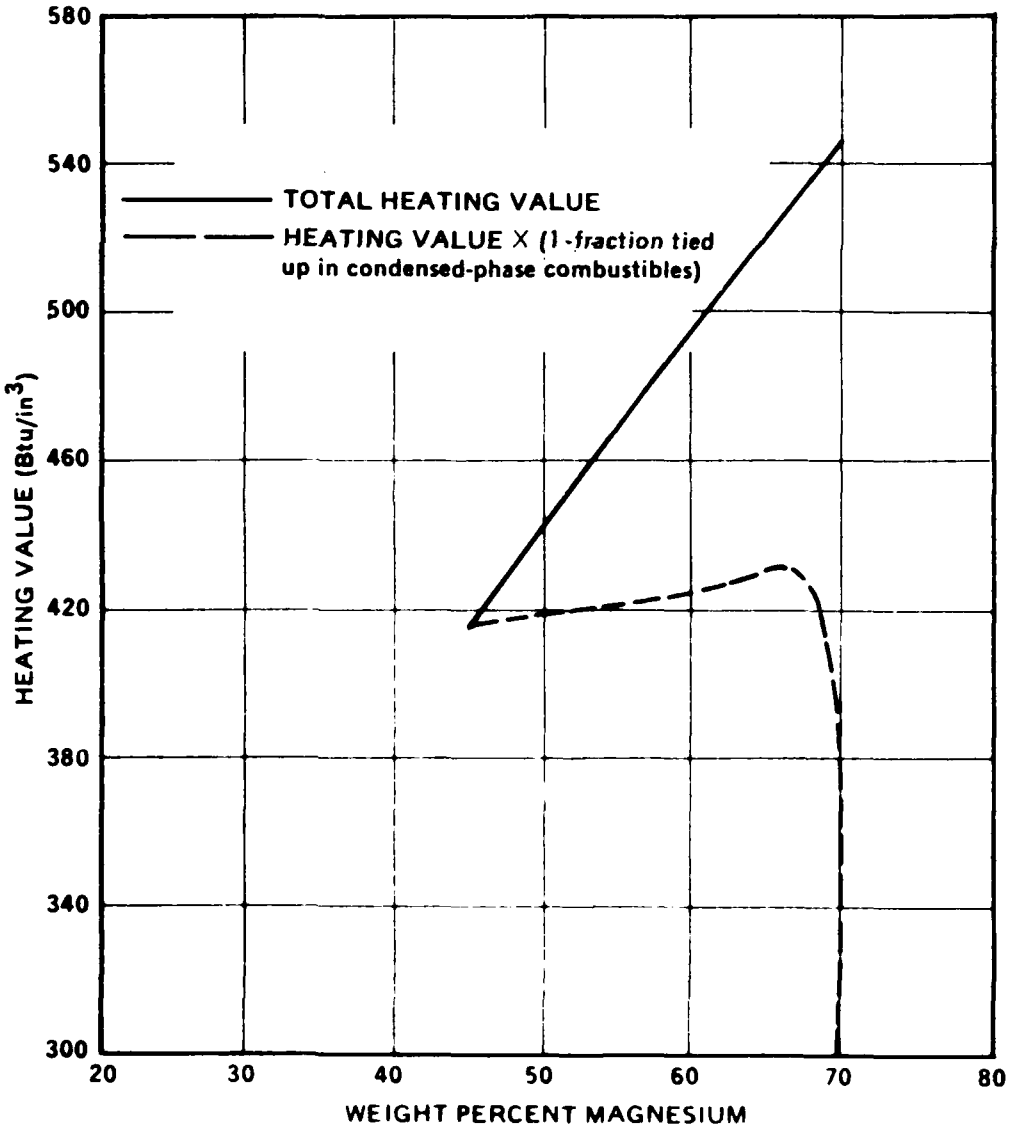

74-612-8

FIGURE 8. HEATING VALUES VERSUS MAGNESIUM LOADINGS FOR NC/DOA/AP/MAGNESIUM SYSTEMS

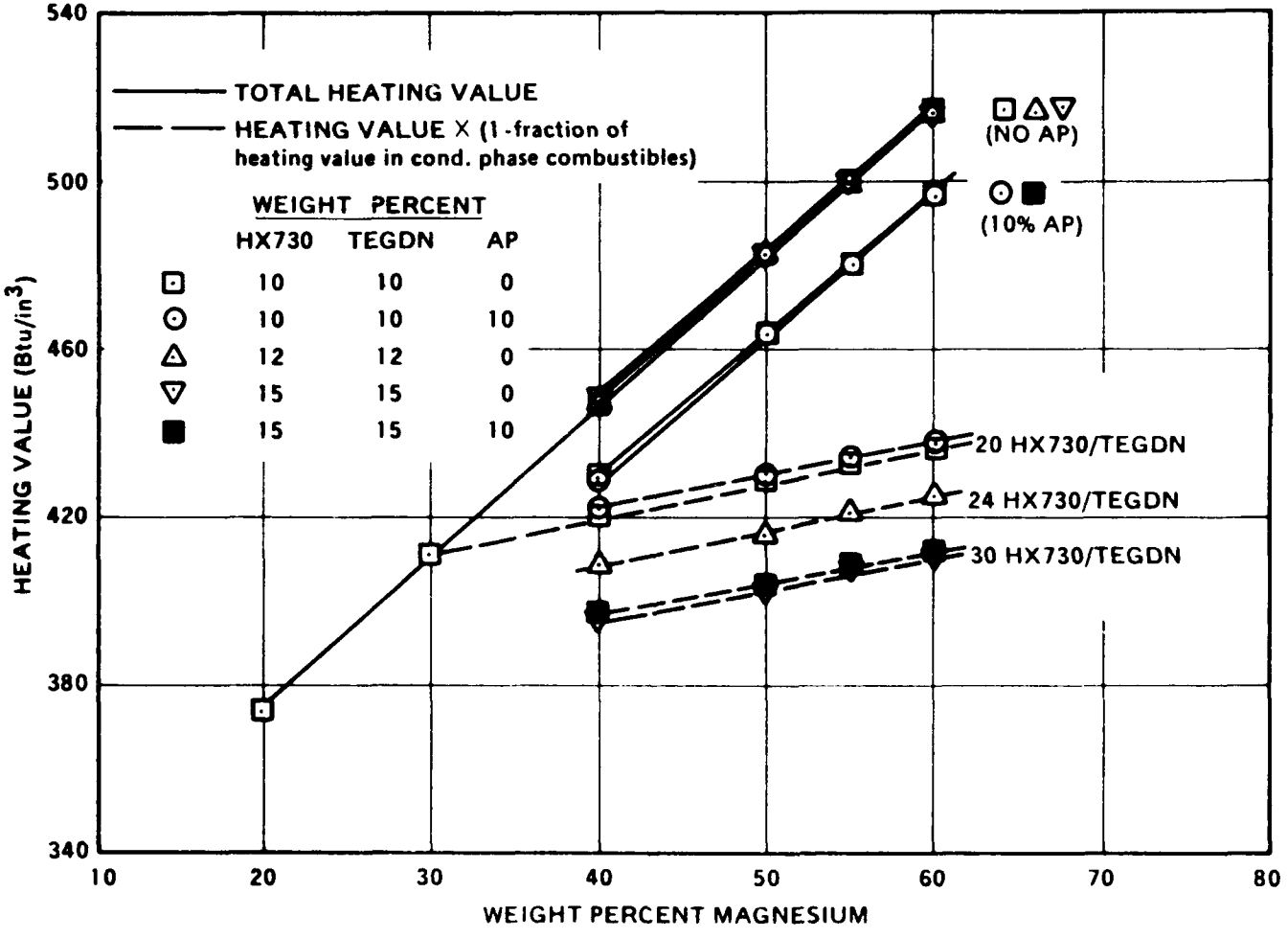

FIGURE 9. HEATING VALUES VERSUS MAGNESIUM LOADINGS FOR HX730/TEGDN/HMX-AP/MAGNESIUM SYSTEMS

74-612-6

heating value minus the heating value tied up in condensed-phase combustibles leaving the primary motor), on the other hand, decreases with increasing binder content (increased carbon), and is essentially independent of replacement of HMX with AP. Primary motor flame temperatures for all cases examined were in excess of 2400°K. As may be seen, total heating values of 500 to 520 BTU/in^3 and reduced heating values of 430 to 440 BTU/in^3 may be obtained with this type of system at 60 to 65% magnesium loading.

A large number of thermodynamic calculations have been performed for the HTPB/HMX/AP/Mg system; only a brief summary of these will be presented here. Among the variables examined were percent binder, the effect of interchange of the HMX and AP oxidizers, and magnesium loading. Typical results are plotted in Figures 10 and 11. Two binder levels, 10% and 15%, representing the probable range of minimum level giving acceptable propellant processing characteristics were examined. As may be seen from Figure 10, the volumetric heating value versus primary motor flame temperature characteristics are nearly identical for the two binder levels; however, the higher binder level does result in approximately 5 percent more of the heating value being tied up in condensed-phase combustibles at any given total heating value. Substitution of small amounts of AP for HMX (experimentally shown to improve propellant burning characteristics) causes a drop in flame temperature for a given heating value, chiefly because more magnesium must be used to achieve a given level of heating value when AP is substituted for HMX. (HMX is a considerably more energetic oxidizer than AP.) The bend to the right of the two curves for AP-containing systems on the right-hand side of Figure 10, is caused by the temperature dropping sufficiently in these cases to cause some condensation of magnesium, thereby tying additional potential heating value up in condensed phase products. Except for this effect, occurring only at the higher heating values, the substitution of AP has very little effect on the percent heating value contained in condensed-phase combustibles at a given total heating value. As may be seen, increasing the magnesium loading increases both the theoretical volumetric heating value and the percent of that value which is tied up in condensed-phase combustibles. However, primary motor temperature is nearly

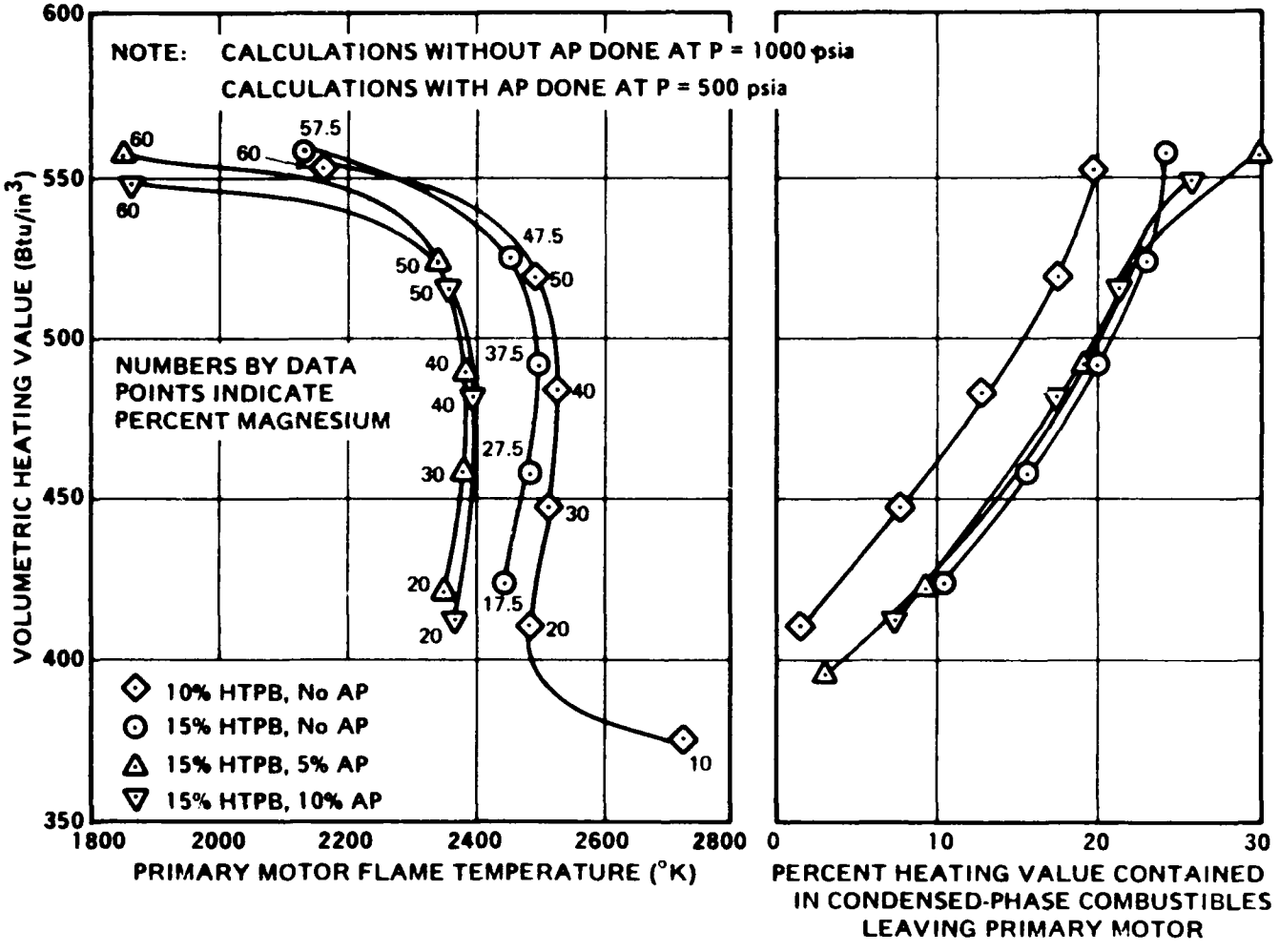

74-612-10

FIGURE 10. THERMODYNAMIC CALCULATIONS FOR HTPB/HMX/AP/MAGNESIUM SYSTEMS.

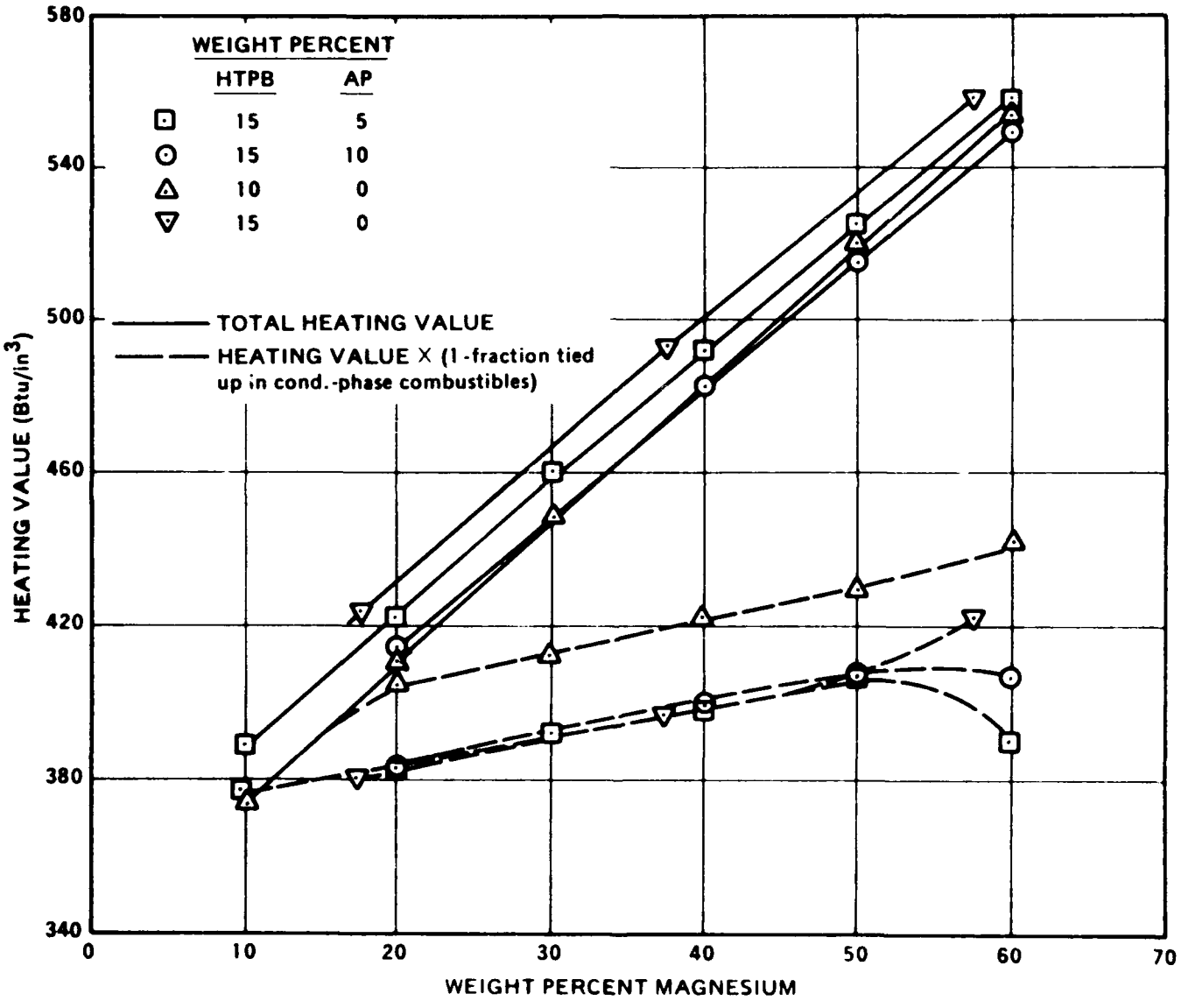

FIGURE 11. HEATING VALUES VERSUS MAGNESIUM LOADINGS FOR HTPB/ HMX-AP/MAGNESIUM SYSTEMS

independent of the magnesium loading up to about 50 to 55 percent due to the highly exothermic reaction, $Mg(g) + CO \rightarrow MgO(s) + C(s)$ - at higher loadings, the CO is exhausted and primary motor temperature decreases drastically with further increases in magnesium content. Thus it appears that the maximum practical magnesium content in this type of system (HTPB/HMX/AP/Mg) is about 60 percent. At this loading, theoretical volumetric heating values of approximately 550-560 BTU per cubic inch are attainable, with maximum reduced volumetric heating values of 420-440 BTU per cubic inch.

Results of thermochemical calculations for two mixed-metal systems (magnesium/aluminum and magnesium/boron) are presented in Figures 12 and 13. Boron and aluminum both have higher heating values than magnesium (10636 BTU/lb for magnesium, 13361 BTU/lb for aluminum, and 23,900 for boron) - however, both are ejected into the afterburner as relatively hard to burn particles. In Figure 12, heating value and reduced heating value are plotted against total metal loading for 15% HTPB binder formulations with HMX oxidizer for all-magnesium, 5/1 magnesium/aluminum, and 1/1 magnesium/aluminum cases. As might be expected, the theoretical heating values increase with substitution of aluminum for magnesium; however, it may also be noted that the maximum obtainable reduced volumetric heating values are essentially independent of Magnesium/Aluminum ratio. With boron/magnesium mixed metal systems, the picture is similar except the reduced heating value actually decreases monotonically with substitution of boron for magnesium.

A summary of maximum volumetric heating values obtainable with each of the castable systems examined is presented as Table 5. With the exception of the mixed-metal systems, the various systems examined give similar maxima, 520 to 550 BTU/in^3 for total volumetric heating value and 430 to 470 BTU/in^3 for reduced volumetric heating value. In terms of total heating value, the HTPB/HMX-AP Magnesium system appears best, while the NC/NG/ADN/Magnesium system yields the highest reduced volumetric heating value. The mixed metal systems permit attainment of higher total volumetric heating values, but at the expense of increasing percentages of the heating value being tied up in condensed-phase combustibles (which are relatively

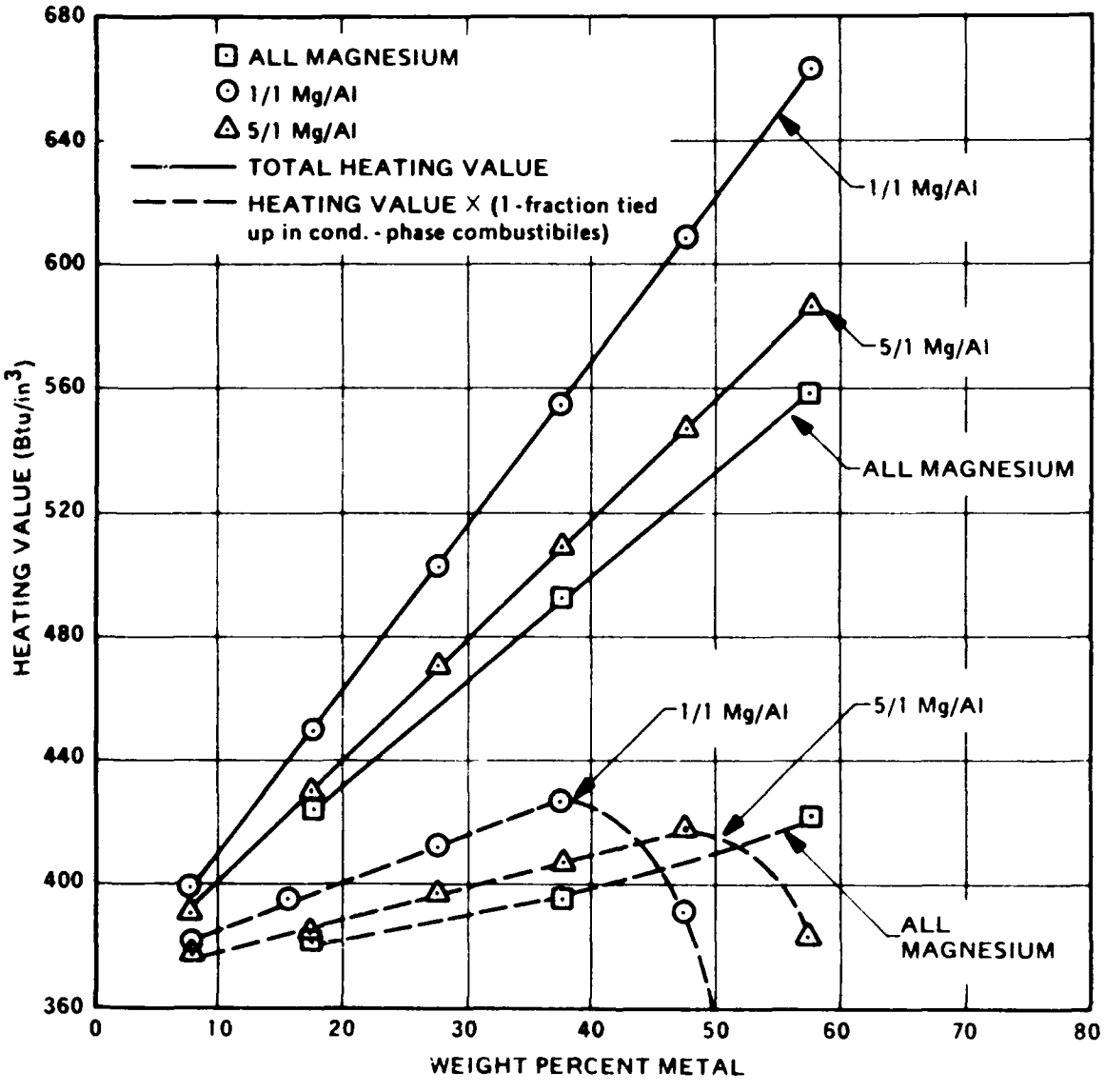

74-612-13

FIGURE 12. HEATING VALUES VERSUS METAL LOADINGS FOR HTPB/HMX/MAGNESIUM/ALUMINUM SYSTEMS.

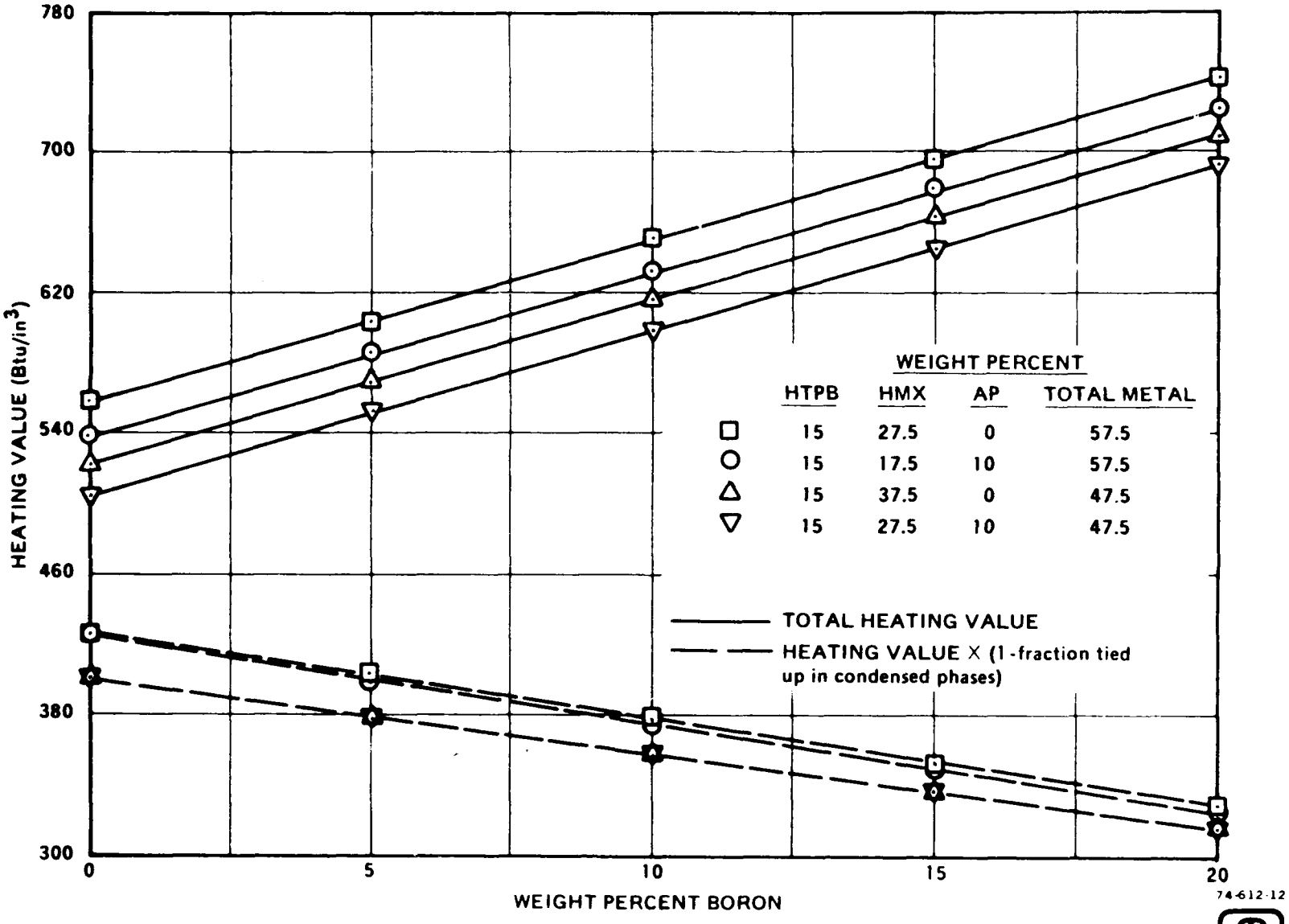

FIGURE 13. HEATING VALUES VERSUS BORON LOADINGS FOR HTPB/HMX-AP/ MAGNESIUM/BORON SYSTEMS

TABLE 5. MAXIMUM VOLUMETRIC HEATING VALUES OBTAINABLE WITH CASTABLE MAGNESIUM SYSTEMS EXAMINED

SYSTEM	MAXIMUM VOLUMETRIC HEATING VALUE (Btu/in^3)	MAXIMUM [VOLUMETRIC H.V. × (1 - FRACTION TIED UP IN COND. PHASE COMBUSTIBLES)] (Btu/in^3)
NC/PEG400/Mg	~ 540	~ 430
HX730/TEGDN/AP/Mg	$\gtrsim$ 520	$\gtrsim$ 440
NC/DOA/AP/Mg	~ 520	~ 430
NC/NG/ADN/Mg	$\gtrsim$ 520	$\gtrsim$ 470
HTPB/HMX-AP/Mg	~ 550	~ 440
HTPB/HMX-AP/Mg/B	~ 740	~ 430 (at zero percent Boron)
HTPB/HMX/Mg/Al	~ 660	~ 430 (at total heating value of $\leq$550)

74-612-14

hard to burn) entering the afterburner. The tradeoff for optimum delivered performance is obviously a function of the severity of the afterburner environment, with maximum total heating value being desired for afterburner operating conditions conducive to complete burning of condensed-phase materials and maximum reduced heating value being desired for conditions where condensed-phase combustibles cannot be ignited and burned.

3. Pressed Compositions

Similar thermodynamic screening calculations were carried out for a large number of potential pressed composition systems:

(1) $Pb(NO_3)$ - Mg - $(CH_2)_n$

(2) $Ca(NO_3)_2$ - Mg - $(CH_2)_n$

(3) $Sr(NO_3)_2$ - Mg - $(CH_2)_n$

(4) $Ba(NO_3)_2$ - Mg - $(CH_2)_n$

(5) KNO_3 - Mg - $(CH_2)_n$

(6) $NaNO_3$ - Mg - $(CH_2)_n$

(7) NH_4NO_3 - Mg - $(CH_2)_n$

(8) Oxalic Acid - Mg

(9) Tartaric Acid - Mg

(10) Sucrose - Mg

(11) AP - Mg - $(CH_2)_n$

(12) HMX - Mg - $(CH_2)_n$

(13) $(NF_4)_2SiF_6$ - Mg - $(CH_2)_n$

(14) NF_4BF_4 - Mg - $(CH_2)_n$

(15) NF_4ASF_6 - Mg - $(CH_2)_n$

(16) Teflon - Mg - $(CH_2)_n$

(17) Delrin - Mg

(18) Polyvinylidene Fluoride - Mg

(19) XXX - Mg - $(CH_2)_n$ XXX = Proprietary ARC Oxidizer

(20) XXX - Mg - Al - $(CH_2)_n$

Within each system containing $(CH_2)_n$ as a pressing aid, levels of this ingredient from 1 to 5 weight percent were examined. At each level, magnesium content was varied over a considerable range, representing a wide variation in fuel/oxidizer ratio. Detailed results of all of these calculations will not be presented herein: rather, detailed results for a few typical systems will be presented and discussed, and results for the other systems will then be summarized.

Detailed results for the Mg - Teflon - 5%$(CH_2)_n$, Mg - Teflon - 1%$(CH_2)_n$, Mg - Polyvinylidene Fluoride, and Mg-Delrin systems are presented in Figures 14 - 17. In Figure 14, volumetric heating value is plotted against primary motor flame temperature, with the percent metal loading for each point designated. As metal loading is increased, in each case, flame temperature decreases while volumetric heating value increases. It is particularly interesting to note the shapes of the curves with the existence of regions where volumetric heating value increases very slowly with large decreases in flame temperature, separated by a region where volumetric heating value increases sharply with only a small sacrifice in flame temperature. Using this criteria alone, it would seem that the most promising composition from these systems would be those at the top of the sharply rising parts of the curves. Thus, for the four systems, in the order listed above, it would appear that the optimal magnesium loadings would be about 60 to 65%, 65 to 70%, 60% and 60%.

Since pressed composition of these types tend to be poor in terms of gas production, and since gas production is needed to break up clinkers and give efficient propellant ejection from a motor, plots of volumetric heating value versus moles of gas produced per 100 grams of propellant, as plotted in Figure 15, are also of interest. As may be seen, there is, in general, an optimum metal loading in terms of gas production,

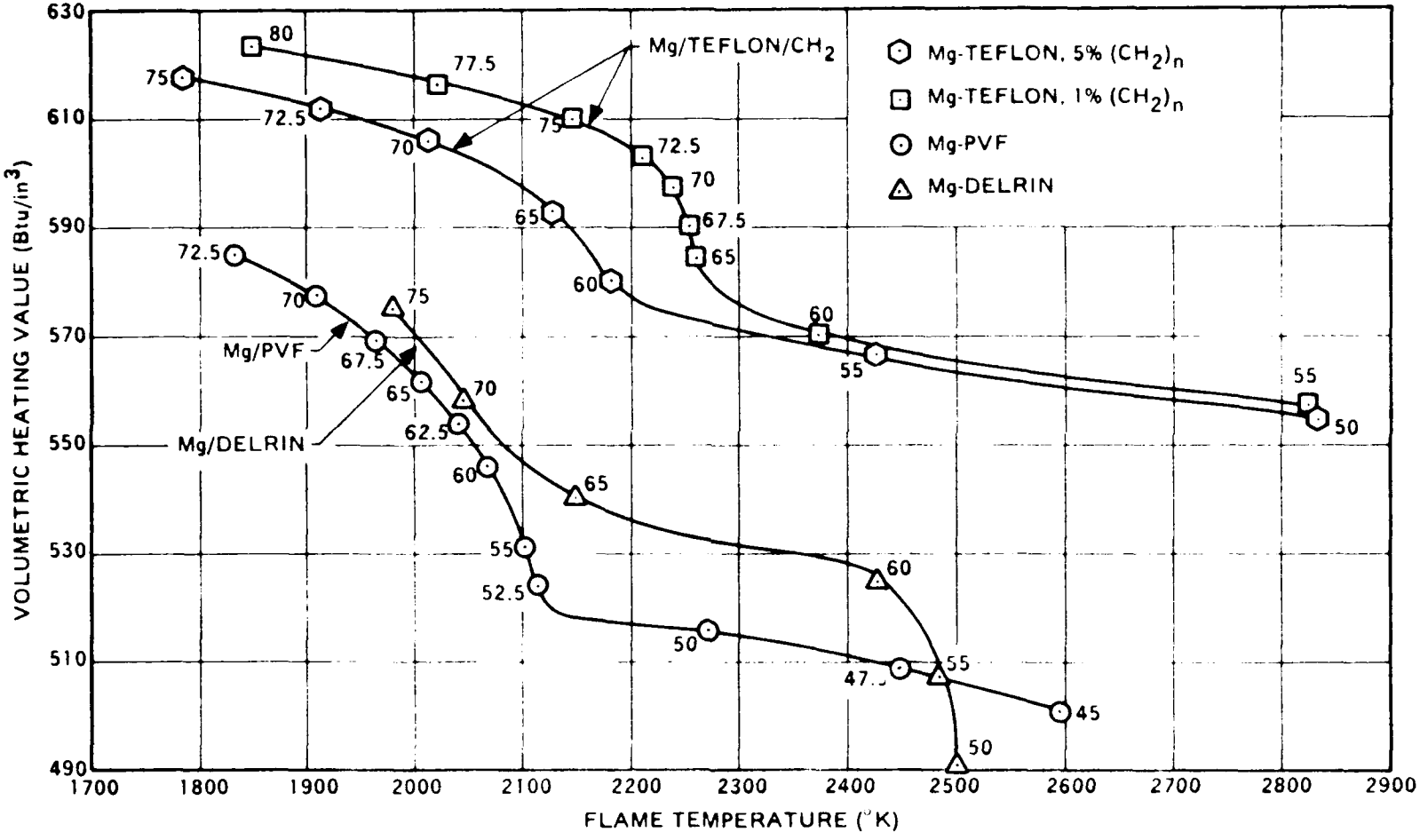

Figure 14. Volumetric Heating Value Versus Flame Temperature for Four Potential Pressed Composition Systems

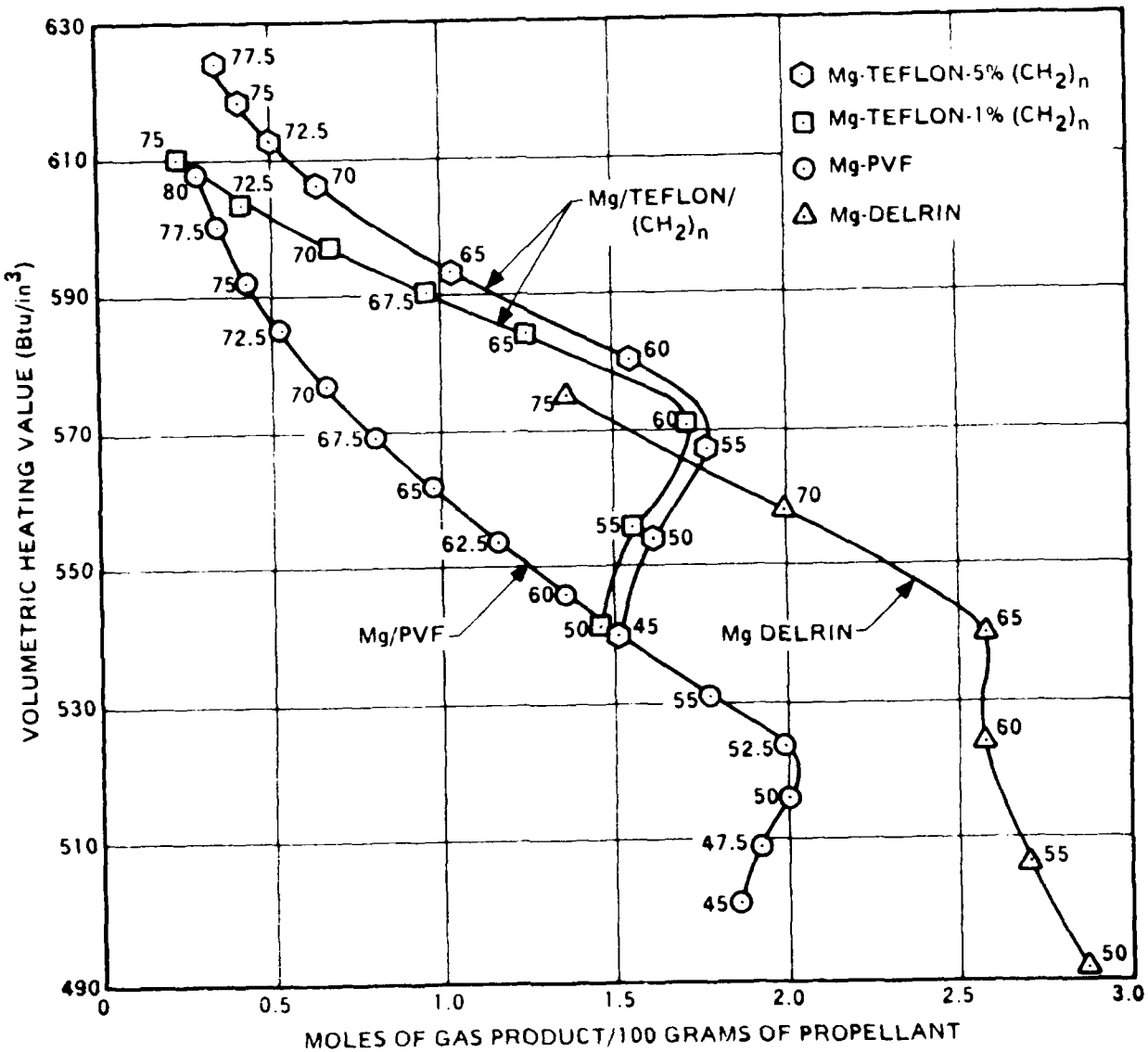

Figure 15. Volumetric Heating Value Versus Moles of Gas/100 Grams of Propellant for Four Potential Pressed Composition Systems.

with gas production dropping rapidly with further increases in metal loading (accompanied by only modest increase in heating value). On this basis, the optimum magnesium loadings for the four systems, in the order listed above, are about 55 to 60%, 60 to 65%, 52.5 to 55% and 65%.

In Figure 16, volumetric heating value is plotted against percent heating value in condensed-phase combustible primary motor products for the same four systems. Again, knees appear in the curves indicating optimal metal loadings based on balancing off the benefit of increased heating value with increasing metal loading against less ready availability of that heating value with increased metal loading. Based upon this criterion, the optimal metal loadings for the four systems in the same order, appear to be about 55 to 60%, 60 to 65%, 52.5 to 55%, and 65%.

Thus, it appears that selection of optimal metal loadings for these systems on the basis of the three criteria discussed above lead to fairly similar conclusions. The optimal metal loadings are:

System	Optimal Metal Loading (Wt%)
Mg - Teflon - 5% $(CH_2)_n$	~60%
Mg - Teflon - 1% $(CH_2)_n$	~65%
Mg - Polyvinylidene Fluoride	~55%
Mg - Delrin	~60%

In Figure 17, total and reduced volumetric heating value are plotted against percent magnesium loading for each of the four systems discussed above. For each system, total volumetric heating value increases monotonically with metal loading over the range examined, as one would expect. The reduced volumetric heating value curves, however, show maxima occurring at metal loadings approximately 3 to 4% below those listed above as optimal on the basis of the criteria previously discussed. This slight offset is not unexpected, since the optimal metal loading should not be that at which the reduced volumetric heating value maximizes, but instead some higher value at which its decay with further increase in metal loading has not become very large.

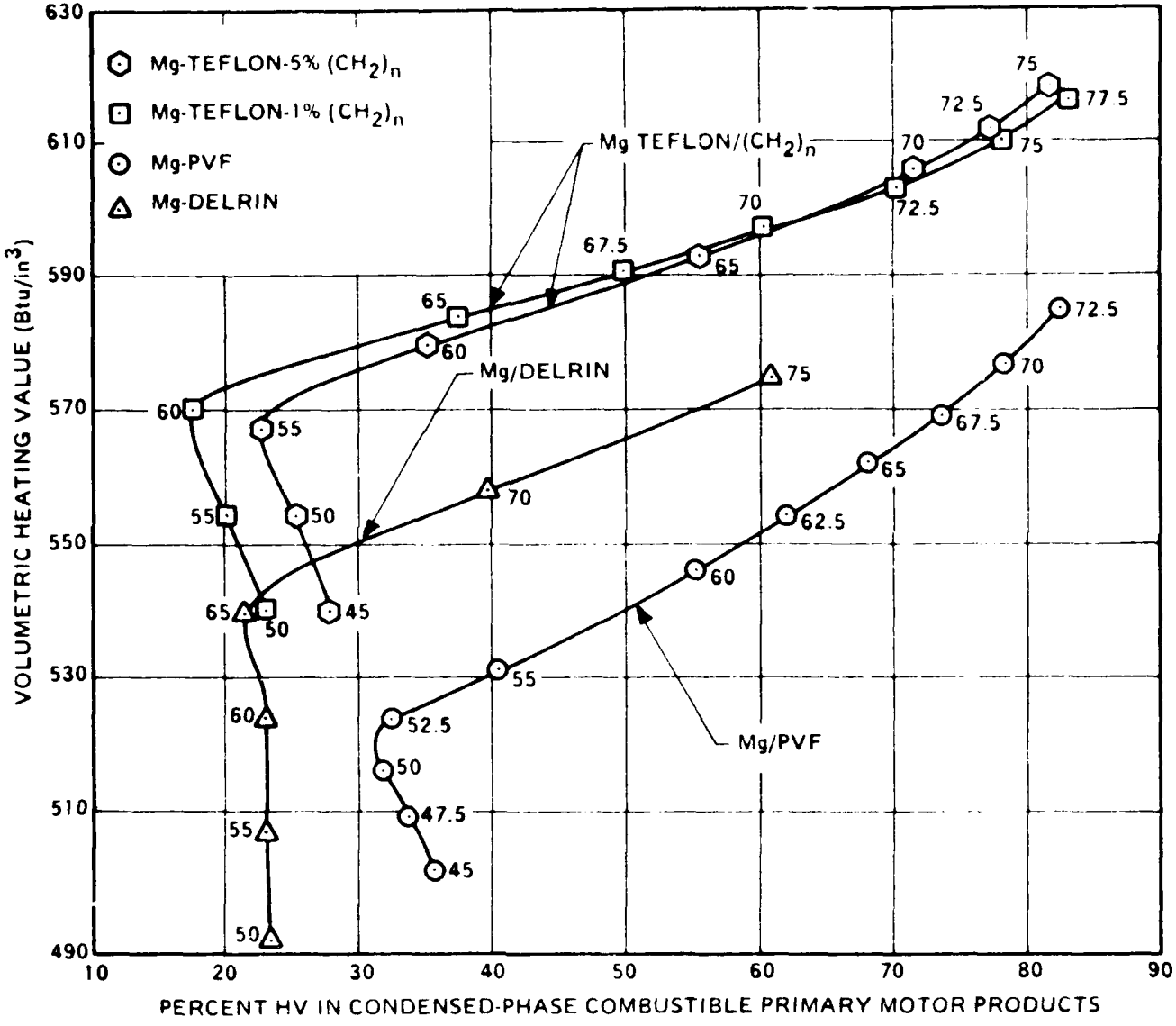

Figure 16. Volumetric Heating Value Versus Percent Heating Value in Condensed-Phase Primary Motor Products for Four Potential Pressed Compositions.

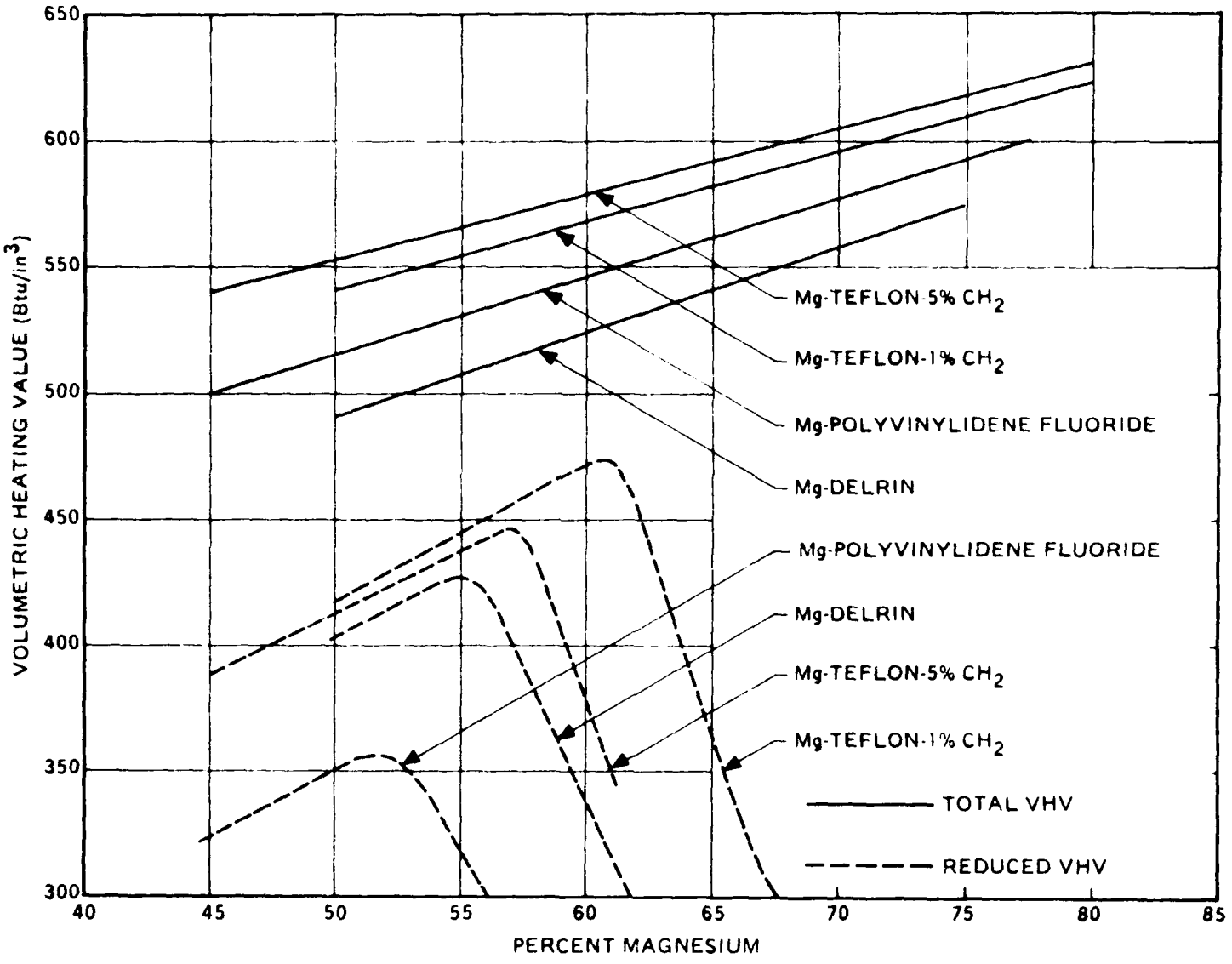

Figure 17. Volumetric Heating Value Versus Metal Loading for Four Possible Pressed Magnesium Composition Systems

The other systems studied in this screening effort showed similar characteristics in general and will not be discussed in detail.

A summary of results for 17 of the pressed composition systems examined, in terms of Total Volumetric Heating Value and Reduced Volumetric Heating Value versus Metal Loading are presented in Figures 18 and 19. (Three of the nitrate systems are not included due to their similarity to the sodium nitrate, potassium nitrate, and ammonium nitrate systems.) Since minimizing use of the pressing aid, $(CH_2)_n$, was found to give optimal results thermodynamically (as shown in Figure 17), only results for the 1% level of this ingredient are shown. In the only system containing mixed metals (magnesium and aluminum) results are presented only for the 10% aluminum level. Table 6 gives a summary of optimized volumetric heating values available from all of the pressed compositions thermodynamically screened. The systems containing the proprietary AKC oxidizer (XXX) are clearly superior in terms of total heating value and, with the exception of the exotic fluorine salt systems (which are not realistic candidates at this time), are also superior in terms of reduced heating value. Other systems which appear attractive include Mg/Teflon/$(CH_2)_n$ and MG/HMX/$(CH_2)_n$, both of which appear respectable in terms of both heating value parameters.

4. Candidate Formulations Selected

At the end of the thermodynamic screening phases, five castable formulations designated MK1, MK2, MK6, MK11, and MK12, and three pressed formulations designated TK1, TK2, and TK3 were selected for further evaluation. Later, when difficulty was encountered in making MK6, it was replaced by a similar formulation (but with lower solids loading) designated MK6A. Detailed compositions of these formulations are not presented here, in order that this report may be unclassified, but general characteristics are presented in Table 7. All of the formulations contain in excess of 50% metal (7 containing magnesium, 1 containing a 2/1 MG/Al alloy, and 1 containing a 5/1 Mg/Al alloy). The magnesium systems have volumetric heating values of 490 to 570 BTU/in^3, with reduced volumetric heating values

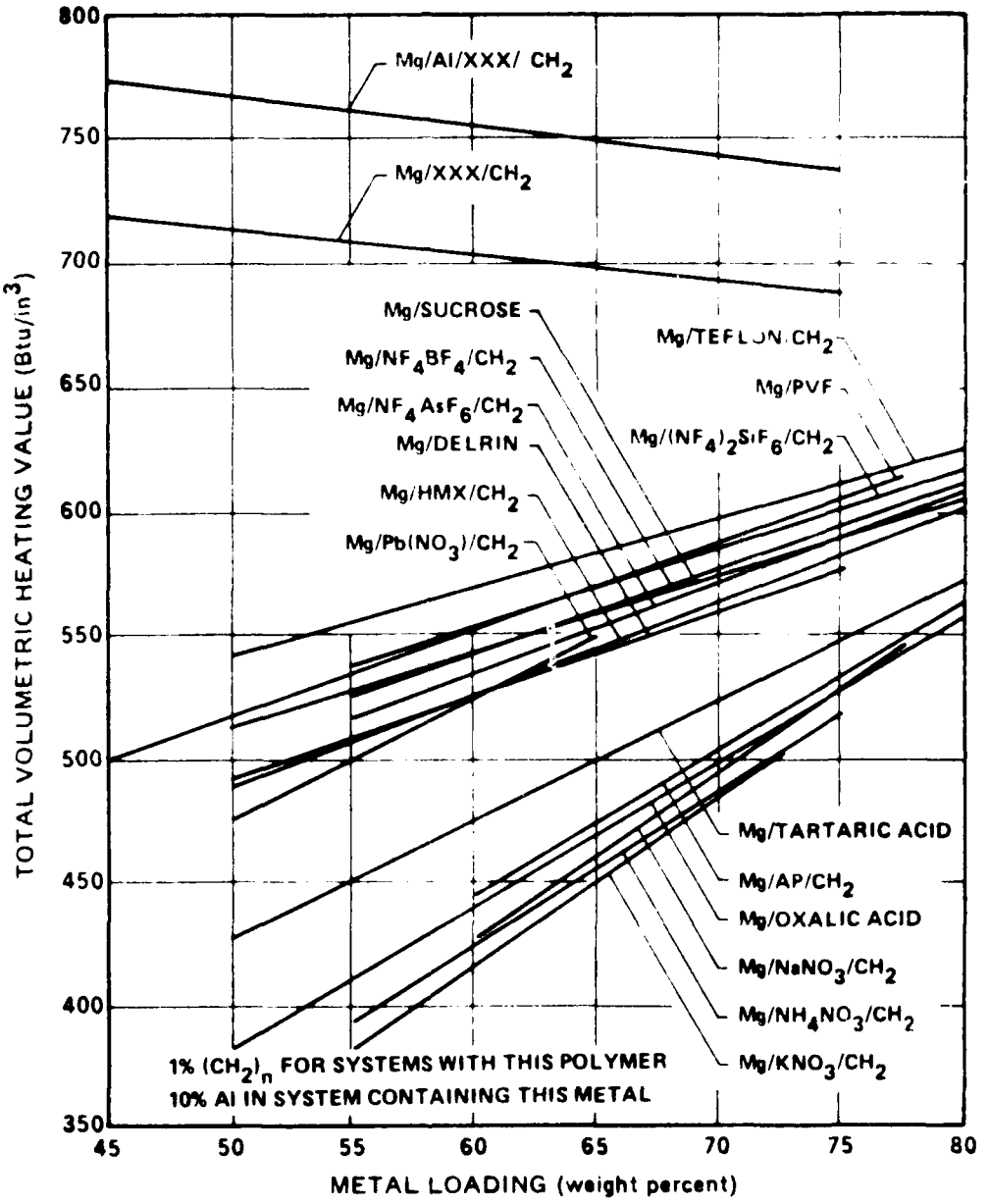

Figure 18. Total Volumetric Heating Value Versus Metal Loading for Various Candidate Pressed Propellant Systems

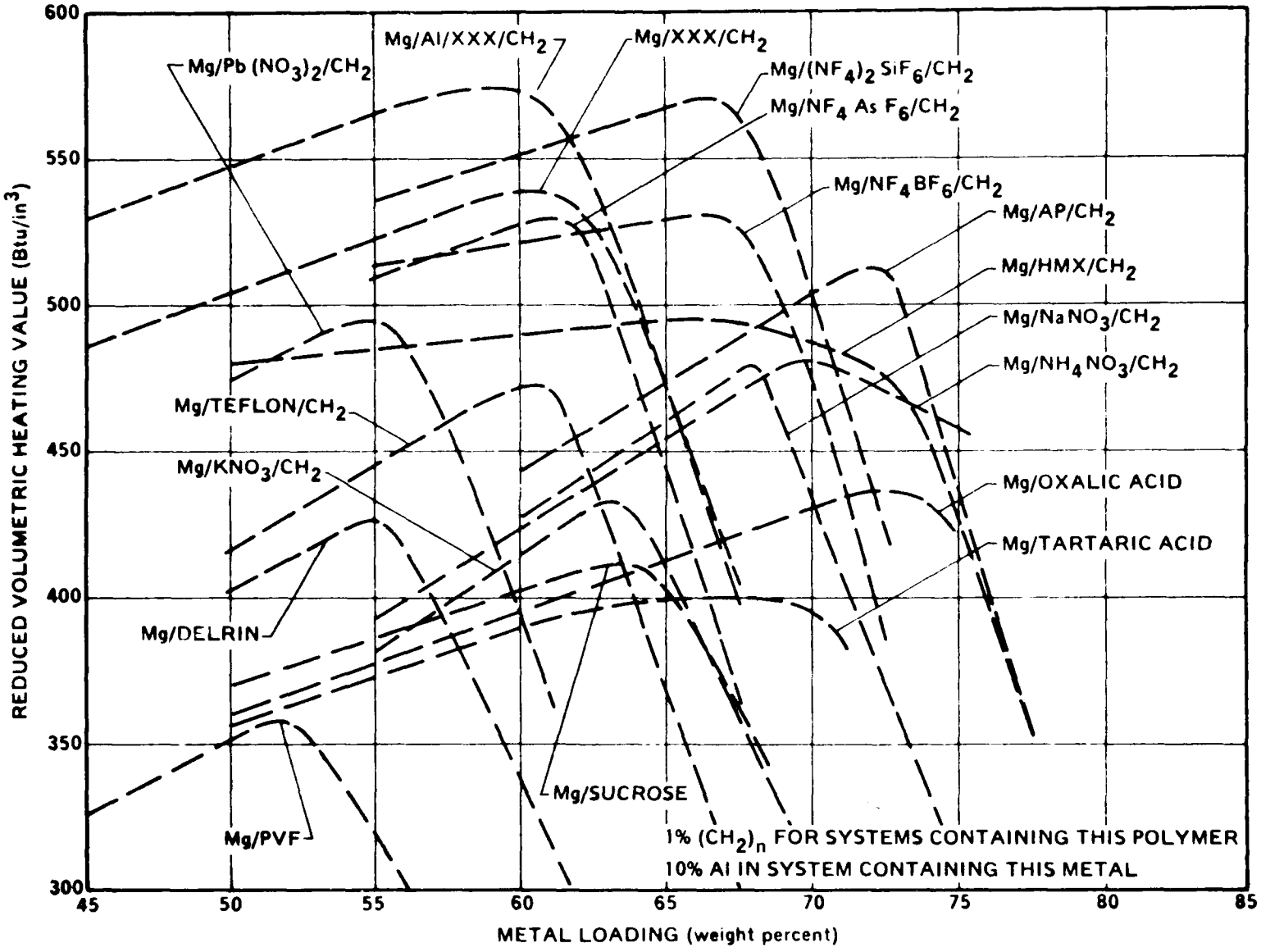

Figure 19. Reduced Volumetric Heating Value Versus Metal Loading for Various Candidate Pressed Propellant Systems

TABLE 6. OPTIMIZED VOLUMETRIC HEATING VALUES OUT OF VARIOUS POSSIBLE MAGNESIUM PRESSED COMPOSITIONS

SYSTEM	MAXIMUM REDUCED VHV (Btu/in^3)	CORRESPONDING TOTAL VHV (Btu/in^3)	APPROXIMATE MAXIMUM TOTAL VHV BEFORE BREAK IN REDUCED VHV, TEMPERATURE, AND MOLS GAS/100 gms VERSUS METAL LOADING CURVES	Gm-MOLS OF GAS PER 100 gms OF PROPELLANT
$Mg/CH_2/Pb(NO_3)_2$	497	501	~520	1.8-1.9
$Mg/CH_2/Ca(NO_3)_2$	480	487	~500	2.1-2.3
$Mg/CH_2/Sr(NO_3)_2$	475	482	~500	1.9-2.1
$Mg/CH_2/Ba(NO_3)_2$	447	460	~490	1.7-1.9
$Mg/CH_2/KNO_3$	435	438	~455	1.9-2.1
$Mg/CH_2/NaNO_3$	477	480	~490	2.2-2.4
$Mg/CH_2/NH_4NO_3$	480	490	~520	2.9-3.1
Mg/OXALIC ACID	440	515	~515	1.9-2.0
Mg/TARTARIC ACID	400	510	~510	2.0
Mg/SUCROSE	415	550	~550	2.4
$Mg/CH_2/AP$	513	520	~530	2.7-2.9
$Mg/CH_2/HMX$	497	550	~560	2.7-3.0
$Mg/CH_2/(NF_4)_2SiF_6$	571	573	~575	2.1-2.2
$Mg/CH_2/NF_4BF_4$	530	565	~570	2.0-2.1
$Mg/CH_2/NF_4A_5F_6$	530	540	~545	2.0
Mg/CH_2/TEFLON	474	572	~575	1.7-1.8
Mg/DELRIN	430	508	~510	2.6
Mg/POLYVINYLIDENE FLUORIDE	357	520	~525	2.0
Mg/CH_2/XXX	542	700	~700	1.9-2.0
$Mg/Al/CH_2$/XXX	574	752	~755	2.0-2.1

TABLE 7. CANDIDATE COMPOSITIONS SELECTED FOR FURTHER EVALUATION*

Designation	Metal[a]	Binder	Oxidizer	Heating Value (Btu/lb)	Heating Value (Btu/in^3)	Reduced Volumetric Heating Value (Btu/in^3)	Flame Temperature (°k)
MK 1	Mg	HTPB	AP	8700	496	413	2450
MK 2	Mg	HTPB	AP/HMX	9055	516	407	2453
MK 6	Mg	LACQUER-GRADE NC	HMX	8300	514	477	2514
MK 11	Mg	NITRO-PLASTICIZED POLYESTER	HMX	8520	506	435	2491
MK 12	Mg/Al(2/1)	HTPB	HMX	9830	590	430	2534
TK 1	Mg/Al(5/1)	$(CH_2)_n$[b]	XXX[d]	10114	751	558	2398
TK 2	Mg	$(CH_2)_n$[b]	HMX	8640	549	488	2345
TK 3	Mg	-	TEFLON	8300	572	475	2340
MK 6A[c]	Mg	LACQUER NC	HMX	8069	490	463	2560

*Detailed compositions classified - may be obtained by authorized personnel from AFOSR.

(a) All formulations contain 50% or more metal by weight.
(b) Less than 5% binder in pressed compositions.
(c) 3% less metal than MK 6, 7% less oxidizer, 10% more binder.
(d) XXX = proprietory ARC oxidizer.

of 410 to 490 BTU/in^3, while the Mg/Al alloy systems have volumetric heating values of 590 to 750 BTU/in^3. All of the castable compositions have theoretical flame temperatures (for 1000 psia combustion) in excess of 2450°K, while the pressed compositions have flame temperatures of 2340 to 2400°K.

An important factor in determining whether or not condensed-phase combustibles emanating from the fuel generator (primary motor) will burn well in the afterburner is the curve of flame temperature in the absence of such burning versus air/fuel ratio, since, given a minimum temperature required for ignition of the condensed-phase combustibles, this determines over what air/fuel ratio range ignition can occur. (A small range indicates that if ignition does not occur in a very limited fraction of the afterburner volume, it will not occur at all, while a large range provides a large fraction of the afterburner volume suitable for ignition.) Such curves are presented for the original five candidate castable formulations, the three candidate pressed compositions, and a typical highly-boron-loaded formulation in Figure 20. As may be seen, the limits are considerably broader for the magnesium-loaded formulations. For example, if a 2000°K temperature is required for particle ignition, this is provided only in an air/fuel ratio envelope of 2/1 to 5/1 for the boron formulation, but for all air/fuel ratios below approximately 8/1 for the magnesium systems (6/1 for the mixed metal system).

In Section III-A, the development of plots [Ratio of Required Flow Rate for a Candidate Formulation to Required Flow Rate for a State-of-the-Art Boron Formulation] was discussed. As stated there, under the highly simplified anlaysis used, this procedure basically involves fixing air flow rate and then calculating the air/fuel ratios for the formulations being compared which will yield the same air vacuum sonic specific impulse (S_A) values for the two fuels. Results of such calculations with MK1, MK2, MK12, TK1, TK2, and TK3 as the candidate fuels are plotted in Figure 21 (Mass Flow Rate Ratio) and Figure 22 (Volume Flow Rate Ratio). (Calculations for MK6, MK6A and MK11 are not included, since they had been dropped by the time this analysis was performed.) As indicated on the figures, high

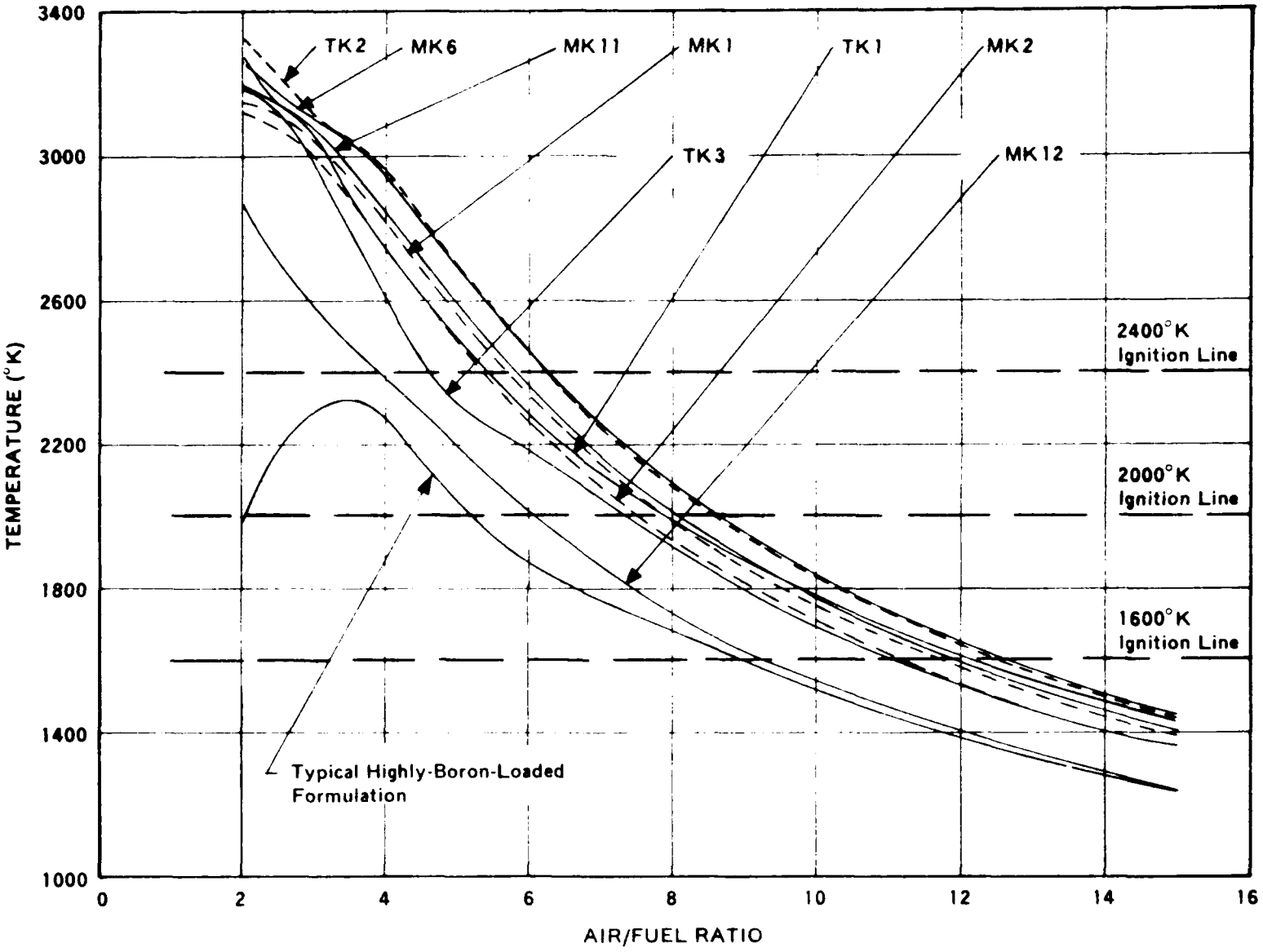

Figure 20. Flame Temperature Versus Air/Fuel Ratio With Condensed-Phase Combustibles from Primary Not Burning (500°K Air) 100 psi.

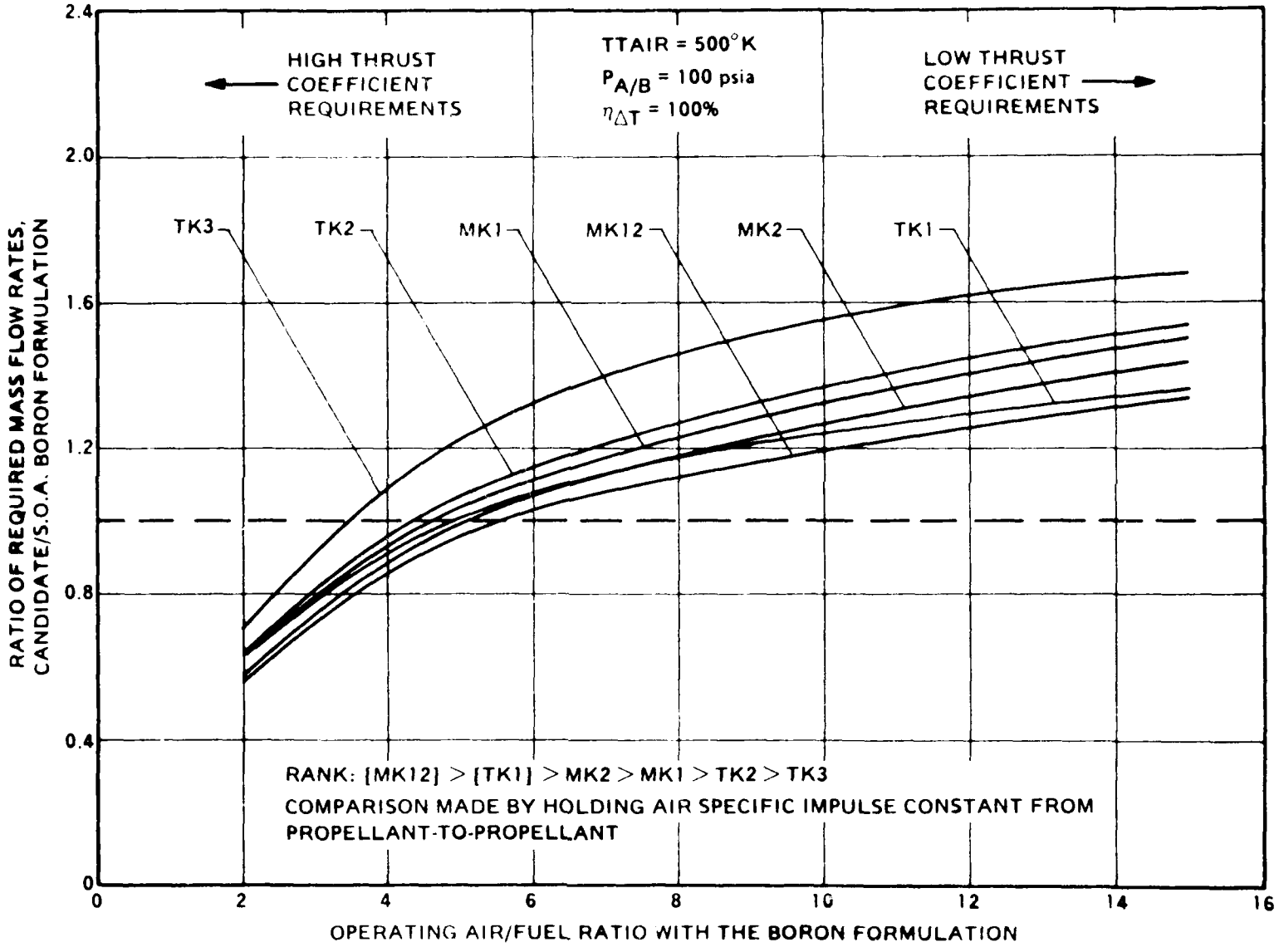

Figure 21. Comparison of Fuel Flow (Mass) Requirements for Given Operating Design Point for Candidiate Formulations versus S.O.A. Boron Formulation

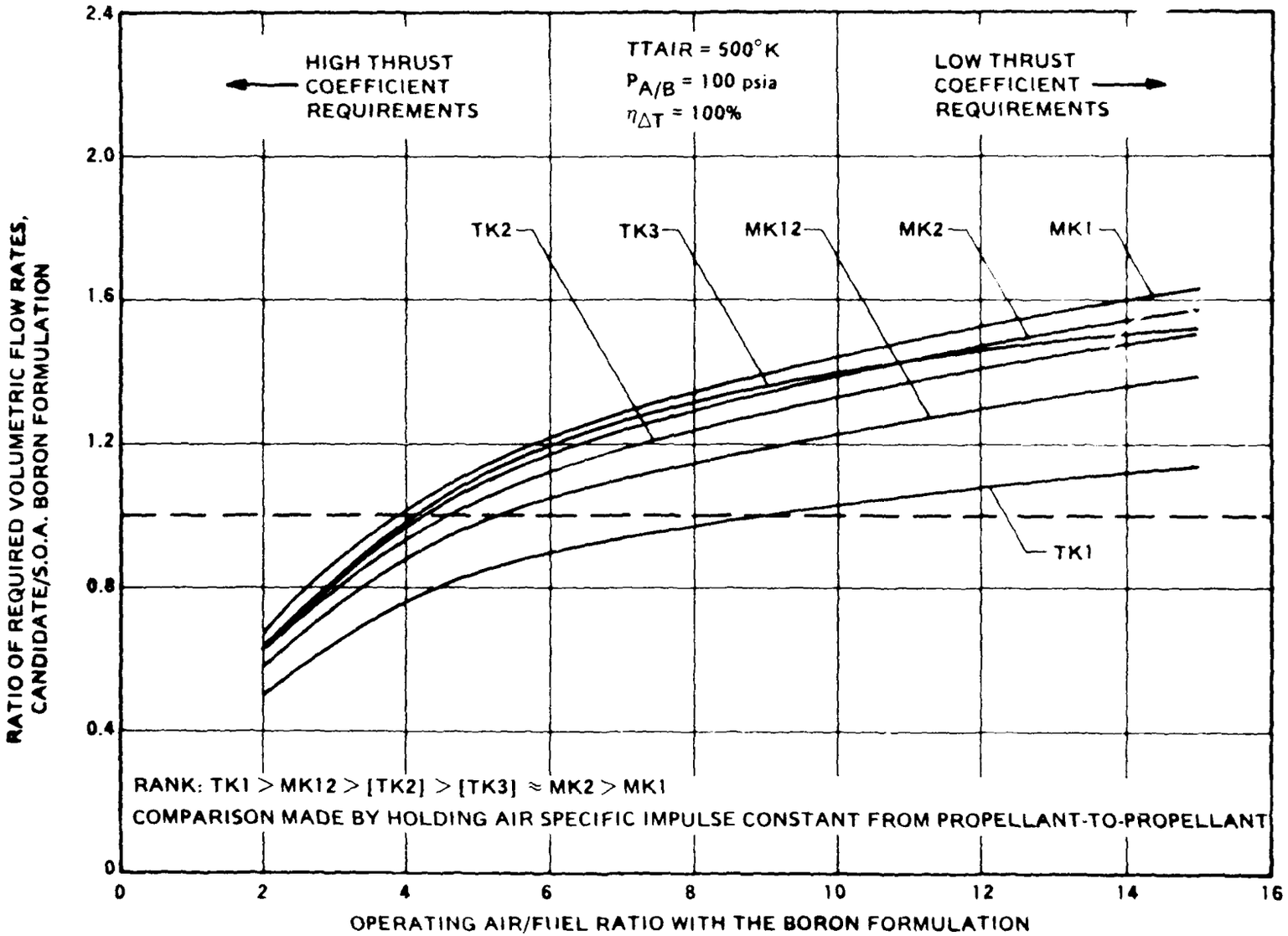

Figure 22. Comparison of Fuel Flow Volumetric Requirements for Given Operating Design Point for Candidate Formulations Versus S.O.A. Boron Formulation

values of the abscissa are indicative of missions with low thrust coefficient requirements while low values are indicative of missions with high thrust coefficient requirements. Straightfoward reasoning indicates that lower lying curves represent more favorable fuels. Thus, as indicated in the figures, for weight-limited systems the candidates rank (in the low air/fuel ratio range of most interest) in the order [MK12] > [TK1] > [MK2] > [MK1] > [TK2] > [TK3], while for the volume-limited systems the rank is [TK1] > [MK12] > [TK2] > [TK3] ≳ [MK2] > [MK1]. As might be expected, this result is essentially in line with the rankings in terms of mass and volumetric heating values, the only exceptions disappearing at high air/fuel ratios (where heating values have more meaning) as curves cross in each figure. As pointed out earlier, for all operating points to the left of the intersection of the curve for a given formulation with the ordinate value of 1.0, the candidate formulation is theoretically superior to the state-of-the-art boron formulation used for comparison.

C. PROPELLANT FORMULATION AND CHARACTERIZATION

1. Preliminary Formulation Work on Magnesium-Loaded Castable Fuel-Rich Composite Propellants (Feasibility Assessment)

Until recent years, the "work horse" binders for composite propellants have been butadiene polymers with carboxyl functionality which have been crosslinked with epoxy and/or imine curing agents. Unlike Al, which has a protective oxide surface, the Mg surface is very reactive. MgO also crosslinks carboxyl groups. It is therefore necessary to passivate or chemically alter Mg powder before it can be incorporated in a carboxyl polymer. This problem was encountered in a previous propellant development effort under an AFRPL program involving development of high boron-loaded fuel-rich propellants. Mg was desired as an additive to improve the boron combustion in the afterburner. However, addition of Mg to the propellant consistently resulted in crosslinking (gelling) of the binder during mixing prior to curing agent addition. Passivation treatments were helpful, but the problem was not solved. Success was attained, however, in using a 65/35 Mg/Al alloy powder which was passivated. Hydroxyl polymers were not evaluated because of boron incompatibility with the cure system.

A series of small mixes was made to assess the extent of the compatibility problem. These are summarized in Table 8. These results point out the serious incompatibility problem between Mg powder and carboxyl polymers. Both polymers evaluated were crosslinked without curing agent, and they gassed badly. On the other hand, hydroxyl polymers did not show this problem, indicating that magnesium-loaded castable formulations could be made with hydroxyl-containing polymers cured with diisocyanate.

As part of this phase of the program, aimed mainly at assessing the feasibility of making castable magnesium-loaded fuel-rich propellants (and carried out before completion of the thermodynamic screening effort described earlier), five processable castable magnesium-loaded fuel-rich propellants were successfully formulated, with magnesium content up to 37.5%. (See Figure 23 for compositions.) The highest magnesium-loaded formulation, designated MFR118 has a theoretical heating value of 8600 BTU/lb or 492 BTU/in^3. Attempts to produce formulations with only 10% binder were unsuccessful; it appears that the lower limit on binder content is 12 or 13%. An attempt was also made to formulate a 15/35/50 HTPB/HMX/Mg propellant. This effort was unsuccessful in that the propellant would not process and gassed badly. It was subsequently found that use of a different cross-linking agent eliminated the gassing problem. Use of spherical HMX in place of the rough crystalline material used in this first effort, and better selection of and control over HMX and Mg particle sizes, solved the processing problem, as evidenced by results described in the next section. In addition to the castable formulation work, dry-packed mixes of 10/80/10, 10/60/30, and 10/40/50 HTPB/HMX/Mg compositions were made for preliminary combustion studies.

None of the above formulations would sustain combustion under nitrogen at one atmosphere, although all burned reasonably well at higher pressures. Substitution of 5 to 10% AP for HMX was found to greatly improve the combustion characteristics of these formulations. The formulations were very "dirty" burners, producing heavy clouds of soot, but they did burn completely, leaving essentially no residue (an important consideration as discussed earlier). The large quantity of soot ejected caused

TABLE 8. SUMMARY OF PRELIMINARY FORMULATION WORK TO DEFINE SUITABLE MAGNESIUM-LOADED COMPOSITE PROPELLANT SYSTEMS

POLYMER[a]	CURING AGENT	AP	RESULTS
HC-434	NONE	NONE	RAPID VISCOSITY INCREASE. TACKY CURE, BAD GASSING
HX-735	NONE	NONE	RAPID VISCOSITY INCREASE. HARD CURE, BAD GASSING
HX-735	NONE	20 μ	RAPID VISCOSITY INCREASE. HARD CURE, BAD GASSING
R-45M	NONE	NONE	NEGLIGIBLE CHANGE TWO HOURS, 50°C
R-45M	DIISOCYANATE	NONE	ADEQUATE POT LIFE, GOOD CURE. NO GASSING
R-45M	DIISOCYANATE	20 μ	ADEQUATE POT LIFE, GOOD CURE. NO GASSING
TELEGEN S	NONE	NONE	NEGLIGIBLE CHANGE TWO HOURS, 50°C
TELEGEN S	DIISOCYANATE	NONE	ADEQUATE POT LIFE, GOOD CURE. NO GASSING
TELEGEN S	DIISOCYANATE	20 μ	ADEQUATE POT LIFE, GOOD CURE. NO GASSING

[a]HC-434 – CARBOXY TERMINATED POLYBUTADIENE
R-45M – HYDROXY TERMINATED POLYBUTADIENE
TELEGEN S – HYDROXY TERMINATED SATURATED HYDROCARBON
HX-735 – CARBOXY TERMINATED POLYESTER

Designations	Weight Percent HTPB	HMX	Mg	Burning Rate Exponent	r_{1000} (in/sec)
◇ - MFR 114	27	63	10	0.17	0.13
○ - MFR 115	24	56	20	0.38	0.23
△ - MFR 116	21	49	30	0.68	0.38
▽ - MFR 117	15	57.5	27.5	0.40	0.25
□ - MFR 118	15	47.5	37.5	0.27	0.25

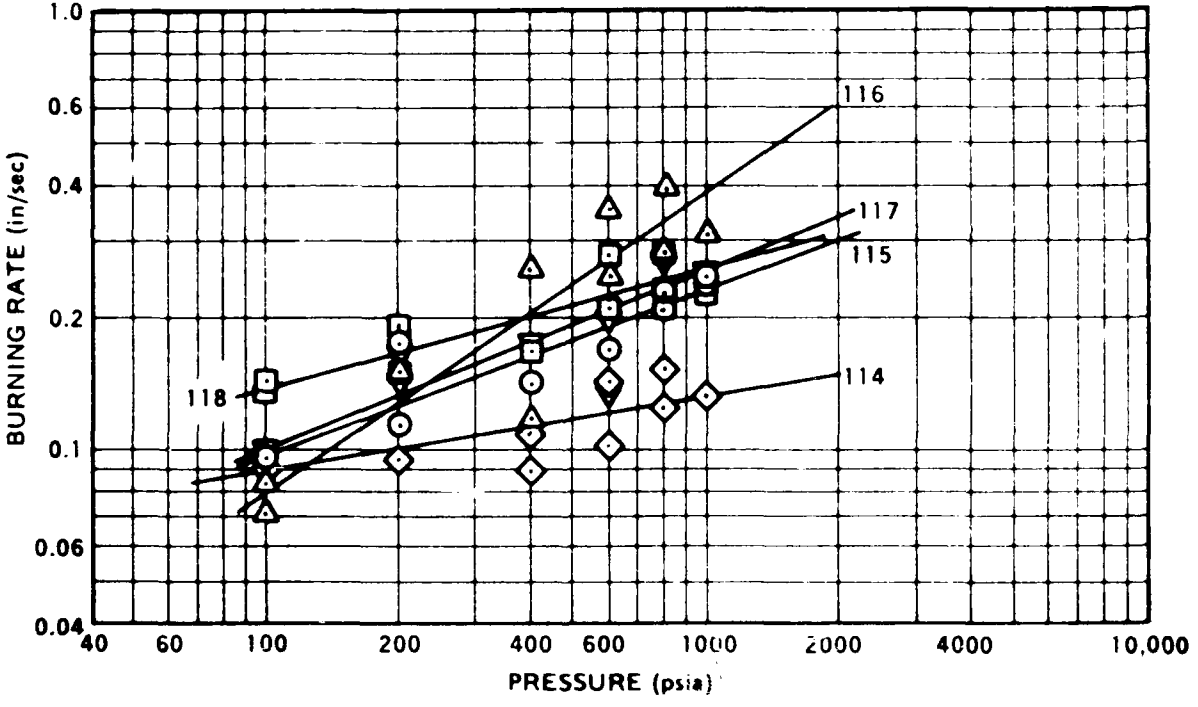

Figure 23. Burning Rate Data for Magnesium-Loaded Fuel-Rich HTPB formulations Made During Preliminary Feasibility Assessment

attempts to obtain burning rate versus pressure curves in the standard strand bomb to fail, due to shorting of the timing trip wires. Accordingly, burning rate data on the five castable formulations were obtained by visual observation of their combustion in a pressurized window bomb, with use of a stopwatch. These data are presented in Figure 23. The scatter was due to the use of the visual timing technique and not to burning irregularities. As may be seen, the burning rate exponents were reasonable, ranging from 0.2 to 0.6, and the burning rates were in the range of typical fuel-rich propellants of other types (0.13 to 0.38 inches per second at 1000 psia).

This preliminary formulation work indicated that production of magnesium-loaded fuel-rich propellants with 12 to 15% HTPB binder and up to 50 to 55% magnesium would present no insurmountable problems and was used in conjunction with the castable propellant thermodynamic screening effort described earlier in selection of the candidate formulations listed in Section III-B-4. It also indicated that for burning rate control, use of some ammonium perchlorate and/or an energetic binder would be necessary since varying HMX particle size has very little effect on burning rate.

2. Formulation of Candidate Castable Compositions Defined In Thermodynamic Screening Effort

As discussed in Section III-B-4, five castable formulations designated MK1, MK2, MK6, MK11, and MK12 were selected for further evaluation. General compositional characteristics and heating values for these formulations are given in Table 7, though detailed compositions are not given for classification reasons. Three of these formulations (MK1, MK2, and MK12) utilize the R45M HTPB binder system, but differ in fuel and oxidizer. MK2 contains both AP and HMX as oxidizers, while MK1 has no HMX and MK12 has no AP. MK12 utilizes Mg/Al (2/1) alloy rather than the pure magnesium metal used in MK1 and MK2.

The other two formulations contain energetic binders with some nitrate ester content. MK6 utilizes a high energy binder developed for smokeless propellants. It is composed of nitroglycerine, lacquer grade nitrocellulose and polyester prepolymer (R-18) crosslinked with isocyanate. The MK11 binder is less complex consisting of BTTN-plasticized polyester

cured with diisocyante. Ingredient incompatibility problems were encountered with both of these propellants, as well as with the modified formulation, MK6A. The solution of these problems will require more time and funding than were available for this program, and further effort on these formulations was eventually abandoned.

MK1, with AP oxidizer, was selected for initial formulation. This formulation was used to optimize particle size fit, to solve gassing and curing problems, and to evaluate processing aids and additives. Most of the trial mixes were made with this propellant. Once the problems were solved, formulation of the other two HTPB propellants was relatively straightforward.

Previous work had indicated that is is necessary to rigorously dry the Mg powder to eliminate gassing. Freshly dried Mg powder (under vacuum at 100°C for a minimum of 6 hours) was therefore routinely used throughout this program.

Optimizing particle size distribution was made more difficult because the spherical Mg powder was available in only 3 average particle sizes: 18, 22, and 50 micron. Formulation with 3 to 5 micron powder was not considered, because the manufacturer would ship it only under non-volatile liquid. HMX was available in only 2 sizes, Class A (large) and Class E (small). AP was available in many sizes.

The first series of MK1 mixes to optimize particle size is summarized in Table 9. The best particle size fit occurred with 50 micron Mg and 7 micron AP. All of the mixes made with IPDI exhibited some gassing. Since those with DDI did not, it was subsequently used as the curing agent. The addition of 3% Velocite plasticizer to the binder did not improve processing so its use was discontinued. Tensile properties were determined on Mix 135, which had a NCO/OH ratio of 0.8/1.0 (74 psi maximum stress, 35% strain at maximum stress and 387 psi modulus). Subsequent mixes were made at 0.9/1.0 to obtain a harder propellant.

Although the end-of-mix (EOM) viscosity of Mix 135 was only 11 KP and it had good flow properties, it was observed to have a very short

TABLE 9. FORMULATION MK1 MIXES TO OPTIMIZE PARTICLE SIZES

Mix No.	Magnesium Size	AP Size	Curing Agent	Other	EOM Viscosity (Kp)	Comments
123	18μ	200μ	IPDI	-	45, Cavitated	Gassed
124	18μ	11/4 200/20μ	IPDI	-	Dry	Discarded
125	22μ	200μ	IPDI	-	40, Cavitated	Did not cure properly
126	18μ	200μ	IPDI	3% Plasticizer	42, Cavitated	Gassed
127	7/4 18/50μ	200μ	IPDI	-	>100	Gassed
128	7/4 50/22μ	200μ	DDI	-	Hard ball	Discarded
129	50μ	7μ	DDI	-	8	1.1/1 NCO/OH, Hard, Good cure
130	22μ	3μ	DDI	-	Dry	
133	20μ	7μ	DDI	3% Plasticizer	25	0.9/1 NCO/OH
135	50μ	7μ	DDI	-	11	0.8/1 NCO/OH, Soft cure

pot life (less than 1 hour). This was attributed to the surface characteristics and impurities of Mg powder. A series of mixes was therefore made to solve this problem. These are shown in Table 10. The problem was essentially solved by changes in the R45M antioxidant in conjunction with bonding agents. Mix 170 was chosen as the final candidate Formulation MK1. It contains HX-752 bonding agent and the NCO/OH ratio was adjusted to 0.85/1 to obtain improved mechanical properties.

Because of the experience gained with formulation of MK1, only four mixes were required for formulation of MK2. The first mix made (No. 131) was processable, but had short pot life. The mixes are summarized in Table 11. Mix 171 is the final MK2 candidate, and had properties very similar to the MK1 candidate.

As with MK2, relatively few mixes were required to develop MK12, due to solution of major problems during formulation of MK1. Two differences in this formulation were noted. The Mg/Al alloy has less interaction effect with the binder, resulting in a softer cure. The absence of AP also changes curing characteristics requiring longer cure times. Table 12 presents a summary of the mixes made. Mix 172 became the candidate MK12 propellant. HX-752 bonding agent was required to get improved tensil properties, probably because of the large Class A HMX. It also exhibited yielding or dewetting to a much greater extent than the other two propellants.

The mechanical properties of the final candidate propellant formulations were included in the preceding tables. However, a comparison of the three propellants is given in Table 13. These are microbone specimens, tested at ambient at a crosshead rate of 1 in/min. JANNAF specimen data were not determined, nor were high and low temperature properties determined.

The safety and hazard characteristics of these formulations were also determined. A summary is given in Table 14. The data indicate that no extreme hazards should be involved in handling these propellants. None of the samples ignited at 6 joules, 5000 volts on the electrostatic discharge apparatus, but all emitted sparks at low joule settings. This is

TABLE 10. FORMULATION MK1 POT LIFE AND MECHANICAL PROPERTY OPTIMIZATION

Mix No.	NCO/OH	Anti-Oxidant	Bonding Agent	EQ! Viscosity (Kp)	Pot Life (Kp) 1 hr	Pot Life (Kp) 2 hrs	Gassing	Max Stress (psi)	Strain at Max. Stress (%)	Modulus (psi)
140	.9/1.0	none	none	10	>100	>100	yes	-	-	-
141	.9/1.0	none	0.3 HX-752	9	41	>100	no	-	-	-
142	.9/1.0	none	0.3 MT-4	20	29	28	no	-	-	-
143	.9/1.0	.06% Plastinox	0.3 MT-4	21	37	>100	no	-	-	-
144	.9/1.0	.06% PBNA	0.3 MT-4	9	31	62	no	228	34	1050
145	.9/1.0	0.1% PX-2	none	9	8	12	no	151	15	1410
147	.9/1.0	0.11% PX-2	none	6	not determined		no	165	22	1230
148	.9/1.0	.01% Plastinox + 0.1% PX-2	none	8	12	13	no	145	20	1170
159	.9/1.0	.01% Plastinox + 0.1% PX-20	none	7	10	10	no	110	25	810
167	.9/1.0	.01% Plastinox + .1% PX-2	0.3 MT-4	15	11	-	no	261	28	1380
170	.85/1	.01% Plastinox + 0.1% PX-2	0.3 HX-752	10	5	7	no	211	34	973

TABLE 11. FORMULATION MK2 MIXES

Mix No	Mg Size	HMX Size	AP Size	NCO/OH	Other	EOM Viscosity (Kp)
131	50μ	Class E	3μ	1.1/1	0.06% Plastinox	10
134	50μ	Class E	3μ	0.8/1	0.06% Plastinox	8
146	50μ	Class E	3μ	0.9/1	0.1% PX-1	11
171	50μ	Class E	3μ	0.85/1	0.01% Plastinox 0.10% PX-2 0.30% HX-752	14

Mix No	Pot-life, Kp at end of 1 hr	2 hrs	Max Stress (psi)	Strain at Max Stress(%)	Modulus (psi)
131	not determinable		-	-	-
134	65	>100	90	47	400
146	16	25	151	34	1000
171	14	-	263	44	963

TABLE 12. FORMULATION MK12 MIXES

Mix No	Mg/Al Size	HMX Size	NCO/OH	Other	EOM Viscosity (Kp)	Pot Life (Kp) 1 hr	Pot Life (Kp) 2 hrs	Max Stress (psi)	Strain at Max Stress (%)	Modulus (psi)
132	20-30	All Class A	1.1/1	.06% Plastinox	30 (cavitated)	Not determined		not determined		
136	20-30	5/2 A/E	.85/1	.06% Plastinox	26	>100	-	not determined		
137	20-30	5/2 A/E	.35/1	.06% Plastinox + .5% HAA	33	44	-	incomplete cure		
152	20-30	5/2 A/E	.85/1	.01% Plastinox + .1% PX-2	22	17	20	79	27	500
161	20-30	5/2 A/E	.95/1	.01% Plastinox + .1% PX-1	16	19	25	98	19	825
172	20-30	5/2 A/E	.85/1	.01% Plastinox .1% PX-2 .3% HX-752	30	32	31	91	34	420

TABLE 13. TENSILE PROPERTIES OF FINAL CANDIDATE FORMULATIONS

Formulation	1	2	12
Mix No.	170	171	172
Max Stress (psi)	211	263	91
Strain at Max Stress (%)	34	44	34
Rupture Stress (psi)	195	258	67
Strain at Rupture (%)	41	48	64
Tangent Modulus (psi)	973	963	420

TABLE 14. HAZARD PROPERTIES OF FINAL CANDIDATE FORMULATIONS

	FORMULATION DESIGNATION		
	MK 1	MK 2	MK 12
MIX NUMBER	170	171	172
UNCURED PROPELLANT			
ESSO FRICTION SCREW			
PYREX GRIT	NEGATIVE	NEGATIVE	NEGATIVE
SiC GRIT	NEGATIVE	NEGATIVE	NEGATIVE
ELECTROSTATIC DISCHARGE (5 K volts)	NO BURN AT 6 joules SPARKS AT 0.012 joules	NO BURN AT 6 joules SPARKS AT 0.0056 joules	NO BURN AT 6 joules SPARKS AT 0.012 joules
AUTOIGNITION TEMPERATURE, °C	288	238	258 (Smoke Only)
CURED PROPELLANT			
IMPACT SENSITIVITY, E_o, kg cm	270	60	80
ESSO FRICTION SCREW			
PYREX GRIT	POSITIVE	NEGATIVE	NEGATIVE
SiC GRIT	NEGATIVE	NEGATIVE	NEGATIVE
ELECTROSTATIC DISCHARGE (5 K volts)	NO BURN AT 6 joules SPARKS AT 0.048 joules	NO BURN AT 6 joules SPARKS AT 0.024 joules	NO BURN AT 6 joules SPARKS AT 0.048 joules
AUTOIGNITION TEMPERATURE, °C	316	242	>350

typical of Mg and Zr propellants, and is due to metal particles flying off the propellant surface. Whether or not these could result in an ignition of a large sample is not known. The HMX propellants are more sensitive to impact, but are less sensitive than composite propellants containing ultrafine AP. One positive test out of 10 (9 negatives) was observed with the cured AP propellant on the ESSO 8crew with pyrex grit. This may be a freak, since the other 9 are negative. Further friction testing is indicated before conclusions are drawn. All of the propellants have high rapid-rise autoignition temperatures, indicating good thermal stability.

The ejection characteristics were compared at ambient pressure in air. The MK1 propellant (Mg, AP) exhibits excellent ejection, burning like a stoichiometric aluminized propellant. The MK12 propellant (HMX, alloy) was difficult to ignite and exhibited poor ejection. The MK2 candidate was intermediate in its ejection properties.

Burning rate data for MK1, MK2, and MK12 are presented in Figures 24 - 26. Initially, data were obtained in a conventional strand bomb. Extreme difficulty was encountered in obtaining reproducible strand burning rates in this device. This was attributed to the very reactive Mg vapor from combustion in the bomb. The Teflon washers and insulation were severely attacked. Premature clock starting and stopping, and clock chattering were consistently observed. This was attributed to arcing and shorting out due to Mg vapor and condensed Mg. It was necessary to verify some of the data points in the window bomb using a stopwatch. This technique is not too accurate. The burning rates of the three propellants, as obtained by this technique, are shown in Figures 24 - 26 as the hexagonal points. The MK1 and MK2 rates are quite similar in the upper pressure (700 to 2000 psi) range (0.40 vs 0.38 in/sec at 1000 psia). However, MK2 has a much lower exponent, with higher rates at lower pressures. This is a typical effect of HMX. The MK12 rates are considerably lower and this propellant burned erratically at lower pressures. (It would not sustain combustion below 100 psia.) This is consistent with the ejection observation and indicates marginal combustion.

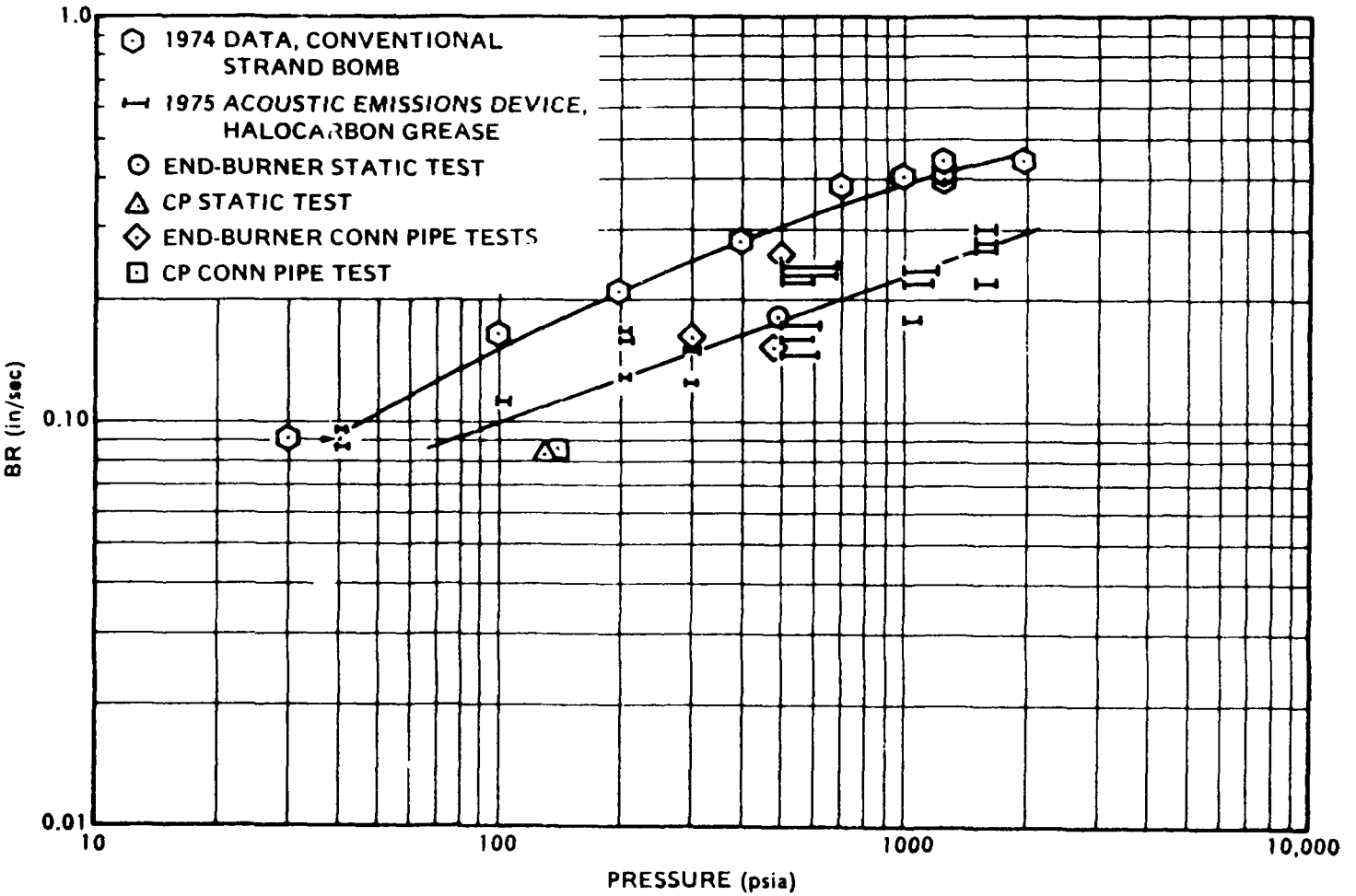

FIGURE 24. Burning Rate Data for MK1

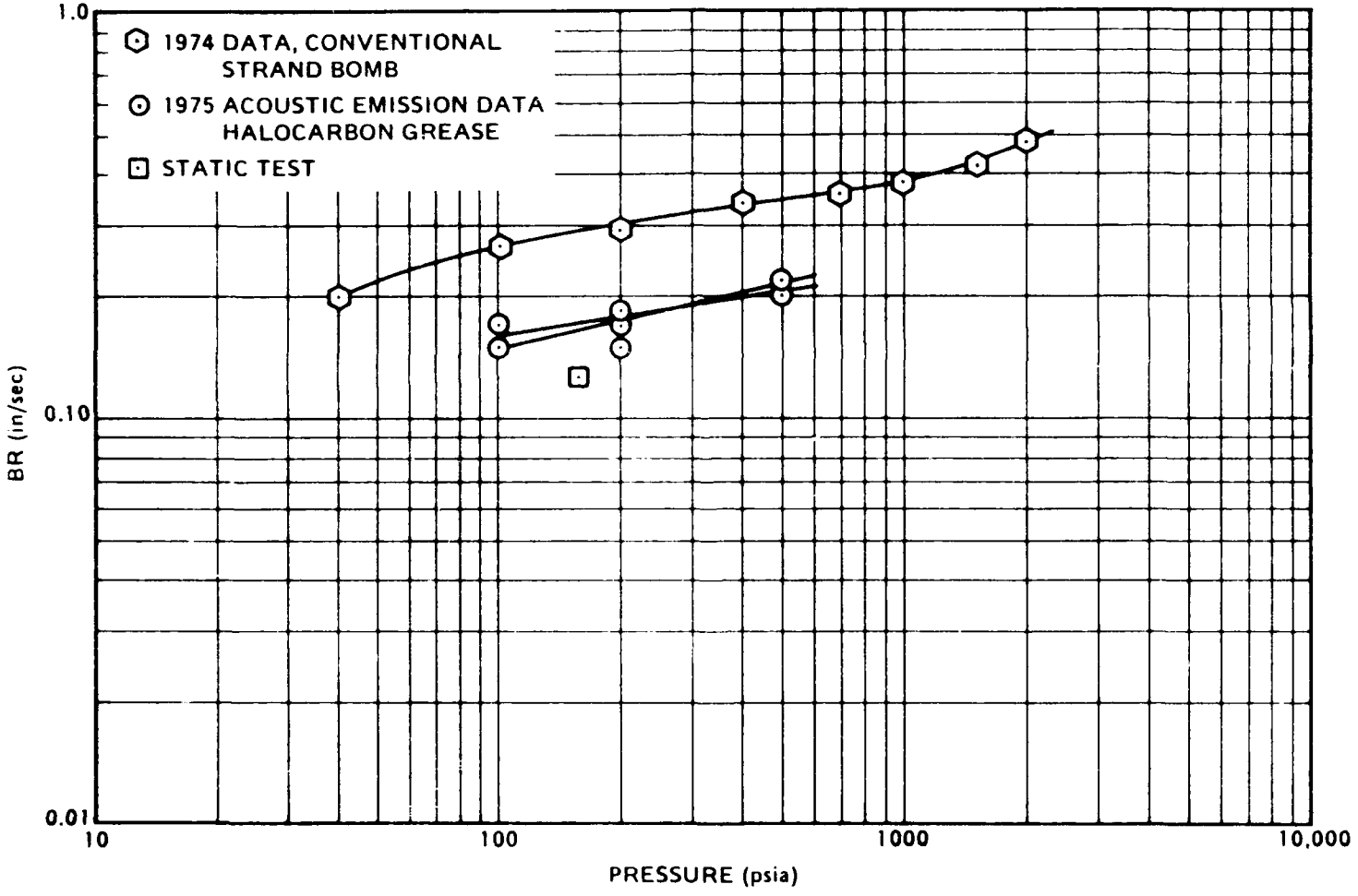

Figure 25. Burning Rate Data For MK2

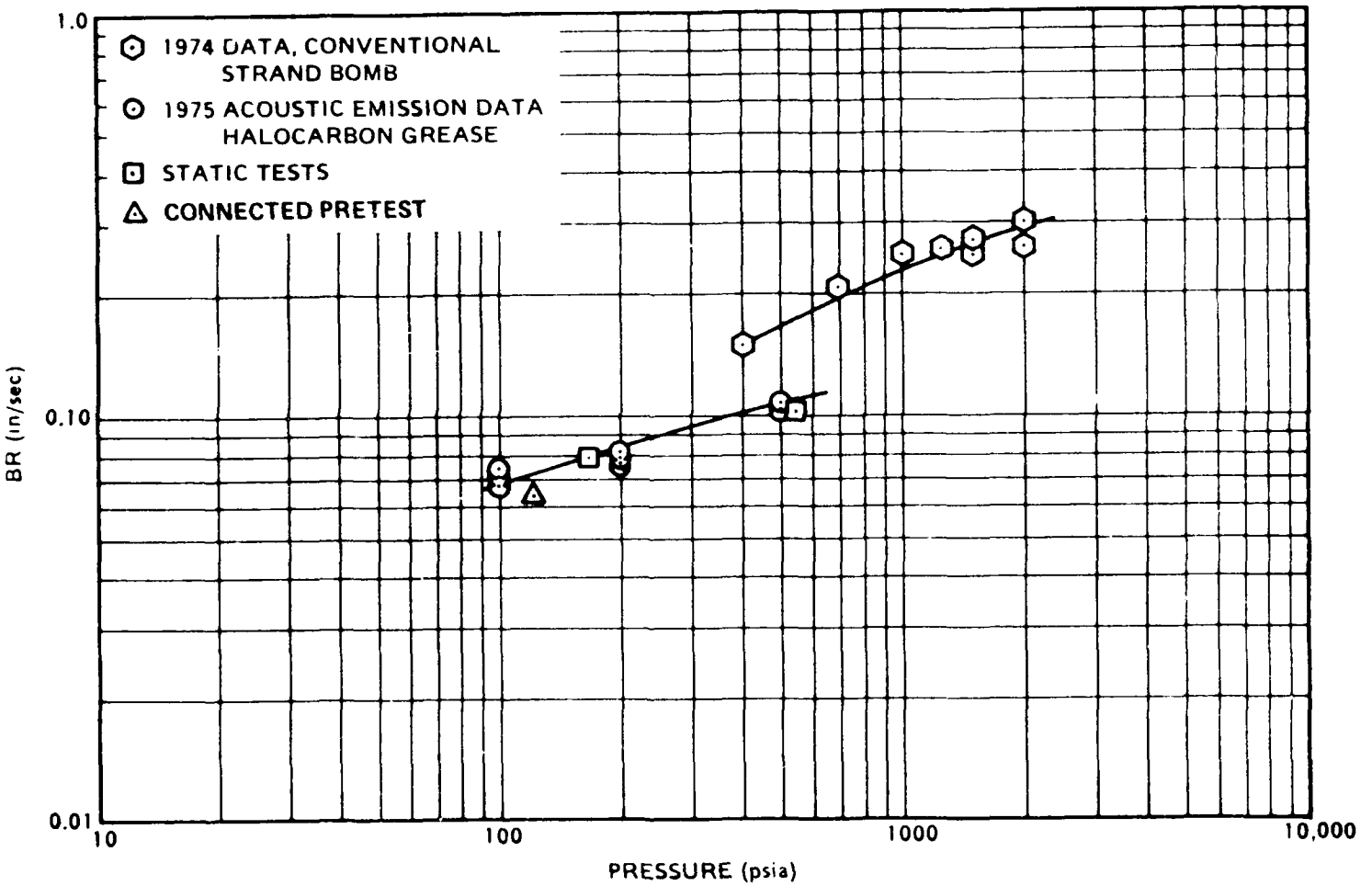

Figure 26. Burning Rate Data for MK12

Later, additional burning rate data were obtained, using an acoustic emissions technique to determine the beginning and end of burning of a known length strand. In these tests, the strands were coated with halocarbon grease. Rates obtained in these tests are presented as the horizontal bars in Figures 24 - 26: these bars indicate the variation in pressure during the tests due to use of a closed, rather than vented, strand bomb to prevent noise interference from flow from the strand bomb to the surge tank. As may be seen, these tests indicate rates of about 60 to 70% of those obtained in the conventional strand bomb tests.

Motor tests with these propellants, described later in this report, were used to obtain motor burning rate versus pressure points which are also presented in Figures 24 - 26. These tests indicated that the strand data obtained with the acoustic emissions technique were considerably more reliable than those obtained in the conventional strand bomb.

3. Formulation of Candidate Pressed Compositions Defined in Thermodynamic Screening Effort

The three candidate pressed compositions identified in Section III-B-4 (TK1, TK2, and TK3) were formulated and evaluated for safety and ballistic properties. All of these compositions are highly magnesium loaded, with TK1 containing some aluminum metal as well (approximately 5/1 Mg/Al). TK1 contains a proprietary fluorine-containing oxidizer, TK2 employs HMX as its oxidizer, and TK3 contains polytetrafluoroethylene (Teflon) as an oxidizer. All of these compositons are dry blends which are compacted under high pressure. Compositions TK1 and TK2 contain small amounts of isocyanate-cured hydroxy-terminated polybutadiene (HTPB) binder as a composition aid, to impart adequate strength to pressed pieces for handling and use. Composition TK3, made up with Teflon, did not require a binder. Safety properties measured were sensitivity to ignition by impact, friction, electrostatic discharge, and autoignition temperature, using BuMines tools. Results of these tests, presented in Tables 15 through 17, indicate no particular hazards problems associated with these formulations. In terms of ICC Shipping Classifications, TK2 will be a Class A propellant, while TK1 and TK3 will be Class B.

TABLE 15. SUMMARY OF TK1 PROPERTIES

Safety Properties

Impact Sensitivity, Eo	225 kg-cm
Friction Sensitivity, Esso Screw	Negative
Friction Sensitivity, ABL Block	Negative at 500 psi/90°
Electrostatic Discharge	Negative at .09 joules/5000 volts
Autoignition Temperature	> 390°C

Ballistics

In steel tubes	$r = 0.54\ (P/100)^{0.514}$	, P < 300 psia
	$r = 0.96$	, P > 300 psia
Free-Standing	$r = 0.31\ (P/100)^{0.727}$	, P < 360 psia
	$r = 0.85\ (P/1000)^{0.066}$	, P > 360 psia

Burning Characteristics of 1/2" Diameter Strands in Steel Tubes

Burns well with no clinker up to 1000 psia.

Slight degree of clinker on tube walls for p > 1000 psia.

TABLE 16. SUMMARY OF TK2 PROPERTIES

Safety Properties	
Impact Sensitivity, Eo	100 kg-cm
Friction Sensitivity, Esso Screw	Negative
Friction Sensitivity, ABL Block	Negative at 200 psi/90°
Electrostatic Discharge	Negative at .09 joules/5000 volts
Autoignition Temperature	280°C

Ballistics

In steel tubes $r = 0.395\ (P/1000)^{0.3}$

Burning Characteristics of ¼" Diameter Strands in Steel Tubes

Small clinker formed at 100 psia.

Extensive clinker formation at 200 psia.

Clinker is very hard and soot ejection pour at 1000 psia.

TABLE 17. SUMMARY OF TK3 PROPERTIES

Safety Properties	
Impact Sensitivity, -Eo	150 kg-cm
Friction Sensitivity, Esso Screw	Negative
Friction Sensitivity, ABL Block	Negative at 500 psi/90°
Electrostatic Discharge	Negative at .09 joules/5000 volts
Autoignition Temperature	> 390°C

Ballistics

In steel tubes

$r = 0.185\ (P/100)^{0.62}$, P < 500 psia.

$r = 1.15\ (P/1000)^{1.20}$, P > 500 psia.

Burning Characteristics of ½" Diameter Strands in Steel Tubes

No clinker at 100 psia.

Small clinker at 200 psia.

Extensive clinker and poor soot ejection at 500 and 100 psia.

Burning rate versus pressure data were obtained over a pressure range of 100 to 1000 psia for TK1, TK2, and TK3, using cylindrical pellets approximately 1/2-inch in diameter and 1-inch long, pressed at 30,000 psi in steel sleeves. Results of these measurements are given in Tables 15 through 17 and Figures 27 through 29. Both of the compositions containing a fluorinating oxidizer (TK1 and TK3) exhibit a pressure exponent break: the proprietary oxidizer reducing the exponent at P >300 psi, and teflon increasing the exponent at P >500 psi. Burning rate measurements were also made for Composition TK1 pressed as free standing cylindrical pellets $\sim$ 0.5" dia. x $\sim$ 1" L inhibited with fluorocarbon grease. Results are shown in Figure 27. The use of grease as an inhibitor in place of a steel sleeve causes a slight reduction in burning rate, and increase in exponent. The characteristic exponent break is still present, but occurs at a higher pressure (400 psi vs 300 psi with steel).

Burning characteristics (ejection) are summarized in Tables 15 through 17. The best of the compositions, in terms of burning without formation of clinker is TK1; this composition ejects all combustion products when burned at pressures up to 1000 psia, the highest pressure tested.

For motor firings (discussed later), two grains of composition TK1 were pressed up at 30,000 psi, free-standing, in seven increments. The diameter of each grain was 2.05 inches. Grain 1 was 7.02 inches long and weighed 696.5 grams. Grain 2 was 7.03 inches long and weighed 694.1 grams.

D. PROPELLANT COMBUSTION PRODUCT CHARACTERIZATION

Formulations MK1, MK2 and MK12 are thermodynamically predicted to yield product streams containing approximately 1 gm-mole of magnesium vapor per 100 grams of propellant (about 30 to 40 percent by volume of the total gas-phase products of combustion). Since this magnesium vapor should be extremely combustible, and in fact should promote afterburning of other fuel product species as discussed later, it is of interest to know whether or not these theoretical expectations are indeed realized, particularly at the high magnesium loadings involved. If the primary motor combustion is not efficient, they may not be, due to lower than theoretical temperature preventing

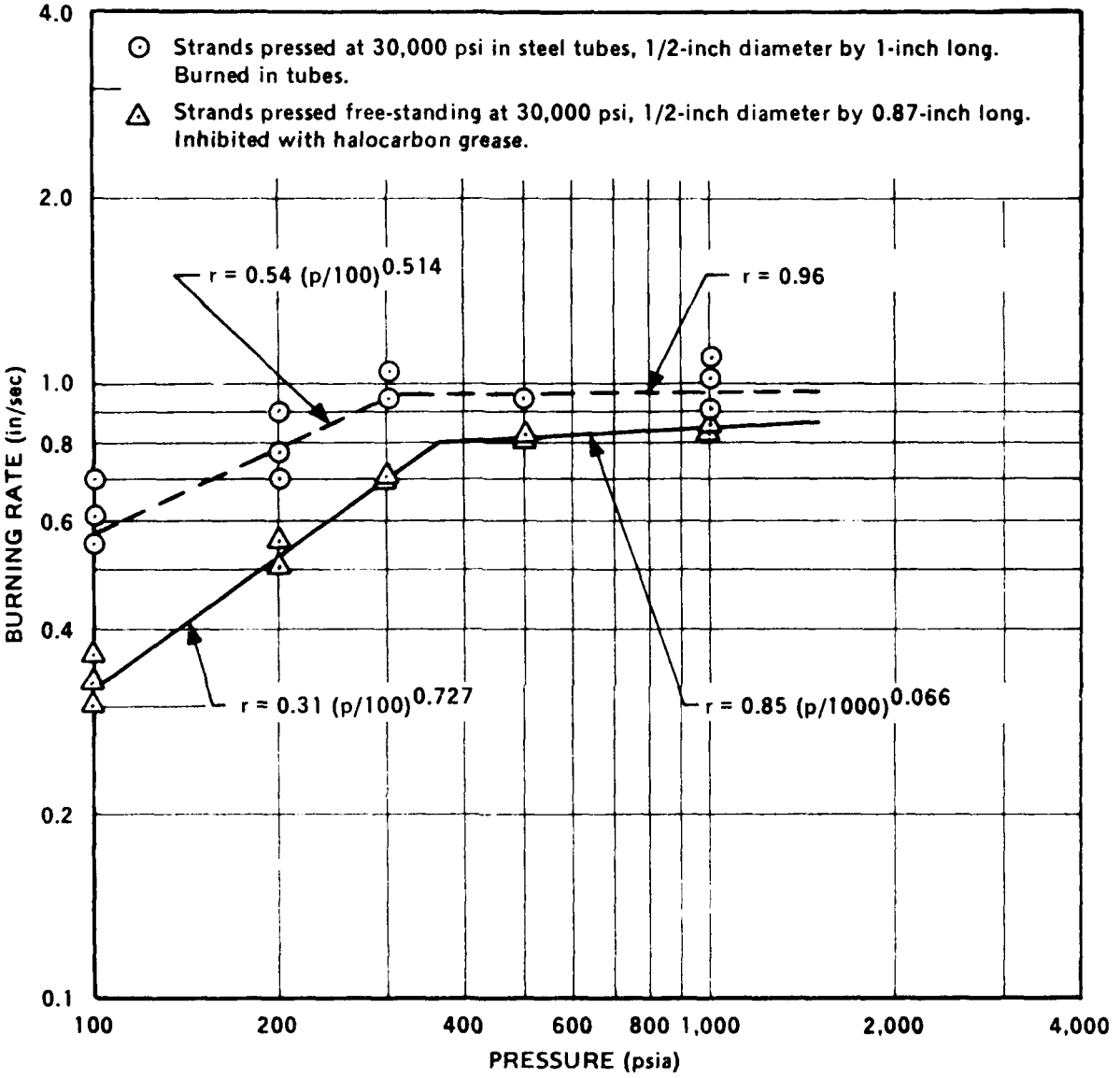

Figure 27. Burning Rate Data for TK1.

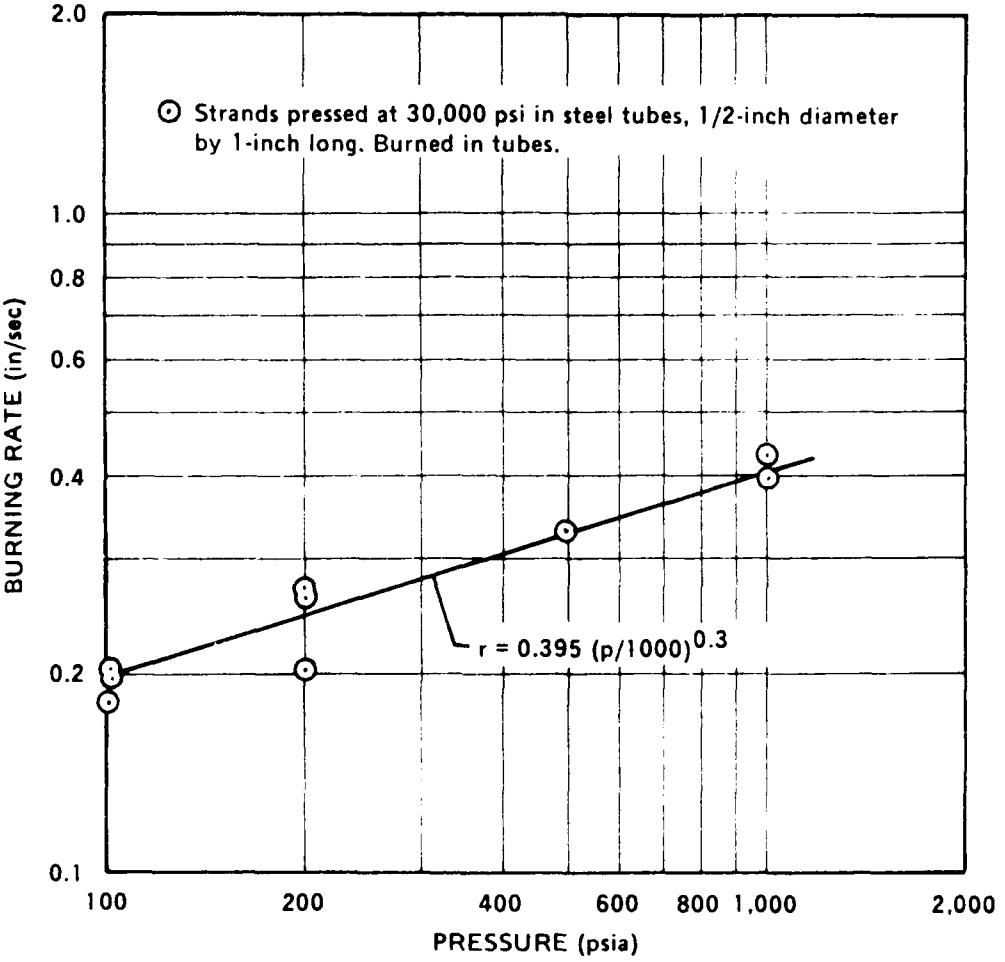

Figure 28. Burning Rate Data for TK2.

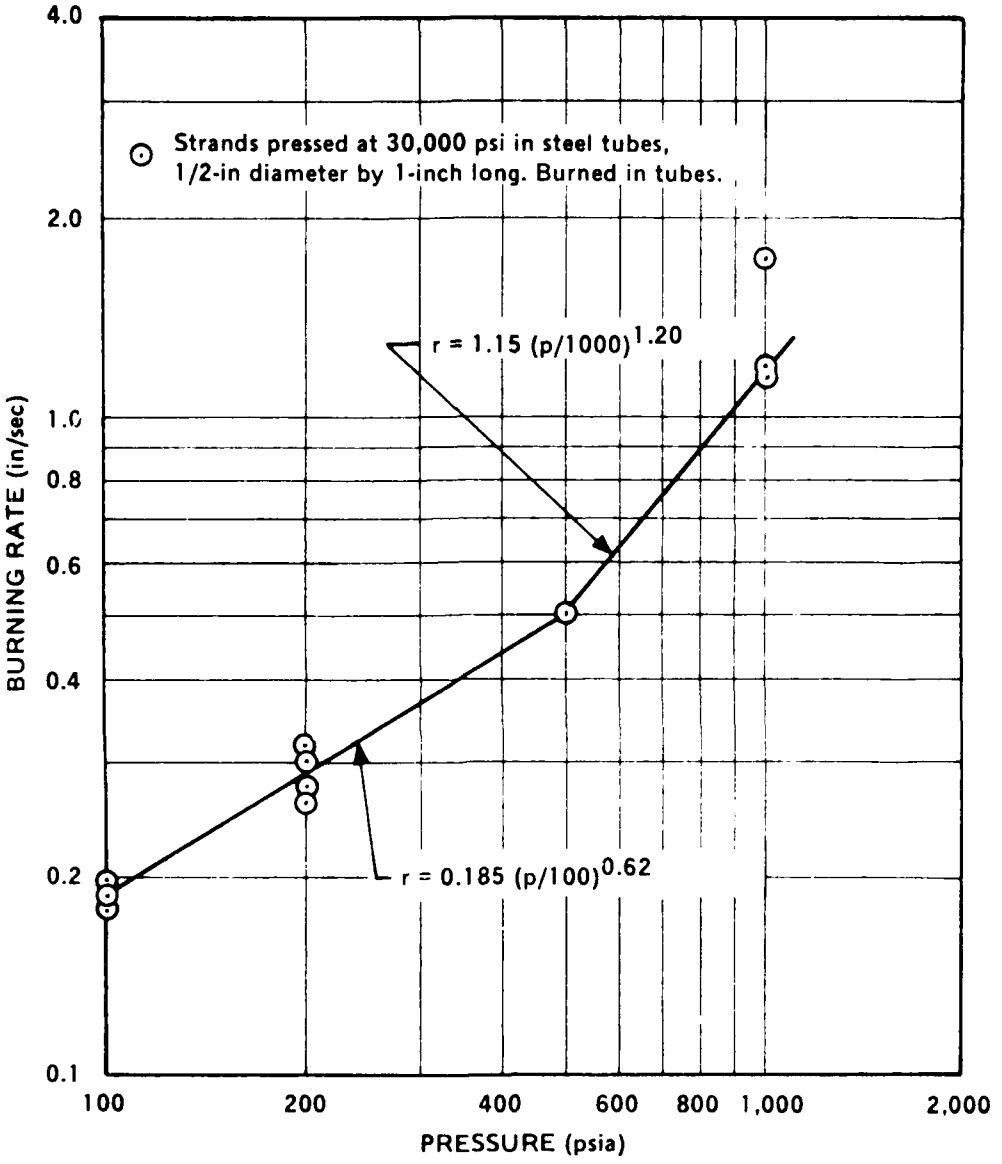

Figure 29. Burning Rate Data for TK3.

vaporization of the magnesium or resulting in a shift of magnesium vapor plus nitrogen to magnesium nitride (thermodynamically predicted at temperatures of 1700 K or less). In addition, while thermochemistry indicates significant amounts of CO and Mg(g), if the magnesium reacts preferentially with the propellant oxygen, due to kinetic limitations, there may be considerably more MgO(s) and C(s) formed and less CO and Mg(g). It is also important that the other products of combustion be characterized and compared to theoretical predictions.

Two types of experiments have been devised for characterization of the combustion products of MK1, MK2, and MK12, the first being an in situ optical absorption measurement of magnesium vapor density above the burning surface of the propellant, and the second being combustion of a propellant sample in a closed bomb with subsequent collection and analysis of the products. The major advantage of the first technique lies in the fact that results should not be confused by events possibly occurring during cooling of the combustion products. For example, thermodynamic calculations indicate that as the products are cooled two shift reactions should occur unless kinetically frozen: $Mg + CO \rightarrow MgO + C$, and $3\ Mg + N_2 \rightarrow Mg_3N_2$. With the second procedure, such shifts may occur, tending to confuse the results. The major disadvantage of the first technique is that it is a very difficult experiment, particularly with the high level of particulates (very fine carbon) in the propellant combustion products.

The apparatus utilized for in situ Mg(g) density measurement is shown in Figures 30 and 31. Figure 30 shows schematically the reaction chamber. The chamber is cruciform and is made out of Plexiglas. The propellant sample, a cylindrical strand 1.3 cm in diameter, 2 to 3 cm long, is placed in the center of the chamber, just upstream of the side arms. Since the fuel-rich, magnesium-containing propellant products ignite and burn vigorously in oxygen, the strands must be protected by an inert gas. Argon is therefore introduced in three streams, one from the extreme upstream location,

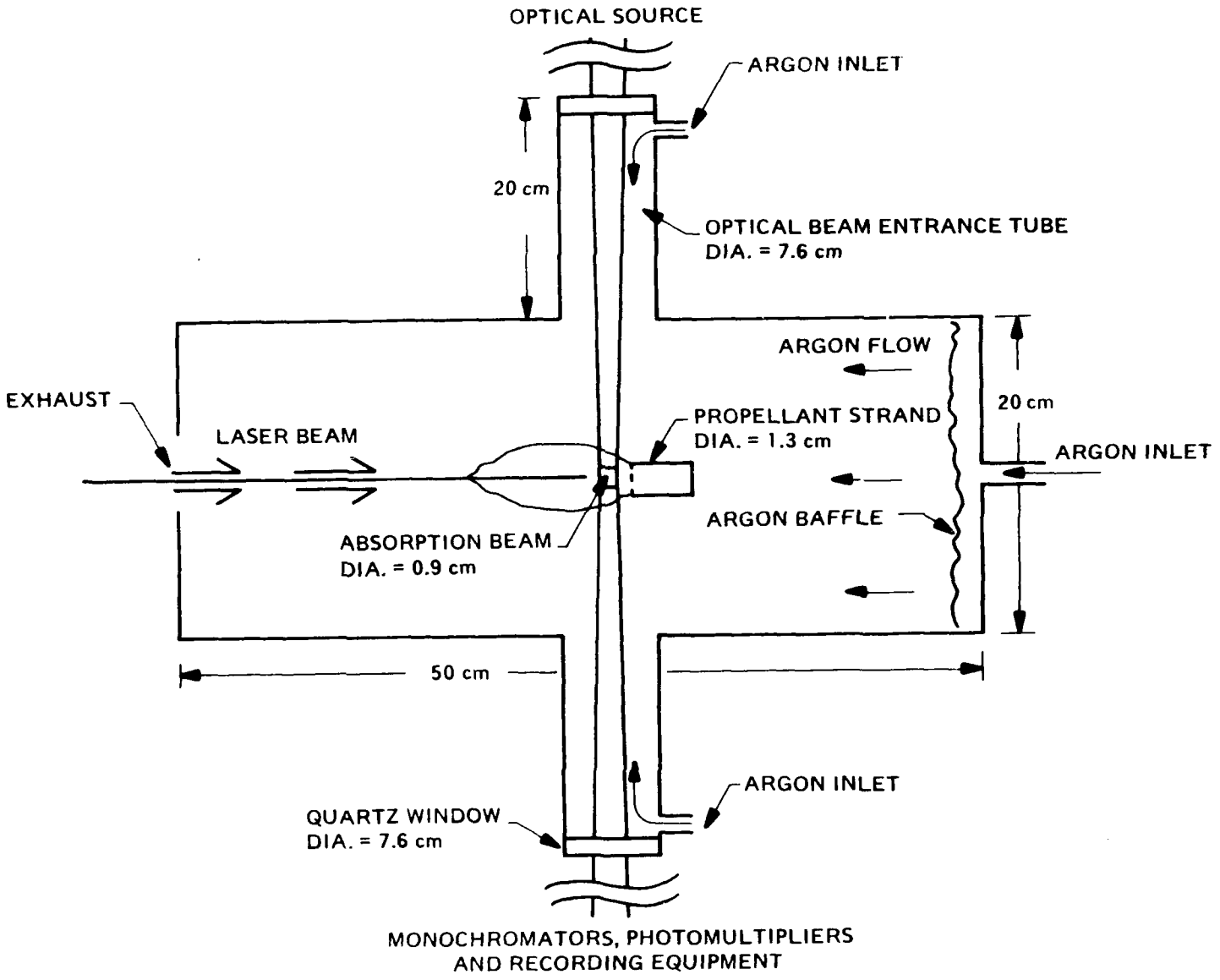

Figure 30. Magnesium Vapor Atom Number Density Experiment Schematic

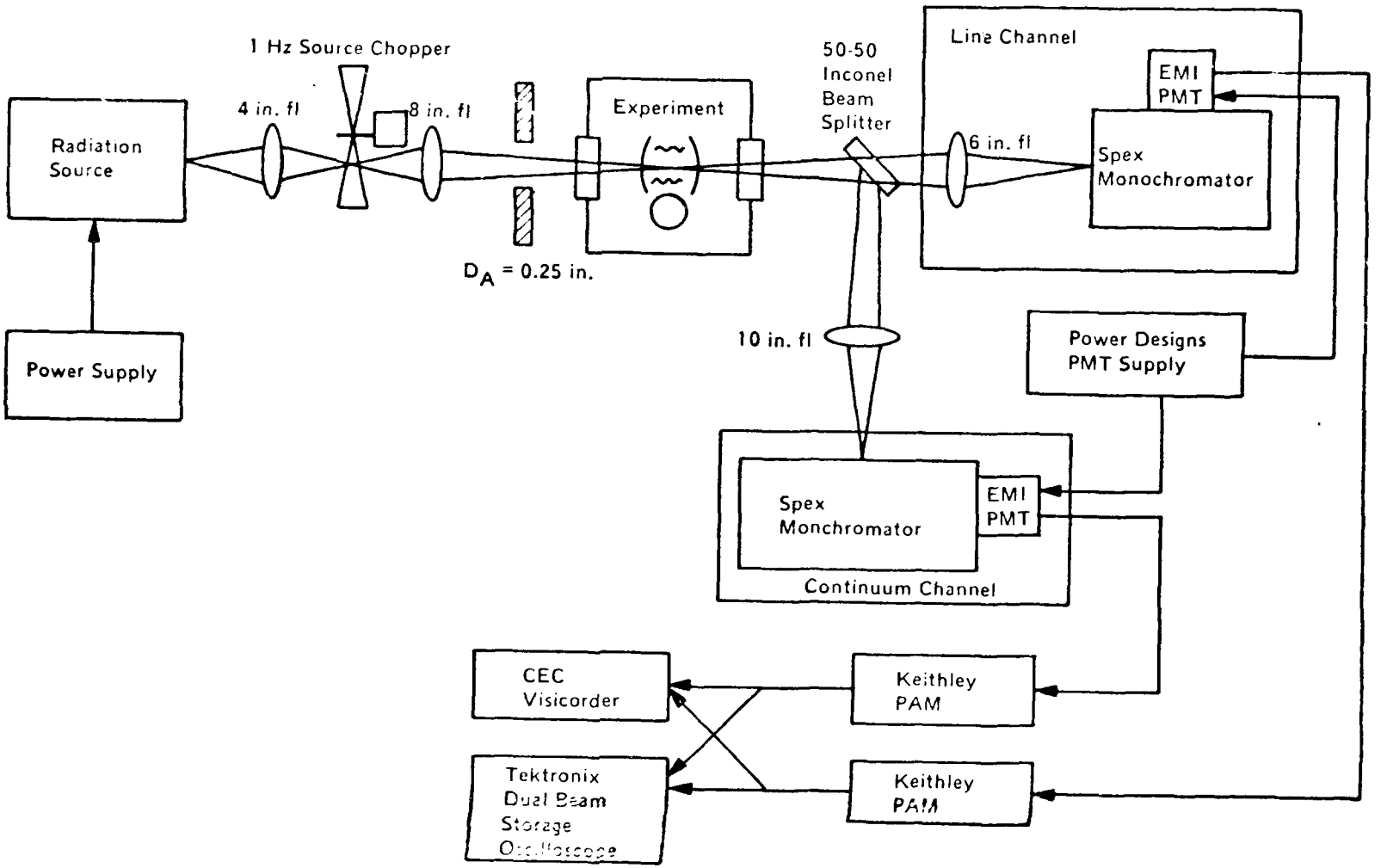

Figure 31. Optical Absorbtion Apparatus

and the other two through the side arms. An optical beam from a tungsten-lamp continuum source intersects the strand jet normal to the main axis of the experiment. Mg(g) densities are measured by the selective absorption of the 2852Å resonance line. Since this wavelength is in the ultraviolet, the entire optical system, including the side-arm windows, must be made of quartz.

Since the Mg-loaded propellants sometimes do not burn well at atmospheric pressure (particularly under argon), the strand combustion was aided by laser radiation, normal to the burning surface. The laser is a 100 watt CW CO_2 instrument, operating in the LWIR at 10.6 μm. This wavelength is convenient, because it is not absorbed selectively by the propellant product gases to any appreciable extent. Some absorption by $H_2O(g)$ and $CO_2(g)$ must be anticipated, but this should not affect the experiment. We found it also very convenient to use the laser radiation for ignition of the strand: in each run, the laser was first turned on to a high power; after the strand ignited the power was turned down, or off, as necessary to give a manageable burning rate.

The optical absorption apparatus is shown in Figure 31. A detailed description of the apparatus and of the newly developed continuum-absorption method is given in Ref. 14. Briefly, a beam from a tungsten-filament lamp, collected by a set of slits and lenses, intersects the jet of propellant strand products. The beam diameter is 0.9 cm. After the passage through the jet, the beam is split into two parts, each entering an identical set of monochromators, preamplifiers, and phototubes. The monochromator slits are 10Å wide. One is centered on the Mg-resonance line, 2852±Å, and the other on an arbitrary nearby wavelength, 3200±Å. The photomultiplier signals from both beams are displayed simultaneously on a dual-channel oscilloscope. The apparent absorption (A) by Mg(g) is obtained by subtracting the control channel absorption from that of the active channel (2852Å):

$$A = 1 - \frac{\left[\dfrac{P_D^{S+F}(\nu_L) - P_D^{F}(\nu_L)}{P_D^{S}(\nu_L)}\right]}{\left[\dfrac{P_D^{S+F}(\nu_C) - P_D^{F}(\nu_C)}{P_D^{S}(\nu_C)}\right]} \qquad (1)$$

$P_{D_F}^{S+F}$ = Power detected when light source is viewed through plume

P_D^{F} = Power detected when plume is viewed alone

P_D^{S} = Power detected when light source is viewed without plume

ν_L = Atomic absorption line frequency

ν_C = Neighboring frequency

The apparent gas absorption, A, is related to the gas volumetric absorption coefficient, K_ν^{GA}, by:

$$A = \frac{\int_{-\infty}^{\infty}\int_{-\infty}^{\infty}\{1 - \exp[-K_\nu^{GA}(S_2-S_1)]\}g|\nu' - \nu|h(\nu')d\nu d\nu'}{\int_{-\infty}^{\infty}\int_{-\infty}^{\infty} g|\nu' - \nu|h(\nu')d\nu d\nu'} \qquad (2)$$

K_ν^{GA} = Gas volumetric absorption coefficient = $f(N_{MG})$

S_2-S_1 = Plume optical path length

$g|\nu'-\nu|$ = Slit function

$h(\nu')$ = Exit slit response

ν = Frequency of incident radiation

ν' = Position in exit slit of monochromator corresponding to frequency ν for an infinitely narrow entrance slit, perfect monochromator optics, and no diffraction effects.

The number density of magnesium vapor atoms is in turn related to the gas volumetric absorption coefficient, K_ν^{GA}, by:

$$N = \frac{[K_\nu^{GA}/S(\nu)]\, m_e C \Sigma\, g_i \exp(-E_i/kT)}{\pi e^2\, g_\ell [\exp(-E_\ell/kT)]\, f_{\ell u}} \qquad (3)$$

$S(\nu)$ = Normalized line shape factor

m_e = Electronic mass

C = Vacuum velocity of light

g_i = Degeneracy of level i

E_i = Energy of level i

k = Boltzmann's constant

T = Temperature

e = Electronic charge

$f_{\ell u}$ = Absorption oscillator strength

ℓ = Lower energy level

Equations 2 and 3 have been evaluated through use of a computer program as described in Ref.14 to develop theoretical curves of apparent gas absorption, A, versus magnesium atom number density, N, for various path lengths as shown in Figure 32. However, since there are considerable uncertainties in this theoretical calculation procedure and since preliminary tests indicated very low (less than 1 percent of theoretical) magnesium vapor yields, it was decided that a series of calibration runs be made to develop corrections (if needed) for the theoretical curves. These tests were conducted with the propellant sample shown in Figure 30 replaced by a magnesium vapor source capable of producing a stream of pure magnesium vapor. The vapor generator consisted of a specially constructed crucible (heated by resistance heating) filled with magnesium ribbon, inside a vessel with a one centimeter diameter orifice through which the vapor exited into the optical absorption test beam. The generator and test apparatus were placed in a vacuum tank and argon was bled in to the desired pressure level for a test. The resistance heater was then activated, producing a jet of magnesium at the vacuum tank pressure and

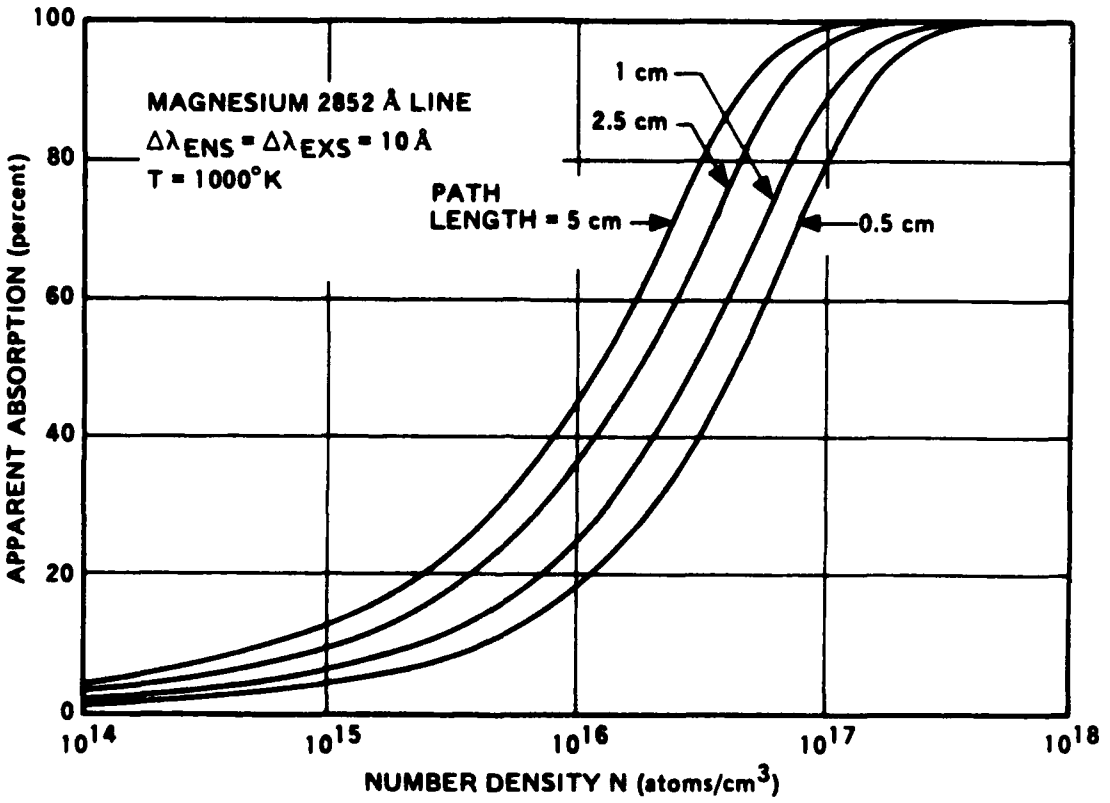

Figure 32. Theoretical Magneisum Vapor Absorption Versus Number Density

a temperature approximately equal to the boiling temperature of magnesium at that pressure. From this pressure and temperature the actual magnesium vapor density could be calculated. The apparent absorption A calculated from the recorded optical beam power level oscilloscope traces by Equation 1 was then combined with Figure 32 (the 1 centimeter path length curve) for calculation of a magnesium vapor density based on atomic absorption measurements, for comparison with the actual density. Results of a series of four tests are presented in Table 18. As may be seen, use of the theoretical curves of A vs. N tends to underestimate the magnesium atom density by approximately a factor of 4. Accordingly, on subsequent propellant tests the atom densities calculated by use of these curves were multiplied by a factor of 4.

Early in the program, strands of four different uncured mixes (hand-tamped into strands) were tested by this technique. These formulations, designated 118, 119, 120, and 122, contained 37.5, 30, 10, and 10% magnesium respectively. The first contained 15% HTPB binder, with the remainder of the formulation being HMX. The second and third were each 10% HTPB with the remainder HMX, and the final formulation was identical with the third, except for 5% AP replacing part of the HMX.

The 37.5% Mg formulation gave absorption results which were difficult to read, because the beams were very highly attenuated by product particles, probably C(s) and MgO(s). Both the 10% and the 30% Mg formulations gave readable apparent absorption measurements, fluctuating considerably over any given run, and varying from run to run. The absorptions were 18.5, 11.6, 7.0, and 9.5% for the four formulations (in numerical order). Results are presented in Table 19. As indicated, in all cases, the number density of magnesium vapor atoms were considerably less than predicted by thermochemical equilibrium calculations.

Approximately 10 to 15 optical absorption tests each were conducted with Formulations MK1, MK2, and MK12 burning at 1 atmosphere. Due to problems with particulate absorption tending to flood both data channels (giving absorption readings of 100 percent) and producing large amounts of noise even when the did not flood the channels, only about half of the tests

TABLE 18. RESULTS OF CALIBRATION TESTS FOR OPTICAL ABSORPTION MEASUREMENT OF MAGNESIUM VAPOR DENSITY

Test Number	Pressure (Torr)	Actual Magnesium Vapor Density (Atoms/cc)	Apparent Gas Absorption, A (%)	Magnesium Vapor Density From Theoretical Relation Between A and N (Atoms/cc)	(Actual Density) / (Density According to Absorption Measurement)
1	4.5	$4.4 \cdot 10^{16}$	30	$1.3\ (10^{16})$	3.4
2	14.0	$13.5 \cdot 10^{16}$	60	$4.0\ (10^{16})$	3.4
3	4.5	$4.4 \cdot 10^{16}$	24	$0.95\ (10^{16})$	4.6
4	14.0	$13.5 \cdot 10^{16}$	54	$3.25\ (10^{16})$	4.15

TABLE 19. RESULTS OF ABSORPTION MEASUREMENTS FOR FOUR UNCURED HAND-TAMPED FORMULATIONS BURNING IN ARGON AT ONE ATMOSPHERE.

Formulation Designation	Percent Magnesium	Theoretical Flame Temperature (°K)	Theoretical Number Density of Magnesium Gas Atoms, cc^{-1} ($\times 10^{-17}$)	Apparent Gas (Absorption) (percent)	Number Density of Mg Gas Atoms Corresponding to A (with calibration correction factor), cc^{-1} ($\times 10^{-17}$)	Percent of Theoretical Mg Vapor Yield
118	37.5	1954	9.7	18.5	0.[illegible]0	2.1
119	30	1960	7.4	11.6	0.092	1.2
120	10	2449	1.05	7.0	0.040	3.8
122	10	2504	9.2	9.5	0.072	9.8

TABLE 20. RESULTS OF ABSORPTION MEASUREMENTS FOR FORMULATIONS MK1, MK2, and MK 12 BURNING AT ONE ATMOSPHERE IN ARGON

FORMULATION DESIGNATION	THEORETICAL NUMBER DENSITY OF Mg GAS ATOMS cc^{-1} (X 10^{-17})	APPARENT GAS ABSORPTION (percent)	NUMBER DENSITY OF Mg GAS ATOMS CORRESPONDING TO A (with calibration correction factor), cc^{-1} (X 10^{-17})	PERCENT OF THEORETICAL Mg VAPOR YIELD
MK 1	11.0	49	1.1	10
		53	1.3	12
		30-41	0.5-0.8	5-7
		40-50	0.8-1.1	7-10
		56	1.4	12
MK 2	10.0	25-51	0.4-1.2	4-12
		33-36	0.6-0.7	6-7
		67	1.9	19
		60	1.6	16
MK 12	8.3	16-34	0.3-0.6	4-8
		10-37	0.2-0.7	3-9
		22-27	0.3-0.4	4-5
		35-48	0.6-1.1	8-13
		57	1.4	17
		42-46	0.9-1.0	10-12
		54-60	1.3-1.6	16-19
		58-59	1.5	18

were usable and even in these the uncertainty in the apparent absorption, A, was usually on the order of ± 10 to 20 percent. However, it is felt that the data obtained are at least semi-quantitatively correct. Results are summarized in Table 20. As may be seen, for each formulation the percentage of theoretical magnesium yield measured averages about 10 to 12, with the highest percentage being 19. Three possible explanations for these low yields of magnesium vapor have been suggested:

(1) In the propellant combustion, the magnesium is attacked preferentially by the available oxygen, resulting in $MgO(s) + C(s)$ rather than the thermochemically predicted $Mg(g) + CO(g)$.

(2) Heat losses and/or combustion inefficiency results in sufficient reduction of the flame temperature that an appreciable amount of the magnesium appears as magnesium nitride (thermodynamically favored at temperatures below about 1500°K).

(3) The temperature at the point of optical measurement is so far below theoretical due to inefficient combustion, heat losses, or both, that condensation of much of the magnesium occurs.

Examination of the propellant stoichiometry enables us to quickly rule out the first explanation inasmuch as the three formulations are so fuel rich that even if all of the oxygen thermodynamically predicted to appear as CO instead was used to tie up magnesium, it would only account for 30 to 50 percent of the magnesium. Formation of magnesium nitride, on the other hand could, in combination with the $Mg + CO \rightarrow MgO + C$ shift, tie up all of the magnesium in the cases of Formulations MK2 and MK12: however, in the case of Formulation MK1, even an allowance for both shifts would still result in approximately 50 percent of the theoretical magnesium vapor still being present. Only as the temperature is decreased to approximately 1100-1200°K.

for Formulation MK1 (compared to a 1 atmosphere combustion theoretical flame temperature of 1940°K) does the magnesium level fall to 10-15 percent of that predicted for adiabatic complete combustion, the final decrease being due to magnesium condensation.

Results of a series of thermochemical equilibrium calculations for MK1, MK2, and MK12, in which the enthalpy of the system is adjusted to bring the flame temperature down (corresponding to heat losses), demonstrating the possibilities discussed above are presented in Figure 33. In this figure, the volume percent of the gas phase which is magnesium divided by the same parameter at theoretical adiabatic conditions is plotted against temperature. As may be seen, for the ratio to drop into the 10-15 percent band indicated by the optical absorption tests, the flame temperature must drop from the theoretical value of approximately 1950°K to 1400°K for Formulations MK2 and MK12, or 1100°K for Formulation MK1. In all three cases, this corresponds to approximately a 75 to 80 percent loss of theoretical heat release. At this point, we are unable to conclude whether or not the observed results of our one atmosphere propellant combustion tests can be explained in this manner.

In addition to characterization of the combustion of the three highly-magnesium-loaded, fuel-rich propellants by optical absorption measurements of the products of samples burning at one atmosphere, we also burned samples in a closed bomb at 500 psia (argon) and analyzed the products. The apparatus used is depicted in Figure 34. The procedure is as follows:

The propellant sample to be burned (approximately 10 grams) is inhibited on the sides and placed in a 2700 cc capacity modified Hoke bomb. The bomb is evacuated and flushed several times with argon and finally pressurized to 500 psia with that gas. The sample is then ignited with a hot wire. The combustion causes the pressure in the bomb to rise to approximately 800 - 1000 psia, dropping back to approximately 550 - 600 psia as the bomb

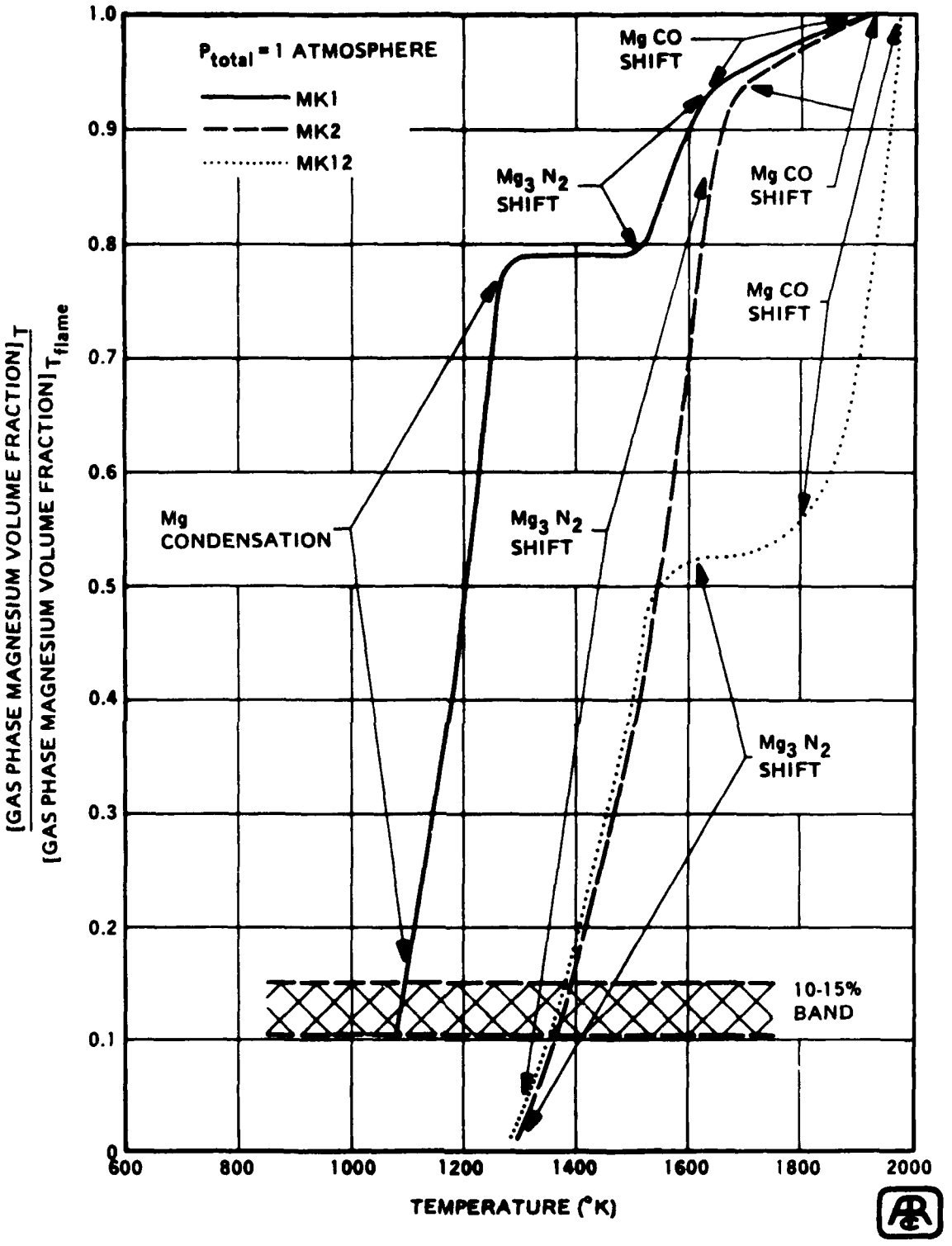

Figure 33. Theoretical Variation of Fraction of Gas-Phase Products which are Magnesium with System Temperature

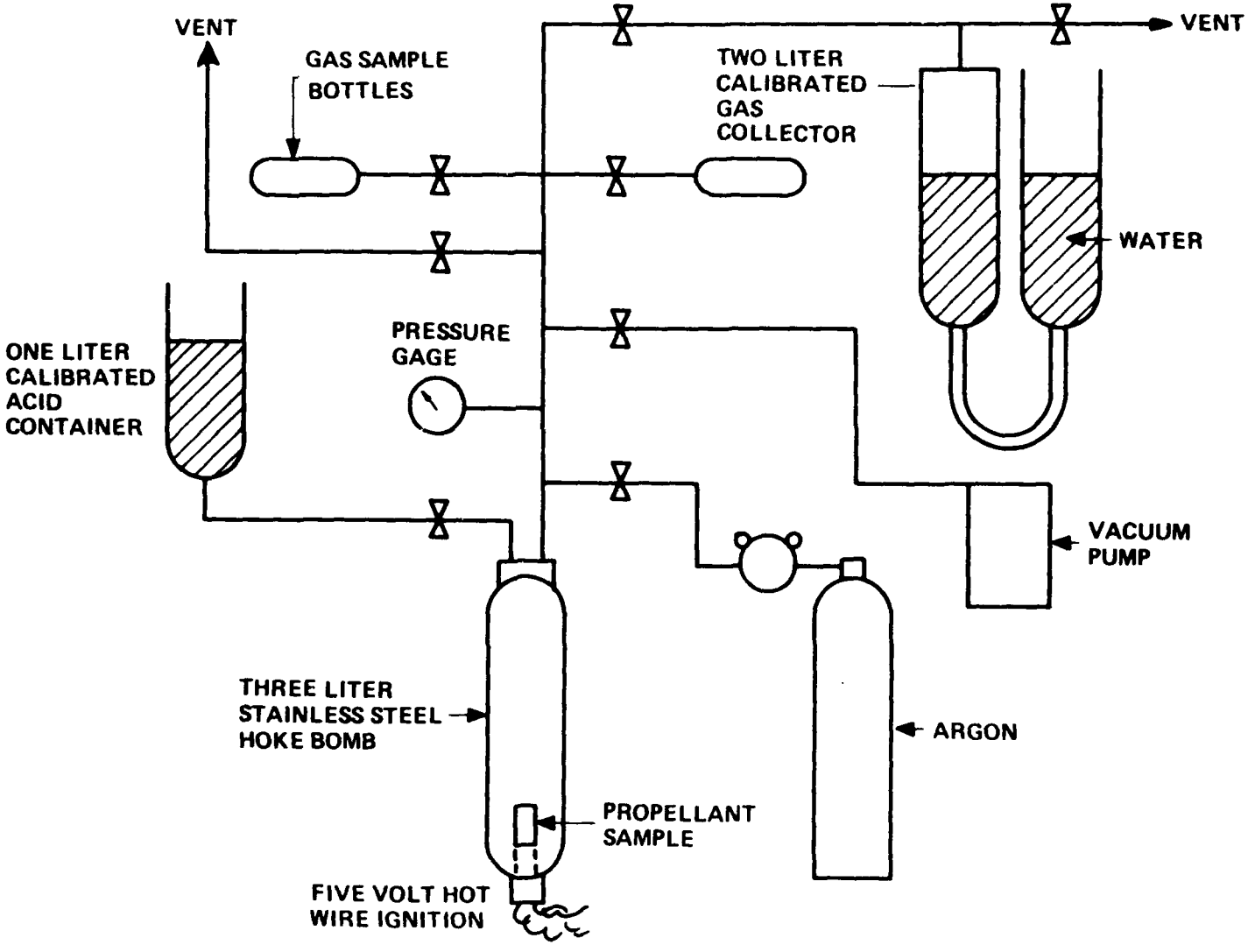

Figure 34. Closed Bomb Propellant Combustion Product Test Apparatus

cools. After the bomb has been permitted to cool thoroughly (and the combustion products to mix well with the argon) a gas sample is taken for chromotographic analysis. The remaining pressure is then bled off and the bomb is connected through argon-filled lines to a modified Orsat apparatus. The bomb is then filled with a 4 percent solution of HCl in water. Tests run with blanks show that the HCl solution will dissolve MgO or Mg_3N_2 with no gas evolution while it will react with any nascent magnesium to yield one gram-mole of hydrogen gas per gram-mole of magnesium. Therefore, collection and measurement of the volume of the gas evolved as the bomb is filled with the HCl solution (with, of course, correction for the displacement of gas initially in the bomb by the solution) permits determination of the amount of magnesium produced by the propellant combustion.

The contents of the gas sample bottles (two per test) are analyzed for volume percent hydrogen, oxygen, nitrogen, hydrocarbon, carbon monoxide, and carbon dioxide. With these numbers and the calculated initial gram-moles of argon in the Hoke bomb (calculated from known pressure, temperature, and volume) the gram-moles of each of these species produced by the propellant combustion can be calculated. These are then compared with theoretical predictions (based on the known propellant sample weight). Results of a test with Formulation MK2 are shown in Table 21. As may be seen, 0.070 gm-moles of magnesium are produced, compared to a theoretical yield of 0.111 gm-moles - the percentage yield is 65 percent. Now, it is most interesting to compare the shortage of magnesium with the shortage of CO and N_2. If we assume that the shortage of these two gases is due to reaction with magnesium, we find that the shortage of CO will account for a shortage of 0.010 gm-moles of magnesium (via $Mg + CO \rightarrow MgO + C$) while the shortage of nitrogen will account for a shortage of 0.030 gm-moles of magnesium (via $3\ Mg + N_2 \rightarrow Mg_3N_2$) for a total shortage of magnesium of 0.040 gm-moles, as compared to the observed shortage of 0.041 gm-moles.

TABLE 21. RESULTS OF SAMPLE TEST OF MK2 BURNED AT 500 PSI IN A CLOSED BOMB

1. INITIAL GM-MOLES ARGON = 3.76

2. MEASURED COMPOSITION OF GAS SAMPLE COLLECTED AFTER COMBUSTION OF 9.31 gram PROPELLANT SAMPLE

COMPOUND	VOLUME (percent)	GM-MOLES IN TOTAL GAS PRODUCT
ARGON	96.06	3.76
H_2	2.90	0.113
N_2	0.61	0.024
CO	0.29	0.011
HC	0.14	0.005

3. GM-MOLES OF Mg, MEASURED BY AMOUNT OF H_2 GAS GENERATED BY ADDITION OF LARGE EXCESS OF 4 PERCENT HCl SOLUTION = 0.070

4. YIELDS ARE THEREFORE:

COMPOUND	THEORY	MEASURED
H_2	0.115	0.113
Mg	0.111	0.070
C	0.105	UK
MgO	0.081	UK
N_2	0.034	0.024
CO	0.021	0.011
HC	0.004	0.005

5. SHORTAGE OF 0.010 MOLES N_2
   0.010 MOLES CO
   0.041 MOLES Mg

6. EXPLANATION: $0.010\ N_2 + 0.030\ Mg \rightarrow 0.010\ Mg_3N_2$
   $0.010\ CO + 0.010\ Mg \rightarrow 0.010\ MgO + 0.010\ C$

Results of two tests each with MK1, MK2, and MK12 are summarized in Table 22. As may be seen, the nascent magnesium yields with MK1 and MK2 are approximately 65 percent of theoretical while that with the mixed-metal propellant, MK12, is about 25-30 percent of theoretical.

It is instructive to examine the theoretical effects of cooling of the products of combustion of the formulations by mixing with argon. (See Figure 35) At 500 psia, the theoretical flame temperature of MK2 is 2353°K, with a total CO yield of 0.227 gm-moles per 100 grams of propellant, 1.191 gm-moles of magnesium vapor per 100 grams, and 0.378 gm-moles of N_2 per 100 grams. As the products cool to 2100°K, all of the CO is thermodynamically predicted to disappear via $Mg + CO \rightarrow MgO + C$. As soon as the CO is exhausted, a second shift, $3\ Mg + N_2 \rightarrow Mg_3N_2$ is predicted to begin, with all of the remaining magnesium being reacted by the time the temperature reaches 1700°K. It is our contention that just such shifts are occurring though kinetic limitations prevent them from going to completion, permitting only about half of the theoretical CO shift and one-third of the theoretical N_2 shift. Accordingly, we feel that this test indicates near equilibrium production of magnesium vapor during propellant combustion at 500 psia with subsequent shift of some of magnesium to MgO and Mg_3N_2 during cool-down. The results of tests with MK1 and MK12 may also be explained in a similar manner (See Figure 35.) In all cases, the experimental nascent magnesium yields, shown by the squares on the theoretical curves, correspond to freezing of the thermodynamically predicted product composition shifts with temperature at about 1900-2000°K.

Carbon particles produced by the strand combustion in one of the MK1 tests were collected from the final acid solution and analyzed for size distribution: the results are presented on a log-probability plot in Figure 36. The straight line indicates that the particles produced have a log-normal size distribution. The mass median particle size is seen to be 1.9 microns, with 80 percent of the mass being contained in particles of 5 microns diameter or less, and 90 percent in particles of 8 microns diameter or less. These small sizes indicate that there should be little trouble encountered in burning this carbon in an air-augmented rocket afterburner, particularly in the presence of burning magnesium vapor.

TABLE 22. NASCENT MAGNESIUM YIELDS IN CLOSED BOMB 500 PSI COMBUSTION TESTS

FORMULATION	TEST NO.	THEORETICAL Mg YIELD (gm-mol/100 gm)	MEASURED Mg YIELD (gm-mol/100 gm)	PERCENT OF THEORETICAL
MK 2	1	1.11	0.73	66
	2	1.11	0.75	67
MK 1	3	1.18	0.79	67
	4	1.18	0.77	65
MK 12	5	0.99	0.26	26
	6	0.99	0.27	27

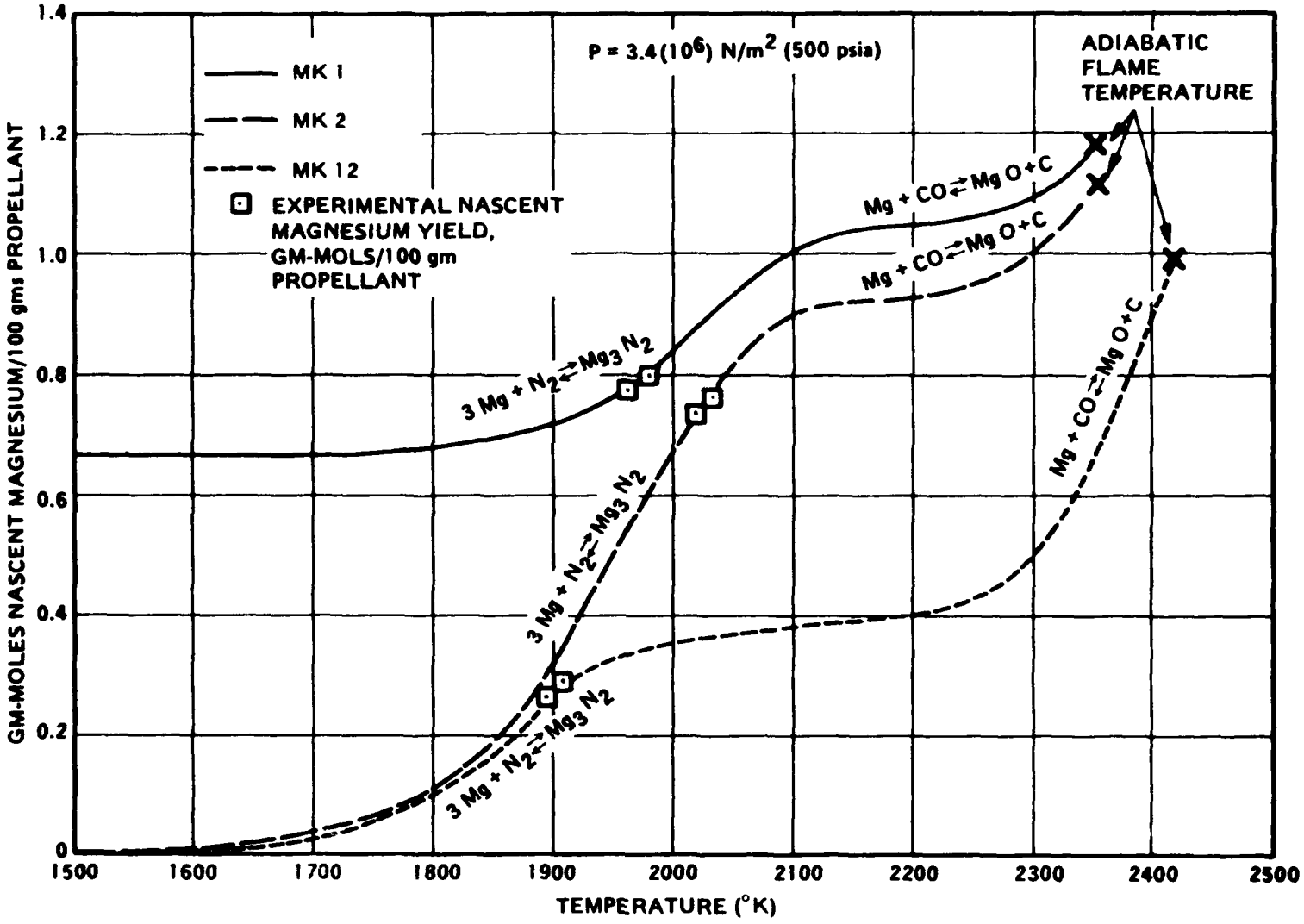

Figure 35. Thermodynamically Predicted Gram-Moles of Nascent Magnesium as a Function of Temperature for MK1, MK2, and MK12

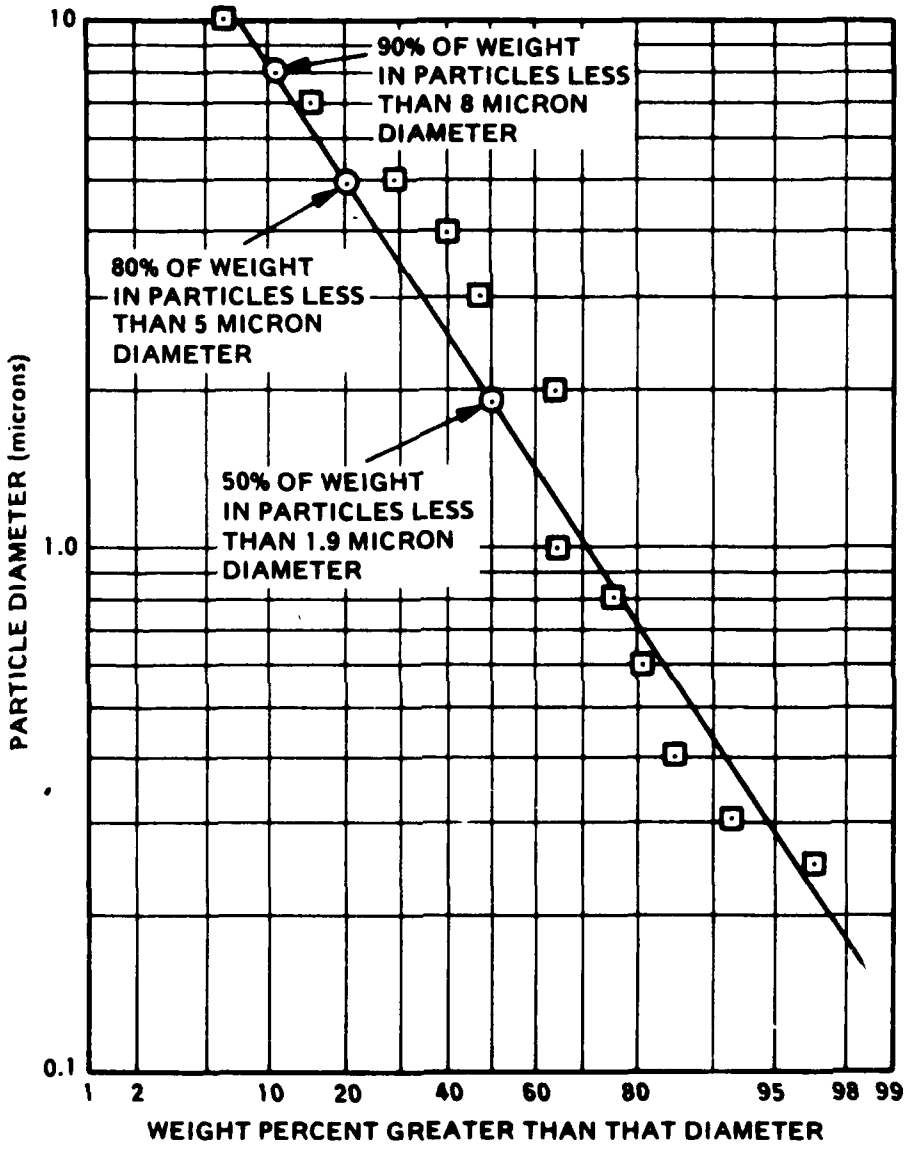

Figure 36. Particle Size Distribution of Carbon Particles Collected from 500 psi Bomb Combustion of Propellant MK1

E. SINGLE-PARTICLE BURNING STUDIES

1. Magnesium

A very brief experimental study of single-particle magnesium combustion was made using the Atlantic Research Corporation flat-flame burner technique. Particles ($d \sim 50$ μm) were injected into hot burner gases, $T_g = 2200 \pm 200$°K. As expceted, the burning times of even such large particles are very short; indeed, so short (<0.5 msec) that they could not be measured quantitatively. The preignition delays, on the other hand, were relatively long, several milliseconds. This may appear surprising, since magnesium has been reported to have a very low ignition temperature, below 1000°K (Ref. 15). The explanation, no doubt lies in the fact that, in this technique, cold (room temperature) magnesium is injected into hot gases, and it must melt before ignition ($T_m = 924$°K). Thus, in addition to the heat-up time from room temperature to ignition temperature, the preignition delay must also include the time, t_m, necessary to melt the particle:

$$t_{TOTAL} = t_{273 \rightarrow 924} + t_m = \frac{\rho d^2 \left[c_{p,Mg} (924 - 273) + \Delta H_{melt} \right]}{12\, k\, (T_{gas} - 924)} \qquad (4)$$

where ρ is the particle density and k is the thermal conductivity of the gas. Substitution of realistic numbers for the various properties in the above equation indicates that approximately 2.5 msec is required to heat a 50μ magnesium particle to its melting point and melt it.

2. Magnesium Nitride

As indicated earlier, it appears likely that magnesium nitride particles are produced in the fuel-rich combustion environment of the primary motor with the formulations of interest; thus, some knowledge of the manner in which magensium nitride burns in an oxygen-containing atmosphere (e.g., a ramburner) is of interest. Accordingly, a brief study of the ignition and combustion of magnesium nitride single particles in the Atlantic Research Corporation flat-flame burner was carried out as part

of this program. A sample of lump magnesium nitride was purchased from a commercial supplier and ground to a fine powder with a mortar and pestle. A nominal 35 to 40 micron cut of this material was then sieved from the ground product for study. Some of this 35 to 40 micron material appeared to be single crystals, but much of it consisted of a number of smaller crystals attached very tightly together (so tightly that vigorous mechanical scrubbing did not break them up). It should be pointed out that the particle size quoted is nominal, since many of the particles were far from spherical or cubic, some being long rods with aspect ratios in excess of 4 to 1.

Ignition and combustion of these particles was carried out at a flat-flame burner temperature of 2350 $\pm$ 100°K at oxygen levels of 5.4 to 20.8%. Ignition delay time was calculated from the distance above the point of injection of the particle into the flame to the appearance of a sudden brightness. This ignition delay time did not appear to be particularly sensitive to the oxygen level, being approximately 3.5 $\pm$ 1.0 msec. In light of the observation that the particles generally have fairly large aspect ratios and thus are likely to have equivalent radii of 20 to 30 microns, we performed heatup calculations for such size particles, initially at 298°K placed in a 2300°K environment. These calculations, which neglect any reaction contributions, indicate that for an ignition time of 3.5 msec, the particle ignition temperatures must be somewhere in the range of 1100 to 1600°K. Burn time data were obtained by observation of burning particle streaks from initial brightness to burn out, through a high speed light chopper wheel. Results of these observations are plotted in Figure 37. As would be expected, burn time decreases strongly with increasing oxygen content, from 6 msec at y_{O_2} = 0.054 to 2.7 msec at y_{O_2} = 0.208.

F. THEORETICAL EFFECT OF MAGNESIUM VAPOR ON PLUME IGNITION

A theoretical examination of the effects of the presence of magnesium vapor on the ignition of a fuel-rich exhaust plume (containing CO and H_2 as other gaseous fuels) mixing with a co-flowing air stream was

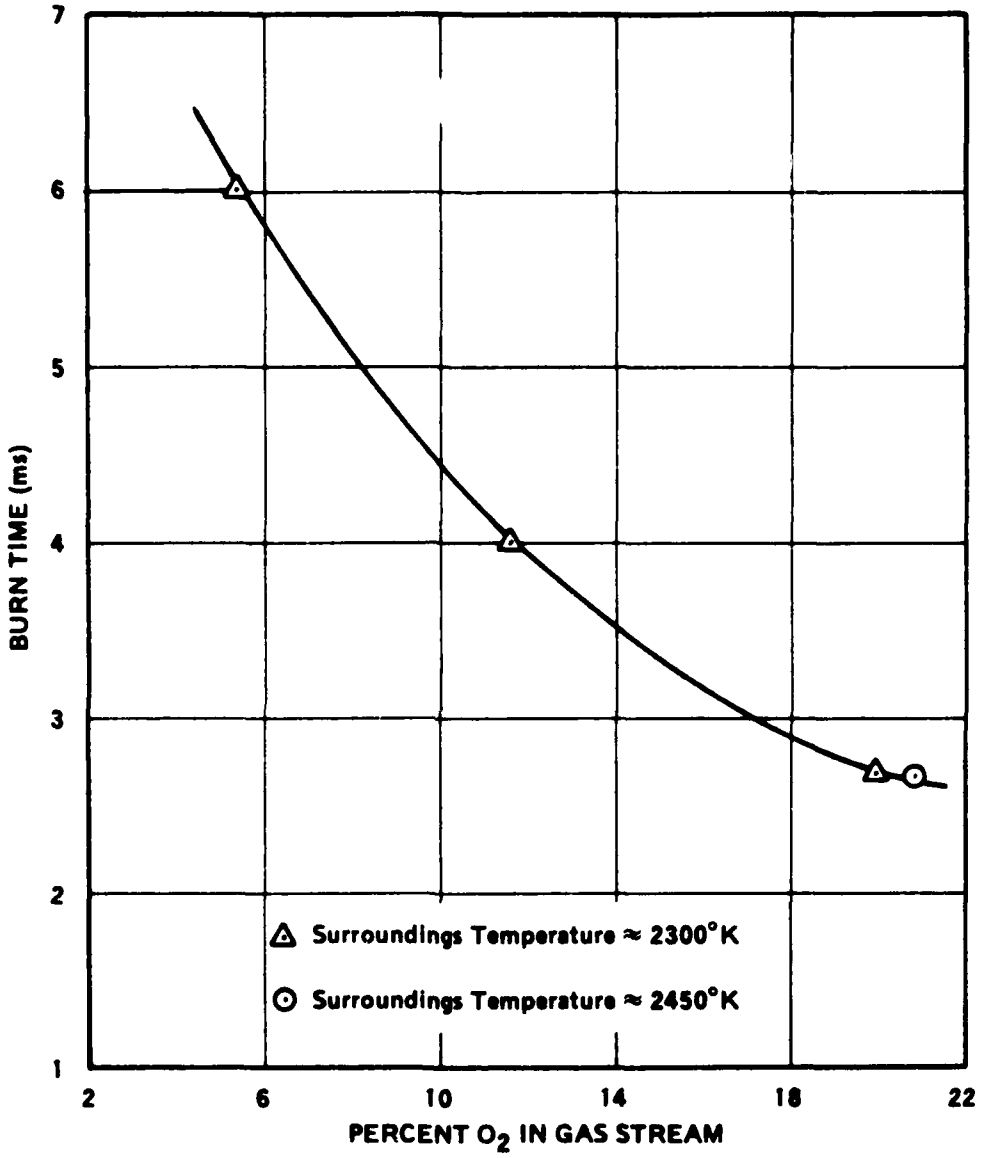

Figure 37. Magnesium Nitride (35-40 micron) Burning Times.

carried out with aid of a modified version of the Aerochem Computer Program for Nonequilibrium Rocket Plume Predictions (Ref. 16). This program treats parallel turbulent mixing between concentric chemically reacting streams, with both mixing and chemical kinetic processes being treated. Outputs of the calculations include detailed temperature and composition profiles in the mixing/combusting plume, and percent of any given fuel burned at any given axial station down the plume.

In the only case examined, the primary motor propellant is a 15/35/50 HTPB/HMX/Magnesium formulation burning at 200 psia. The product stream is expanded through a primary motor nozzle to 15 psia, at which point it enters a coflowing 500°K air stream (also at 15 psia) in a six-inch diameter afterburner with a 5-inch diameter throat. An air/fuel ratio of six is set. Under these conditions, the total mass flow of the air plus fuel streams is (assuming 100% afterburning efficiency) 5.1 lb-m/sec, with a primary motor exhaust flow of 0.73 lb-m/sec. The air velocity is 575 feet/second, while the fuel jet velocity (and initial diameter) is dependent on assumptions regarding the primary motor exhaust temperature, which depends on primary motor combustion inefficiencies and heat losses. For adiabatic, 100% efficient combustion in the primary motor, the fuel jet exhaust temperature is 1871°K, with a resultant jet velocity of 5400 ft/sec and jet radius of 0.058 ft (0.7 inches). For a fuel jet exhaust temperature of 1200°K (a second condition examined), the jet velocity is 4350 ft/sec and the jet radius is 0.052 ft (0.62 inches).

The plume calculations have been carried out under several sets of assumptions. In all cases, the effects of condensed phases are neglected (decoupled) since the Aerochem program cannot treat condensed phases. The sets of assumptions examined are:

Set I: 1871°K primary jet assumed. Standard kinetics used for H_2 and CO combustion reactions. (See Table 23.) Magnesium reactions neglected.

TABLE 23. KINETIC RATE EXPRESSIONS USED FOR HYDROGEN AND CARBON MONOXIDE COMBUSTION REACTIONS IN *PLUME IGNITION/COMBUSTION CALCULATIONS*

$$k_{forward} = A \exp [B/RT]/T^n$$

Reaction	A*	N	B
$OH + H_2 \leftrightharpoons H_2O + H$	$3.46\ (10^{-11})$	0	-5150
$H + O_2 \leftrightharpoons OH + O$	$3.72\ (10^{-10})$	0	-16800
$O + H_2 \leftrightharpoons OH + H$	$2.88\ (10^{-11})$	0	-9450
$OH + CO \rightleftarrows CO_2 + H$	$9.30\ (10^{-13})$	0	-1080
$H_2O + O \rightleftarrows OH + OH$	$9.50\ (10^{-11})$	0	-18000
$CO + O + M \rightleftarrows CO_2 + M$	$1.39\ (10^{-32})$	0	-1800
$H + H + M \rightleftarrows H_2 + M$	$5.50\ (10^{-30})$	1	0
$O + O + M \rightleftarrows O_2 + M$	$1.00\ (10^{-29})$	1	0
$H + OH + M \rightleftarrows H_2O + M$	$2.76\ (10^{-31})$	0	0
$O + H + M \rightleftarrows OH + M$	$1.00\ (10^{-29})$	1	0
$H + O_2 + M \rightleftarrows HO_2 + M$	$4.40\ (10^{-33})$	0	+1000

*CC-molecule-sec units

Set II: Same as Set I except 1200°K primary jet assumed.

Set III: Same as Set II except magnesium reaction kinetics are included. The additional reactions included are Mg(gas) + $O_2 \rightleftarrows$ MgO(gas) + O and Mg(gas) + O + M $\rightleftarrows$ MgO(gas) + M. The heat release obtained from condensation of MgO(gas) is assumed to be released immediately upon formation of MgO(gas). The rate constants for these two additional reactions were estimated to be $k = 10^{-10} \exp [-32000/RT]$ and $k = 10^{-32}$, respectively (in cc-molecule-second units)

Set IV: Same as Set III except data of Kashireninov (Ref. 17) are used to replace the rate constant for Mg(gas) + $O_2 \rightleftarrows$ MgO(g) + O(g) by $k = 3.5\ (10^{-10}) \exp [-16000/RT]$

Set V: Same as Set IV except condensation of the MgO product is neglected (thereby removing the oxide condensation heat effect).

The results of the plume calculations, in terms of percent of potential H_2O formed (representative of degree of completion of burning of the plume) versus distance from the plume origin are plotted in Figure 38. As may be seen from Curve I, at 1871°K primary jet conditions there is no noticeable ignition delay, with the plume combustion being totally mixing limited. When the assumed initial jet temperature is dropped to 1200°K, however, there is an appreciable plume ignition delay, approximately 0.5 - 0.6 feet in the absence of magnesium reactions (Curve II). Allowing magnesium reactions, as controlled by the estimated kinetic parameters (Curve III) significantly decreases the ignition delay length to about 0.3 - 0.4 feet, while use of the kinetic data of Kashireninov (Ref. 17), essentially eliminates the ignition delay, as shown by Curves IV and V. (Note that Curves IV and V are not coincident with Curve I since the mixing rates are different for the 1200°K jet and the 1871°K jet.) Thus, it appears that the presence of magnesium vapor can be quite beneficial to ignition of hydrogen and carbon monoxide in a fuel-rich plume expanding

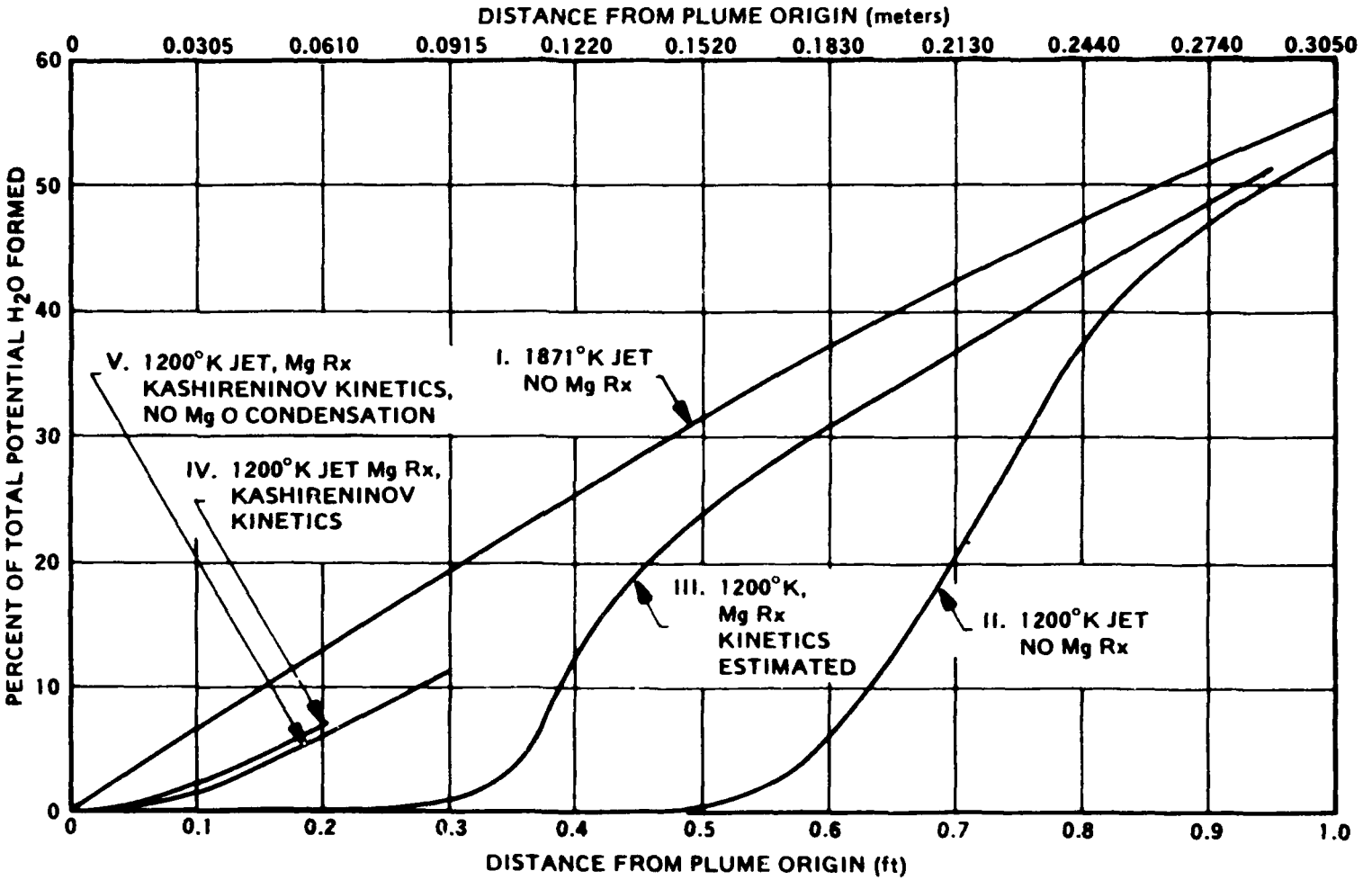

Figure 38. Results of Plume Calculations for Exhaust of 15/35/50 HTPB/HMX/Mg Formulation Mixing with 500°K at P = 1 Atmosphere

into coflowing air. Examination of detailed concentration profiles indicates, as expected, that this enhancement is due to the production of oxygen atoms by the first magnesium reaction, which is quite rapid compared to the consumption of oxygen atoms by the three-body second reaction.

G. COMBUSTION OF SELECTED CANDIDATES IN MOTORS

1. Castable Composition

Motor tests were conducted with formulations MK1, MK2, and MK12 for evaluation of their burning rate versus pressure characteristics in motors (as compared to strands), evaluation of the tendency of the exhaust streams to despoit in and plug nozzles, and evaluation of the efficiency of ejection of the combustion products (as measured in terms of percent residue left in the motors). The burning rate versus pressure data have already been presented in Section III-C; reasonable agreement of the motor data with strand data taken in the acoustic emissions strand-burning apparatus was obtained.

One motor case was employed for all motor tests despite a strong variation in grain sizes. Details of the primary motor assembly are presented in Figure 39. The motor case, designed to withstand 3000 psi operating pressure, is 9.875 inches I.D. with a length of 20.75 inches from the inside of the head wall to the outer edge of the flange, where it mates with the integral blast tube case. A 2-inch diameter blowout port and an igniter wire plug port were located near the aft end of this case, as shown. In addition, two static pressure taps (not shown) were included for measurement of primary motor pressure. A mixing aid was attached to the down stream end of the blast tube in some of the tests.

Both end-burning and center perforated grains were evaluated in tests. Grain size was varied by using inert spacers and volume limiters of various internal dimensions. In some of these tests (referred to as primary motor tests), the product stream was simply exhausted to the atmosphere, while in others (referred to as connected-pipe tests), the products were fed to an afterburner for evaluation of their afterburning

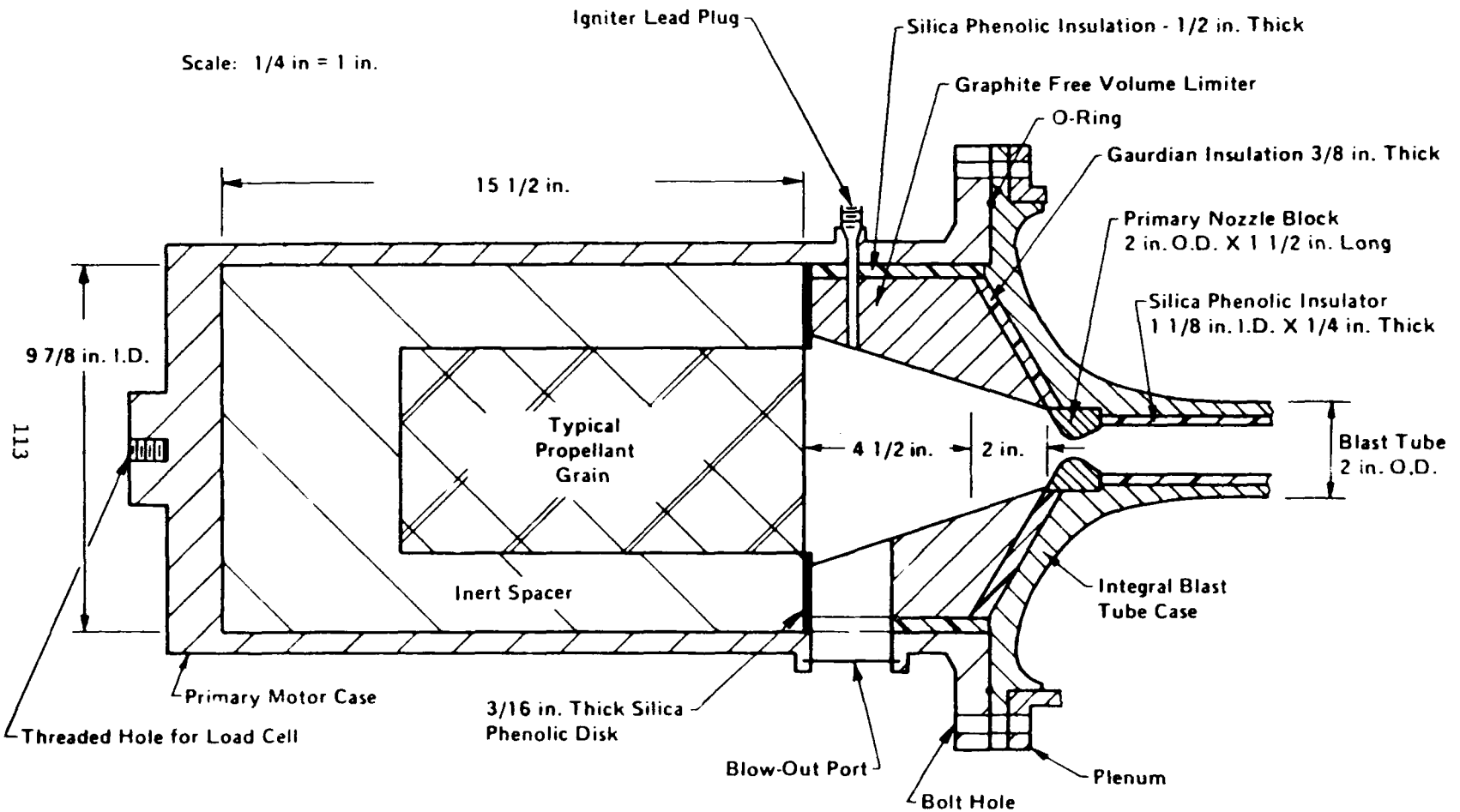

Figure 39. Primary Motor Assembly.

characteristics, to be described in a later section. A total of six motor tests were conducted with MK1, one with MK2, and three with MK12. Grain and nozzle sizes for these tests are given in Table 24. In Test Number 1P, the graphite free-volume limiter was uncoated, providing a severe heat sink to the material flowing through it; in all subsequent tests, it was coated with an insulator, to minimize this problem. Throat closure and residue level data for all tests are presented in Table 25 and Figures 40 and 41.

As may be seen, severe throat closure problems occurred for small graphite nozzles (0.25 to 0.40 inch diemater), probably due to plating out of magnesium/magnesium oxide/magnesium nitride eutectics on these nozzles. Such throat closure would obviously present a severe problem to a motor designer. However, it should be pointed out, that for practical systems, desired fuel flow rates will be such that for single-nozzle primary motors, considerably larger nozzles will be used. The two data points on the right of Figure 40, which correspond to an initial throat diameter of approximately 0.8 inches indicate that the throat closure problem rapidly disappears with increasing nozzle size. If the designer finds that he needs to use multiple nozzles to distribute fuel in a ramburner, and thus finds himself back in the less than 1/2-inch diameter nozzle throat range, substitution of asbestos-phenolic nozzles for graphite nozzles appears to provide another acceptable solution, as shown in Figure 40.

Minimizing residue left in the primary motor is obviously important in providing a useful fuel generator system, since the sensible and possibly chemical enthalpy associated with this residue is not available for utilization in the ramburner, with effective degradation of the heating value of the fuel. Table 25 and Figure 41 indicate that unacceptably high residue levels were obtained in some tests, while quite low levels (10% or less) were obtained in others. Two factors appear to be possible contributors to the differences in residue levels obtained in different tests. First, it may be seen that all tests with cylindrically perforated grains, burning in the central bore, had low residue levels. It appears reasonable that

TABLE 24. GRAIN CONFIGURATIONS AND SIZES USED IN MOTOR TESTS OF CASTABLE FORMULATIONS

Test No.*	Formulation	Grain Configuration	Length (in)	Outside Diam. (in)	Inside Diam. (in.)	Initial Throat Diam. (in.)	Nozzle Type
1 P	MK 1	End-burner	4.85	4.99	Not applicable	0.250	Graphite
2 P	MK 1	Cylindrical Perf	8.75	5.75	3.5	0.812	Graphite
401	MK 1	End-burner	5.06	5.00	Not applicable	0.305	Graphite
401 A	MK 1	End-burner	4.91	4.99	Not applicable	0.305	Graphite
402	MK 1	End-burner	5.10	4.15	Not applicable	0.285	Graphite
451	MK 1	Cylindrical Perf	8.84	5.75	3.5	0.813	Graphite
3 P	MK 2	End-burner	4.80	3.98	Not applicable	0.400	Graphite
4 P	MK 12	End-burner	2.52	5.18	Not applicable	0.275	Graphite
5 P	MK 12	End-burner	2.52	5.18	Not applicable	0.264	Asbestos-Phenolic
403	MK 12	Cylindrical Perf	2.75	4.95	2.98	0.350	Asbestos-Phenolic

* Test Numbers with "P" are tests in which products are simply exhausted to the atmosphere; others are connected-pipe ramburner tests.

TABLE 25. RESIDUE AND THROAT CLOSURE CHARACTERISTICS OF MOTOR FIRINGS OF CASTABLE FORMULATIONS

Test No.	Formulation	Average Pressure (psia)	Percent Residue	Initial Throat Area (in^2)	Percent Reduction in Throat Area During Test
1 P	MK 1	500	34.7	.0491	100
2 P	MK 1	130	4.3 **	.5178	15
401	MK 1	500	18.1	.0731	29
401 A	MK 1	480	24.9	.0731	63
402	MK 1	300	19.0	.0638	53
451	MK 1	140	2.7 **	.5191	19
3P	MK 2	158	4.6	.1257	65
4P	MK 12	540	50	.0594	100
5P	MK 12	165	36	.0547	32*
403	MK 12	120	12**	.0962	13*

* Asbestos - Phenolic Nozzles; graphite nozzles used in all other tests.

** Cylindrically perforated grain configuration; all others were end-burners.

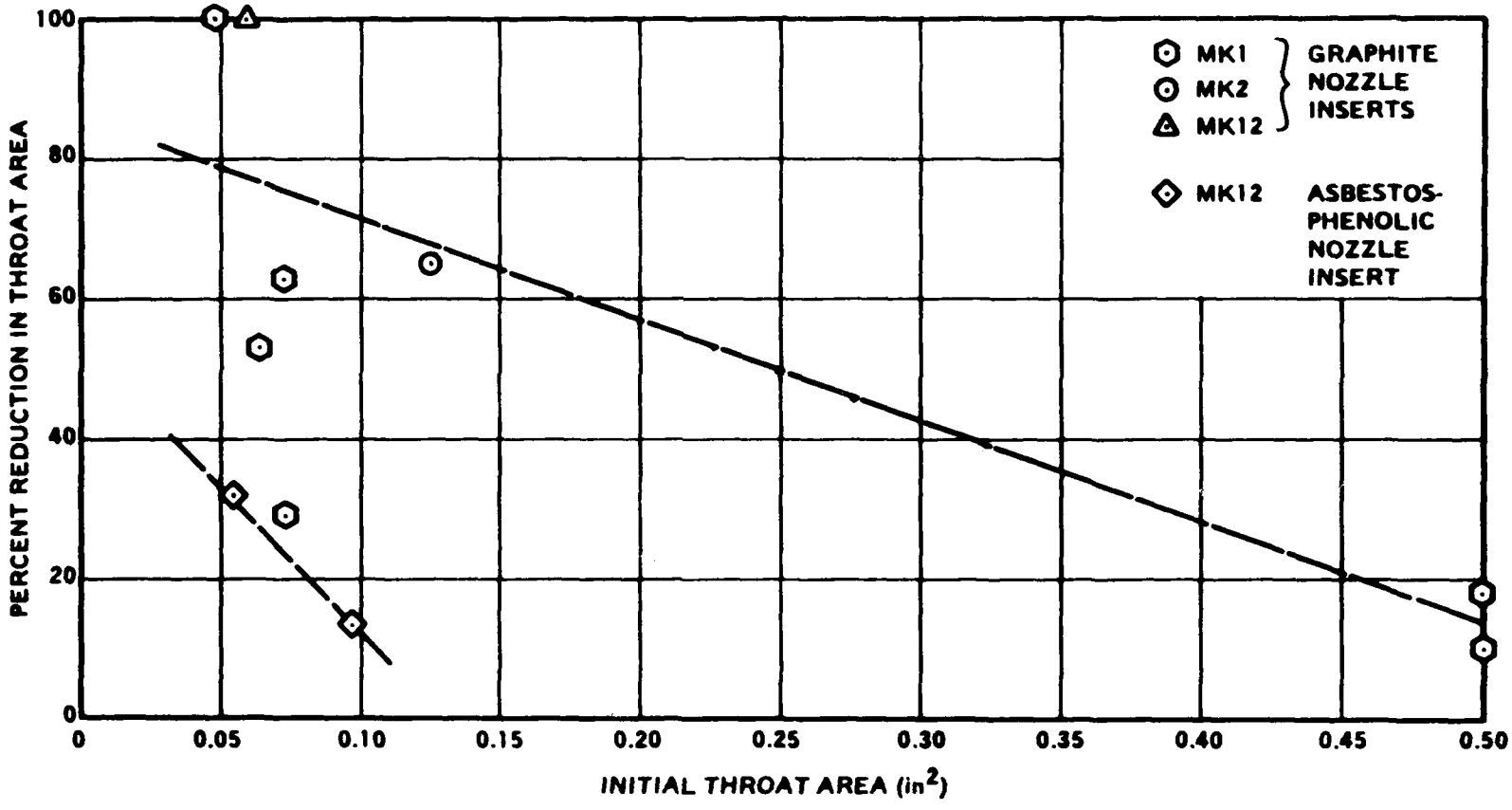

Figure 40. Throat Closures in Motor Firings of MK1, MK2, and MK12

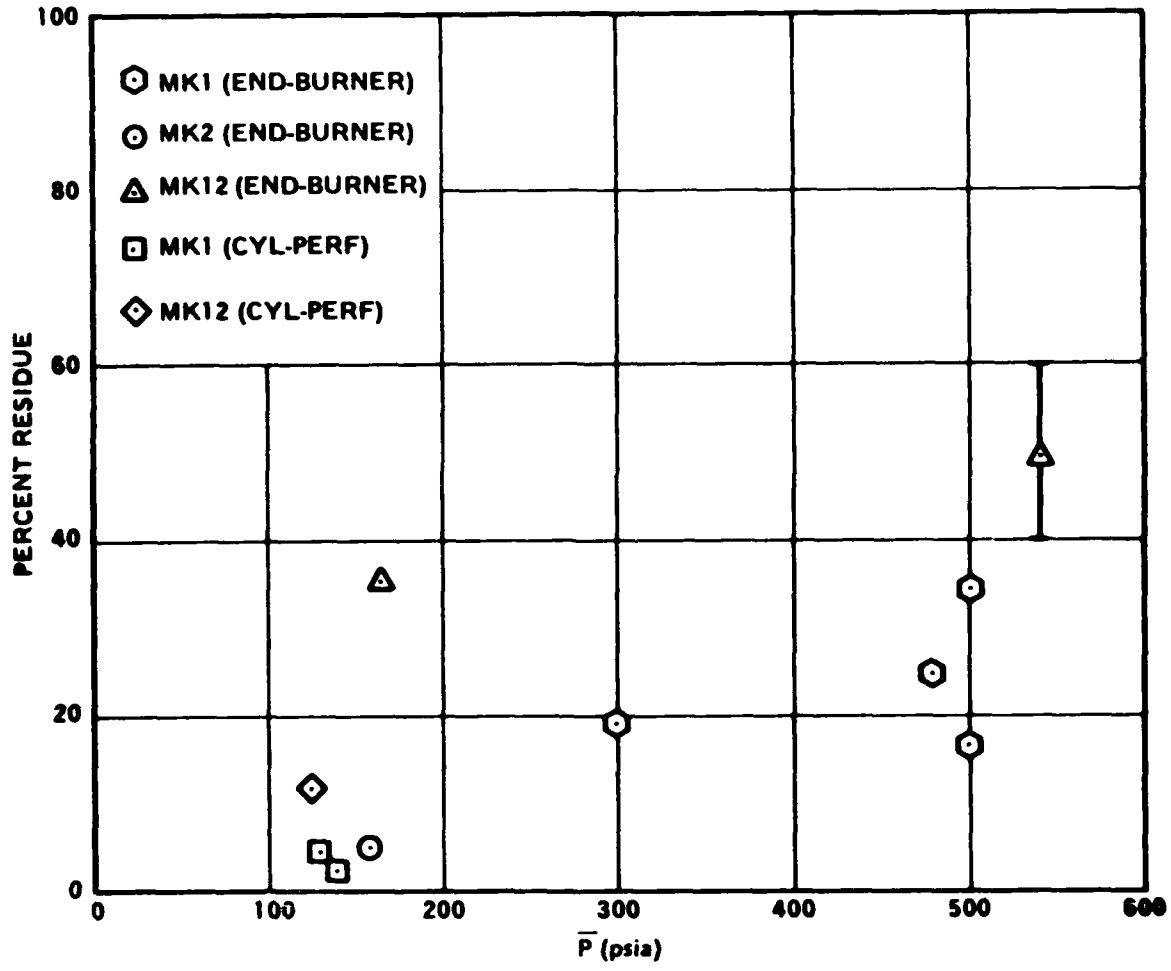

Figure 41. Residue Levels in Motor Firings of MK1, MK2, and MK12

cylindrically perforated grains should be less susceptible to residue formation than end-burning grains, since residues generally form as a growing ash structure on the burning surface which builds up by trapping carbon, magnesium oxide, and other such condensed-phase products as they are produced in the combustion zone: with cylindrically perforated grains, the sweeping action of gases moving through the grain port would be expected to tend to continuously break up this ash structure before it can form a hard clinker which cannot be dislodged.

However, it is not unequivocally clear that the dominant factor in determining the residue level is grain configuration, inasmuch as the cylindrically-perforated grain tests were all run at comparatively low pressure (100 to 150 psia), while most of the end-burner tests were run at somewhat higher pressure ($\tilde{\sim}$ 500 psia). Examination of Figure 41, in which residue level is plotted against average pressure during the test indicates a fair degree of correlation of residue level with pressure. In fact, one end-burner test conducted with MK2 at low pressure resulted in a residue level of only 5.6%. (However, another test with MK12 in an end-burning configuration at nearly the same pressure yielded a residue level of 36%.) Thus, it is not clear whether grain configuration or operating pressure level are dominant in determination of ejection efficiency, or whether (most likely) both play important roles in this area.

A series of tests was conducted in which strands of MK1 were burned at various pressures from 200 to 2200 psia, to see whether there was a critical pressure level at which residue began to form (though it is recognized that this level may be quite different for strands than for motors). Up to 1200 psia, these strands (1-inch long, 1/2-inch diameter cylinders cast in epoxy tubes) ejected completely when burned. At the next pressure level tested, 1500 psia, approximately 28% of the propellant mass was left in the epoxy tube, while at 2000 and 2200 psia, the residue levels were 40 and 47% respectively. Thus, there does appear to be a pressure effect on residue formation, at least for MK1.

A pressure effect on formation of residue, residue increasing with increasing pressure, for end-burning grains in particular, is not

unreasonable on theoretical grounds. If we assume that the flow of gases from a burning fuel-rich propellant past initiating residue clusters on the surface is such that the gas drag on the "particles" is in the Stokes Law flow regime, then the force tending to pull these clusters away from the surface is proportional to the gas velocity away from the surface, as indicated by Equations 5 through 7.

$$\text{Drag Force} = \left(\frac{\rho V^2}{2}\right) A_{cluster} C_D \tag{5}$$

$$C_D = \text{drag coefficient} = 24/\text{Reynolds Number} = \frac{24\mu}{D_{cluster} V\rho} \tag{6}$$

$$\therefore \text{Drag Force} = \frac{\rho V^2}{2} A_{cluster} \frac{24\mu}{D_{cluster}\rho V} = kV \tag{7}$$

The velocity of gases away from the surface depends upon pressure through several factors:

(1) Effect of pressure on gas density.
(2) Effect of pressure on propellant burning rate.
(3) Effect of pressure on moles of gas produced per gram of propellant.

A series of calculations has been performed for the velocity of gas flow away from the surface of MK1, MK2, and MK12 as a function of pressure under assumptions of adiabatic combustion, 20% heat loss, and 40% heat loss: results are presented in Figure 42. These calculations were performed using thermochemical equilibrium calculations to calculate the gas molar yield under the three different assumptions regarding heat loss, and using measured burning rate versus pressure data. As may be seen, gas velocity away from the surface decreases strongly with increasing pressure, particularly in the 100 to 500 psia range of interest, lending strong support to the idea that pressure is a critical facator in the formation of residue.

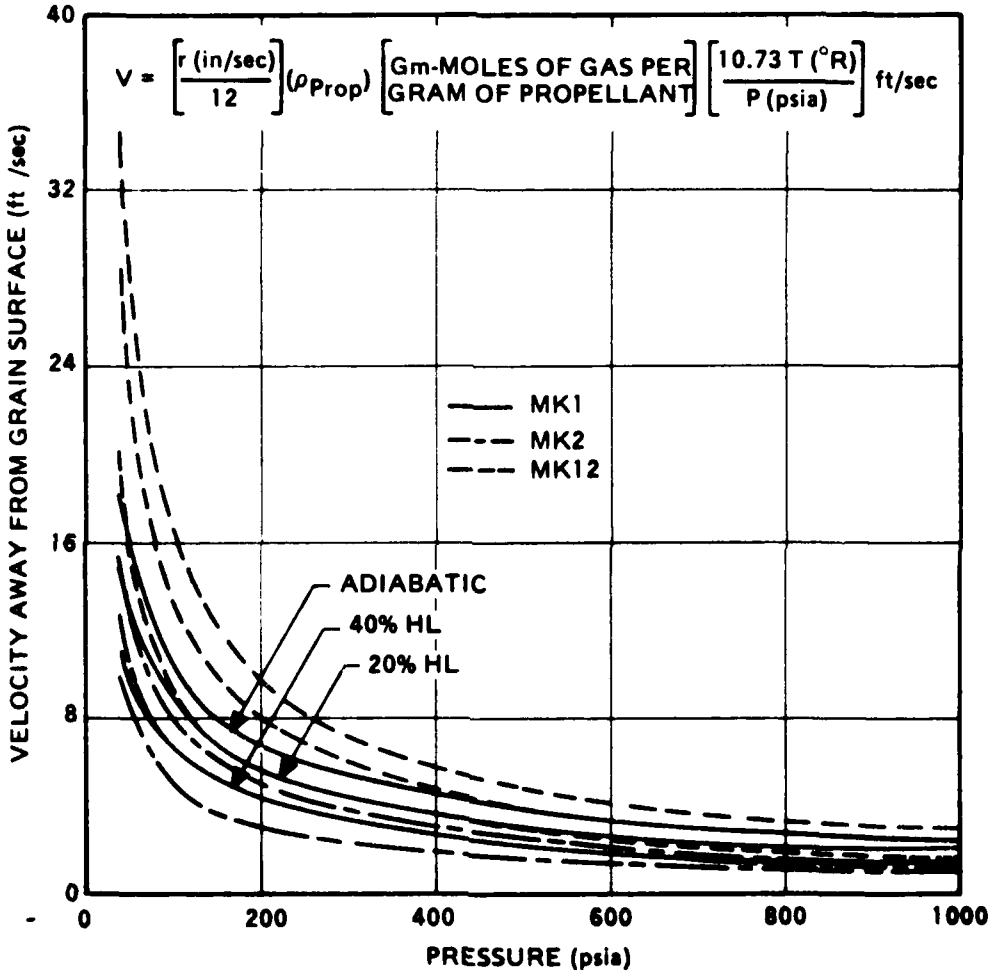

Figure 42. Velocity of Gases Away from Surface of Burning Propellant Versus Pressure

An alternate possible explanation for increase in residue with increasing pressure is demonstrated in Figure 43. A series of thermochemical calculations were run for MK1 with the system enthalpy being fixed at various levels, representing different levels of heat loss (either due to combustion inefficiencies, or losses to the massive hardware used). These calculations permitted definition of the percent heat loss level which would result in the appearance of condensed-phase (liquid) magnesium in the combustion products. These calculations were carried out at various pressure levels from 100 to 1000 psia. As may be seen, the percent heat loss required for appearance of magnesium liquid decreases with increasing pressure. Since the appearance of liquid magnesium (in combination with carbon and solid magnesium oxide) may be a key to producing a clinker structure, this mechanism may lead to increased residue with increasing pressure.

Analyses of residue from one test with MK1 (Test 1P) and one test with MK12 (Test 5P) were carried out to determine what type of material (particularly in terms of potential heating value) was being left in the primary motor in tests yielding appreciable amounts of residue. With the MK1 propellant, the residue was found to be approximately 22% carbon and 78% magnesium oxide, with essentially no unreacted magnesium being present. Comparison with the amounts of carbon and magnesium oxide which should have been produced thermodynamically by the motor indicates that about 70% of the carbon product and 75% of the magnesium oxide product remained in the motor. The chemical enthalpy available in the carbon left behind represents approximately 11% of the total theoretical heating value of MK1. In addition, sensible heat, which would have contributed to heating of air in a ramburner, was lost.

With the MK12 propellant, the residue was approximately 27% carbon, 12% MgO, 18% Al_2O_3 (with perhaps some combination of the MgO and Al_2O_3 to $MgAl_2O_4$, spinel), 32% aluminum, and 11% miscellaneous (probably nitrides and carbides). Thus, approximately half the carbon and nearly all of the aluminum remained in the residue, with only a small

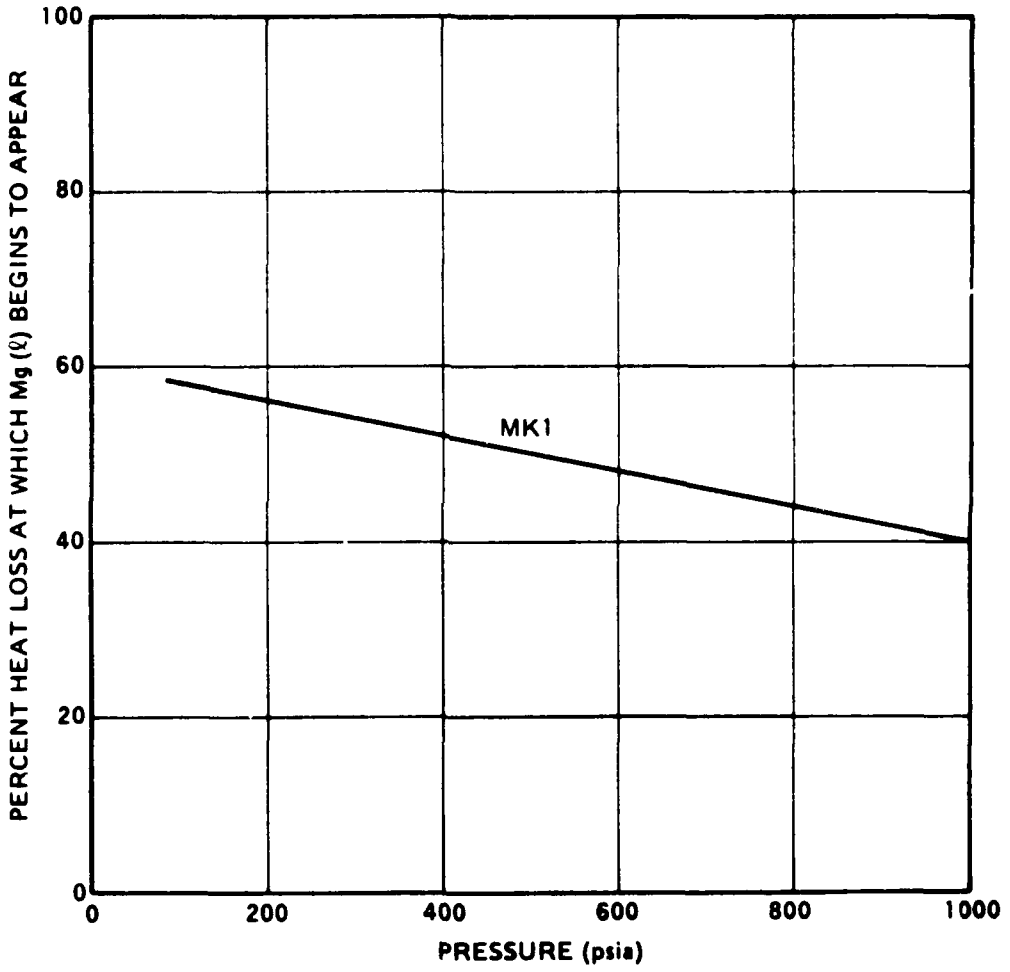

Figure 43. Alternate Possible Explanation for Increase in Residue Level with Increasing Pressure

fraction of the magnesium being left behind. The carbon and magnesium in the slag represent approximately 30% of the potential heating value of MK12.

2. Pressed Compositions

Two TK1 propellant grains were fired in motor tests during this program, one in a test in which the exhaust was simply dumped into the atmosphere and one in which the exhaust was burned in a ramburner in a connected-pipe air facility test. The grains employed were end-burners, 2.05 inches in diameter and approximatley 7 inches long, weighing approximately 1.5 pounds each. Both were designed to operate at about 200 to 300 psia, with a planned burn time of approximately 10 seconds, and a fuel-flow rate of 0.15 pounds/second, using an asbestos-phenolic nozzle of 0.25 inch diameter.

Unfortunately, it appears that in both tests, the propellant either sideburned (liner separation from the propellant), or cracked upon ignition, leading to much higher than planned surface area early in the test (with consequent attainment of much higher pressure and mass expulsion rate early in the test) with subsequent rapid decay of pressure and mass expulsion rate as the propellant consumed itself. In the first test, the residue level was approximately 13%, while in the second (connected-pipe air facility) test, the residue was 10%. Pressure-time traces for the first 8 seconds of each test are shown in Figure 44. The propellant continued to eject at a very low level for several seconds beyond this time period. Depletion of funds prevented further examination of the problem and attempts to avoid it. However, it should be pointed out that a formulation of similar composition (slightly lower heating value) was successfully fired in two tests on an Internal Research and Development Program: accordingly, it is felt that further effort would result in successful firing of motors using the TK1 formulation.

H. CONNECTED-PIPE AFTERBURNER TESTS

1. Castable Compositions

A total of five connected-pipe air-augmented rocket tests

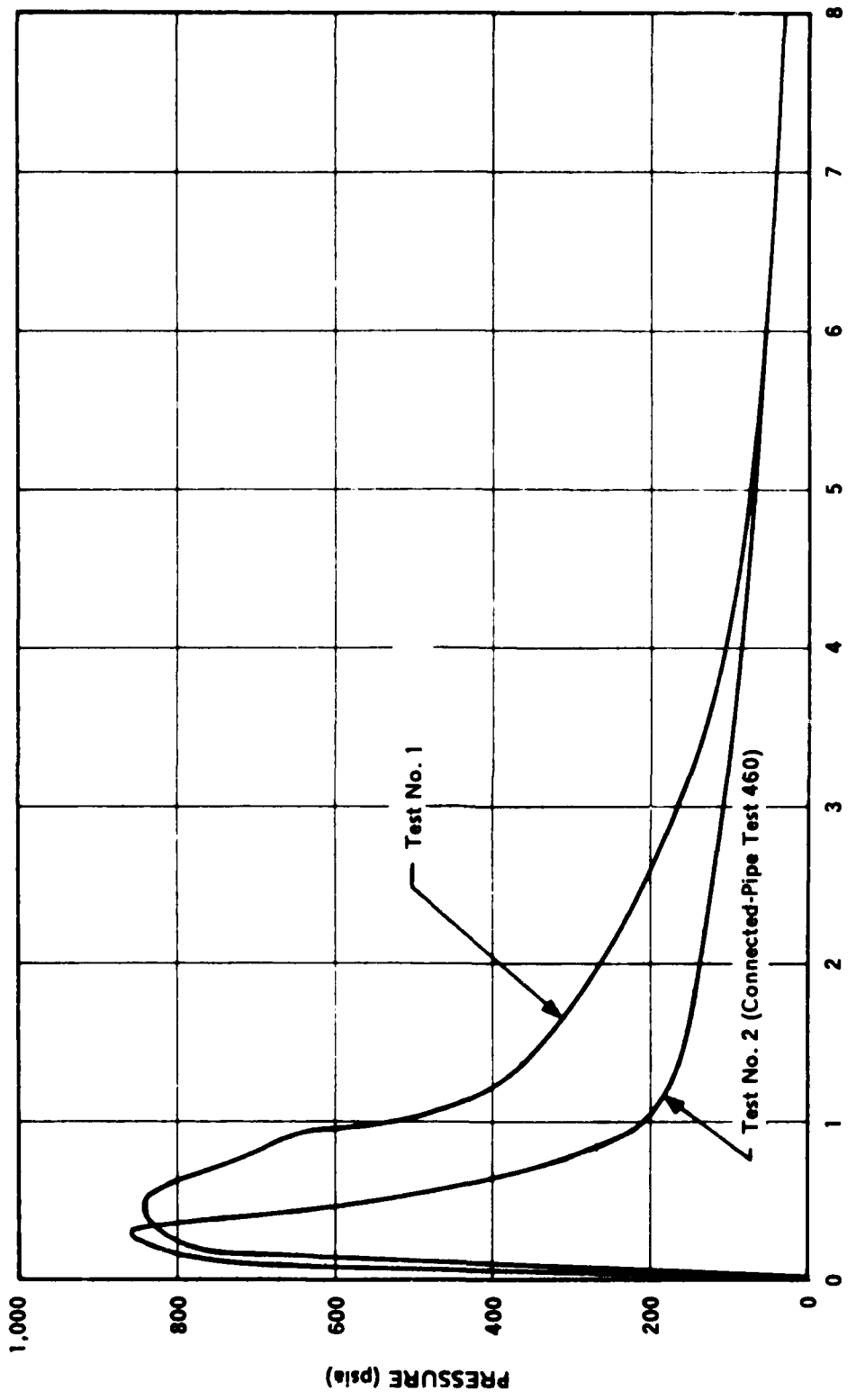

Figure 44. Pressure-Time Traces for Two Motor Tests With TK1.

were carried out with the castable Mg-loaded fuel-rich propellants formulated during this program. These tests were conducted at test conditions highly adverse to efficient afterburning (low pressure, high air/fuel ratio), conditions under which state-of-the-art boron formulations do not burn well. Four of these test were conducted with MK1 grains (Tests 401, 401A, 402, 451) and one with an MK12 grain (Test 403). Grain sizes for these tests were presented earlier in Section III-G, as was a description of the primary motor hardware.

The fuel-rich solid propellant motors of MK1 and MK12 were fired into a secondary duct where the primary rocket exhuast mixed and burned with air injected coaxially from a high-pressure blowdown facility. (Desired air temperature was achieved by passage of part of the air through a pebble-bed heat exchanger.) Static pressures in the secondary duct just upstream of the afterburner nozzle were measured and used in combination with measured air flow rate and total temperature and propellant flow rate (determinable from metering chamber measurements of pressure as described later) to determine the efficiency of mixing and combustion in the afterburner. In addition, force balance measurements were made and used with the air and propellant mass flow rates for an independent determination of afterburning efficiency. Afterburner tube outside wall temperature measurements were also made to permit correction of efficiency data for heat loss to the uninsulated nickel afterburner tube used in this study.

A schematic drawing of the test hardware employed for the connected pipe tests is presented as Figure 45. As shown, the entire test hardware assembly was suspended in pendulum fashion from a knuckle joint near the top end of the hot air downpipe, the knuckle joint permitting the entire test assembly to swing in one dimension through up to 1/2 degree of arc. Fastened to the end of this downpipe was a plenum, open at both ends. The fully assembled primary motor (including metering chamber and mixing/flameholding aid) bolted to the upstream side of the plenum. The boss on the front end of this motor was sized such that a load cell fastened to it just contacted a stationary thrust backstop when the downpipe was exactly

Figure 45. Schematic of Primary Motor-Ramburner Test Hardware

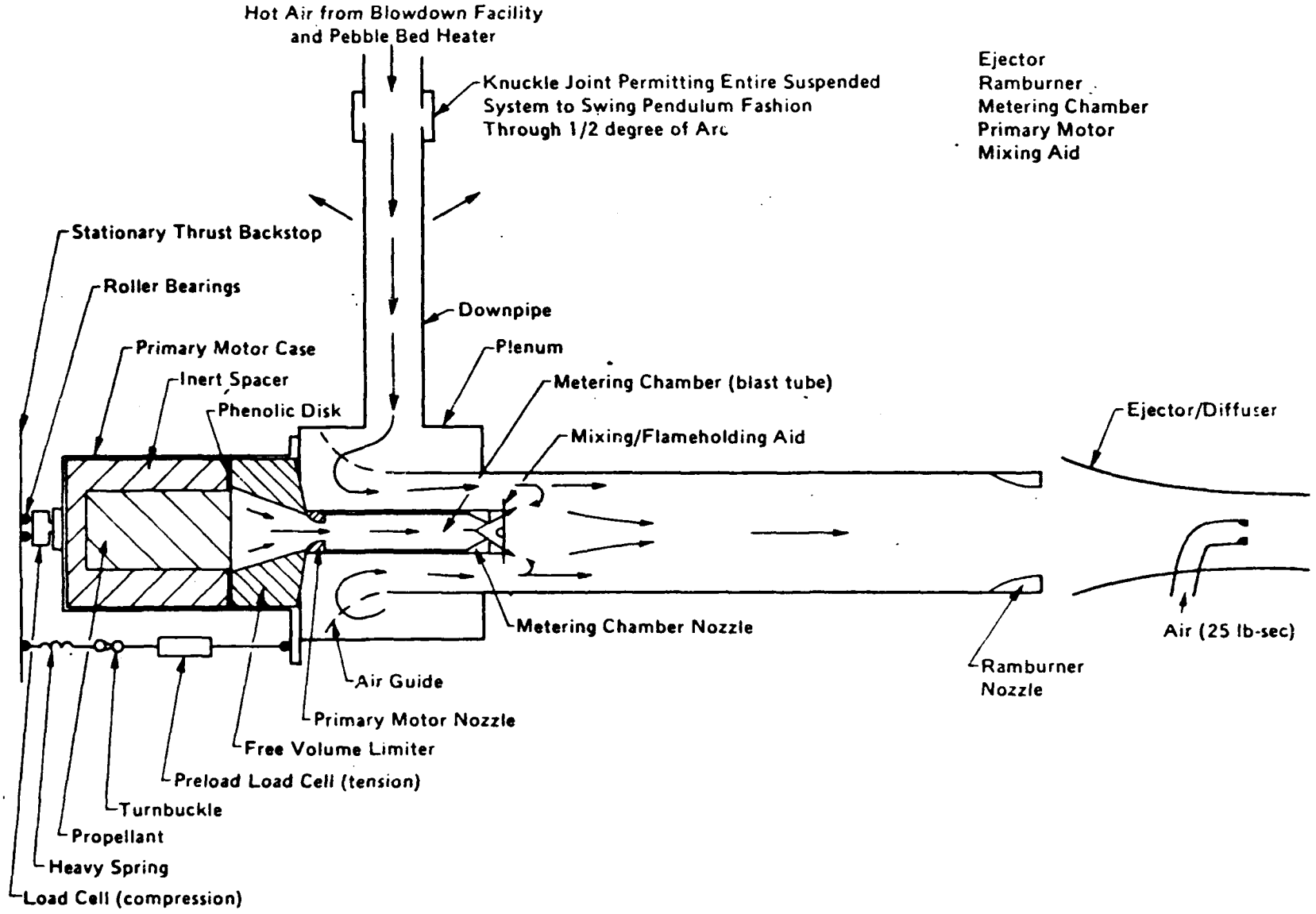

vertical. This thrust backstop included a thrust plate mounted on a roller bearing to permit vertical movement of the entire assembly resulting from thermal growth of the downpipe as it heated up. The system was so balanced that in the absence of operation of the motor or ejector/diffuser, the above mentioned load cell received a positive compressive load. However, with the ejector/diffuser operating and the primary motor not operating (the ejector was activated several seconds before ignition), the ramburner base pressure reduction was sufficient to result in a net force away from the stationary mount; consequently, in tests where the ejector/diffuser was employed, a "preload" load cell operating in tension was added to the system. As may be seen, fuel generator (primary motor) products exhausted from the fuel generator through a blast tube which carried them to a throat where they passed through the mixing/flameholding aid into a coaxially flowing air stream. (Air from the downpipe was passed through an air guide providing a uniform coaxial flow around the blast tube.) The two streams were then mixed and burned in an afterburner tube and exhausted through a sonic nozzle. Since the afterburner operating pressure in these tests was sufficiently low to cause unchoking of the afterburner for an ambient pressure downstream of the nozzle of 14.7 psia, the ejector/diffuser was used in these tests to lower the base pressure sufficiently to insure choked afterburner operation. The ejector, which was mounted on the ground, was separated from this assembly by a small gap.

The outside diameter of the blast tube, extending through the plenum into the ramburner, was 2.0 inches. This tube was constructed of stainless steel with a wall thickness of 3/16 inches. A silica-phenolic tube of 1/4-inch wall thickness was slipped inside this tube to thermally protect it from the hot primary motor exhuast products. The length of this blast tube from the downstream side of the primary motor nozzle to the upstream edge of the metering chamber nozzle was 8.75 inches. The metering chamber nozzle, located at the end of the blast tube was machined from a 1.625 inch O.D., 1.125-inch long graphite cylinder. This nozzle insert was machined to taper smoothly from the silica-phenolic tube inside diameter

(1.125 inches) to the desired throat diameter with no further expansion (sonic throat). In all tests except Test 451, a mixing/flameholding aid, described later in more detail was attached to the end of the blast tube.

As mentioned earlier, air of the desired temperature (nominally 900°R) was brought into the system by means of the downpipe from which the entire test system was suspended. This pipe was precisely at right angles to the ramburner axis and the system pivot point was on the centerline of this pipe, with the result that thrust generated by the system did not have to be corrected for air inlet momentum in calculation of system performance. The air leaving the downpipe entered an annular section around a tube with the same inside diameter as the ramburner. From this annulus it passed through a high resistance (large pressure drop) perforated grid, turning into the annular section between the above-mentioned tube and the blast tube. This annular section of constant cross-sectional area extended 8 inches to the end of the blast tube and an additional 2-1/2 inches to the spoiler disk on the mixing/flameholding aid. A picture of this aid, which screwed onto the end of the blast tube, just downstream of the metering chamber nozzle, is shown in Figure 46. This aid was a copy of the one developed by Marquardt Corporation in slurry ramjet testing and used previously by Atlantic Research with beneficial results. The barrel and wedge converted the primary exhaust to a subsonic stream and diverted it away from the centerline into the coaxially flowing air. The serrated disk spoiled the airstream near the center of the ramburner, causing it to recirculate (entraining at least part of the primary exhaust) and thereby serving as a piloting flameholder. The outer diameter of the serrated disk was 3.75 inches, resulting in blockage of approximately 25% of the air flow passage around the blast tube. In the aforementioned previous Atlantic Research experience with this aid, difficulty in avoiding burning up of the aid was encountered. In that work a stainless steel barrel was used, with failure generally occurring in this region. Accordingly, for the current program, the barrel was made of molybdenum and the wedge of silver-impregnated tungsten.

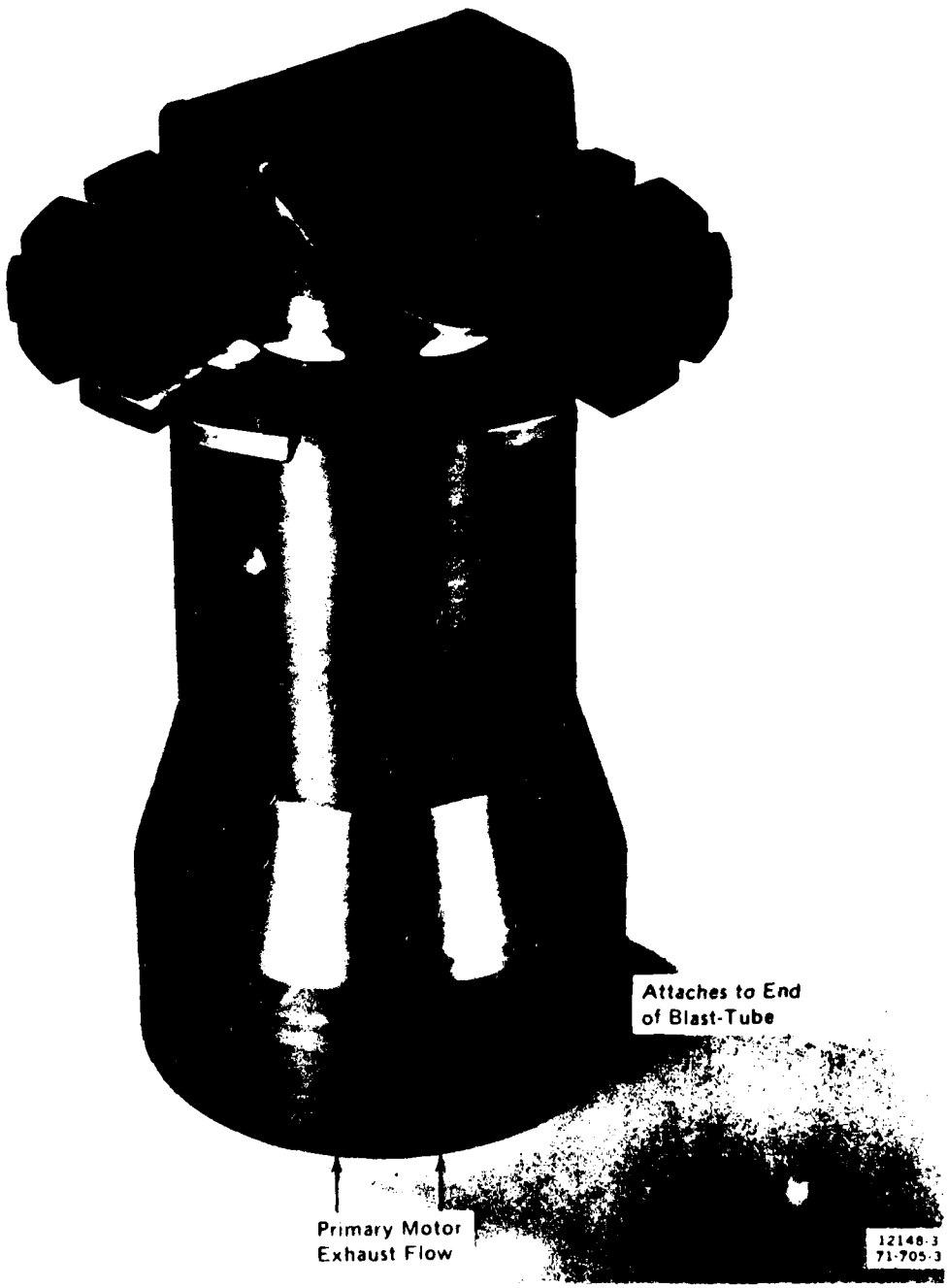

Figure 46. Mixing/Flameholding Aid used in this Study

The ramburner chamber itself, which was attached to the downstream side of the plenum by means of Marmon flanges and a Marmon clamp, was a 43.5-inch long, 5.89-inch I.D., 0.33-inch thick nickel pipe. The nozzle housing for the ramburner nozzle was constructed of stainless steel, with the nozzle insert being made of graphite. The overall length of the nozzle package (which fastened to the ramburner tube with a Marmon clamp arrangement) was 3.4 inches. The nominal nozzle throat diameter was 4.62 inches. The graphite insert tapered from the ramburner tube inside diameter to this throat diameter in approximately 2 inches, the remainder of the nozzle being constant area (sonic nozzle).

The end of the mixing/flameholding aid extended approximately 3.6 inches into the ramburner tube. Thus, the effective length of the ramburner was approximately 40 inches and the L* was 65 inches (nominal residence time of 5 milliseconds).

During each test, up to 48 channels of data were continuously measured and recorded on three Honeywell Model 1508 Visicorders with M-100-350 Galvanometers providing flat frequency response up to 60 cycles per second. These data were read from the visicorder traces at intervals selected as needed throughout each test by means of a Data Scaler Model 400. Two basic types of measuring devices were employed: (1) strain gauges (load cells and pressure transducers); and (2) thermocouples. Four-step calibrations were used to convert strain-gauge measurements to engineering unit data, while manufacturers calibrations and/or standard thermocouple EMF tables were used to obtain engineering unit data from the thermocouple traces. The quantities measured continuously during each test are listed in Table 26. In addition, the following pretest and post-test measurements were made:

(1) Initial propellant weight.
(2) Residue weight.
(3) Initial metering chamber throat diameter.
(4) Final metering chamber throat diameter.
(5) Initial ramburner throat diameter.
(6) Final ramburner throat diameter.

TABLE 26. PARAMETERS MEASURED CONTINUOUSLY DURING EACH CONNECTED-PIPE RAMBURNER TEST.

A.	Static Pressure Upstream of Air Mass Flow Venturi	2 channels
B.	Total Temperature Upstream of Air Mass Flow Venturi	2 channels
C.	Air Total Temperature At Plenum	2 channels
D.	Primary Motor Static Pressure	2 channels
E.	Primary Motor Total Temperature	0 to 2 channels
F.	Metering Chamber Static Pressure	2 channels
G.	Metering Chamber Total Temperature	0 to 2 channels
H.	Compressive force on Primary Load Cell	2 channels
I.	Tension Force on Preload Load Cell	2 channels
J.	Pressure on Base of Ramburner Nozzle	4 channels
K.	Static Wall Pressure in Ramburner 2" Upstream of Nozzle Entrance	4 channels
L.	Static Wall Pressure in Ramburner 10" Upstream of Nozzle Entrance	1 or 2 channels
M.	Static Wall Pressure in Ramburner 18" Upstream of Nozzle Entrance	2 channels
N.	Static Wall Pressure in Ramburner 26" Upstream of Nozzle Entrance	2 channels
O.	Static Wall Pressure in Ramburner 34" Upstream of Nozzle Entrance	2 channels
P.	Outside Ramburner Wall Temperature 4" Upstream of Nozzle Entrance	Up to 4 channels
Q.	Outside Ramburner Wall Temperature 12" Upstream of Nozzle Entrance	Up to 2 channels
R.	Outside Ramburner Wall Temperature 20" Upstream of Nozzle Entrance	Up to 2 channels
S.	Outside Ramburner Wall Temperature 28" Upstream of Nozzle Entrance	Up to 2 channels
T.	Outside Ramburner Wall Temperature 36" Upstream of Nozzle Entrance	Up to 4 channels

(7) Ambient pressure.

(8) Air total temperature at the aft end of the ramburner (prior to ignition).

Measurements of pressure and temperature upstream of the air mass flow venturi were used straightforwardly for calculation of instantaneous air mass flow rate throughout each test. Initial and final propellant weight, initial and final metering chamber throat diameter and primary motor pressure versus time data were used to calculate instantaneous fuel flow rate, assuming a primary motor C* independent of time and assuming a linear variation of throat area with time from initial area to final area.

Once the fuel flow rate and air flow rate were determined, they were used in combination with the measured air total temperature at the plenum, the measured ramburner static pressure, and a thermodynamic equilibrium computer program (or tabular lookup) for determination of theoretical ramburner flame temperature, polytropic constant for expansion of the mixed, burned stream from the ramburner to the ramburner nozzle throat, and throat molecular weight. The fuel and air mass flow rates were then used in combination with the static wall pressure just upstream of the ramburner nozzle, the nozzle throat area, an assumed or calibrated nozzle discharge coefficient (representing the deviation of mass flow rate from that to be expected in the absence of boundary layer effects) and the aforementioned polytropic constant and throat molecular weight to determine actual ramburner product total temperature. Alternatively, a force balance, using the force data from the two load cells, the measured pressure on the ramburner nozzle base, and ambient pressure, could be used to calculate the vacuum sonic thrust generated. From this quantity, along with the nozzle area, discharge coefficient, polytropic constant, and throat molecular weight, an alternate calculation of actual total temperature in the ramburner could be made. In general it was found that use of static wall pressure data at the end of the ramburner was more reliable than the force balance procedure.

The ramburner outside wall temperature versus time data was used with the known thermal capacitance properties of the ramburner to estimate the rate of heat loss from the stream flowing through the ramburner at any given time. This heat loss rate was then used in combination with the total mass flow rate through the ramburner and the thermodynamically calculated heat capacity of the burned air/fuel mixture to calculate a stream temperature loss due to heat transfer to the ramburner walls, and this latter quantity was then added to the calculated actual total temperature to yield a "delivered adiabatic ramburner stream total temperature." Finally, this temperature was combined with the theoretical ramburner stream total temperature and the measured air temperature to yield a temperature-rise efficiency.

The equations used in this data reduction procedure were:

$$WDOTA = K_{venturi} P_{venturi} / \sqrt{T_{venturi}} \tag{8}$$

$$WDOTF = (\text{Propellant Weight} - \text{Residue Weight}) \frac{P_{mc} A_{mc}}{\int P_{mc} A_{mc} d\theta} \tag{9}$$

$$TT4T = f_1(WDOTF/WDOTA,\ P4,\ TTAIR) \tag{10}$$

$$\gamma = f_2(WDOTF/WDOTA,\ P4,\ TTAIR) \tag{11}$$

$$MW = f_3(WDOTF/WDOTA,\ P4,\ TTAIR) \tag{12}$$

$$TT4P = \frac{\gamma(MW) g_c}{R} \left(\frac{2}{\gamma + 1}\right)^{(\gamma+1)/(\gamma-1)} \frac{A_t^2 K_e^2 (P4)^2}{(WDOTA + WDOTF)^2} \left[1 + \left(\frac{(\gamma-1)}{2}\right)(M4)^2\right]^{\frac{2\gamma}{\gamma-1}} \tag{13}$$

$$M4 = \frac{A_t}{A_{ramburner}} \left[\frac{2}{\gamma - 1} \left\{1 + \left(\frac{\gamma - 1}{2}\right)(M4)^2\right\}\right]^{(\gamma+1)/2(\gamma-1)} \tag{14}$$

$$\frac{dQ}{d\theta} = (\text{Ramburner Mass})(C_{p,\text{ramburner}})\frac{dT_{\text{ramburner,backside,avg}}}{d\theta} \tag{15}$$

$$(TT4P)_{\text{corrected}} = TT4P + \frac{dQ/d\theta}{(WDOTA + WDOTF)C_{p,\text{ product stream}}} \tag{16}$$

$$\eta\Delta T = \frac{(TT4P)_{\text{corrected}} - TTAIR}{TT4T - TTair} \tag{17}$$

where:

WDOTA = Air Mass Flow Rate

WDOTF = Fuel Mass Flow Rate

$K_{venturi}$ = Venturi Constant

$P_{venturi}$ = Pressure upstream of flow venturi

$T_{venturi}$ = Temperature at flow venturi

P_{mc} = Metering chamber throat area

TT4T = Theoretical total temperature for 100% efficient afterburning

γ = Theoretical specific heat ratio for 100% efficient afterburning

MW = Theoretical product molecular weight for 100% efficient afterburning

P4 = Static pressure at entrance to afterburner nozzle contraction section

TTAIR = Air total pressure

f_1, f_2, f_3 = Functional relationships calculated using equilibrium thermochemistry program for the propellant being tested

TT4P = Total temperature at end of ramburner based on pressure measured there

g_c = Gravitational constant

R = Universal gas law constant

A_t = Ramburner throat area

K_e = Ramburner discharge coefficient

M4 = Mach number at entrance to afterburner nozzle contraction section

$A_{ramburner}$ = Ramburner cross-sectional area

$dQ/d\theta$ = rate of heat loss to hardware

$(TT4P)_{corrected}$ = TT4P corrected for heat loss to hardware

$\eta\Delta T$ = Temperature-rise efficiency.

In all tests, the air total temperature was approximately 900°R, the afterburner residence time was 5 to 6 milliseconds, and the afterburner length/diameter ratio was approximately 8. Afterburner operating pressures ranged from about 20 psia at the higher air/fuel ratios to 30 to 40 psia at the lower air/fuel ratios tested. Efficiency results for three test with MK1 employing the PLAAR mixing/flameholding aid are presented in Figure 47, while efficiency results for an MK1 test with no mixing/flameholding aid appear in Figure 48. As may be seen, the afterburning efficiencies in general were quite good, generally in excess of 90% with use of the PLAAR aid, and in the 82 to 95% range without it.

It is of interest to compare the three tests with MK1 with a PLAAR aid to the one test without it, since this is the only formulation which was tested both with and without the aid. It appears that the aid is worth approximately 10 percentage points in terms of temperature-rise efficiency, though obviously at the expense of increased combustor drag (not measured in these tests). It appears likely that the relatively low efficiency without the aid is due to mixing limitations rather than flameholding considerations. The primary motor nozzle exit diameter for this test was 0.833 inches, while the ramburner was 45 inches long; thus, there were only about 54 primary nozzle diameters available for mixing. This is probably not sufficient mixing length, since the relatively low overall air/fuel ratio prevailing through most of this test requires nearly total mixing to get sufficient air to all of the fuel. During the test, a very bright flame was observed in the gap between ramburner and ejector, indicating the mixing/combustion was still taking place. In tests with the PLAAR

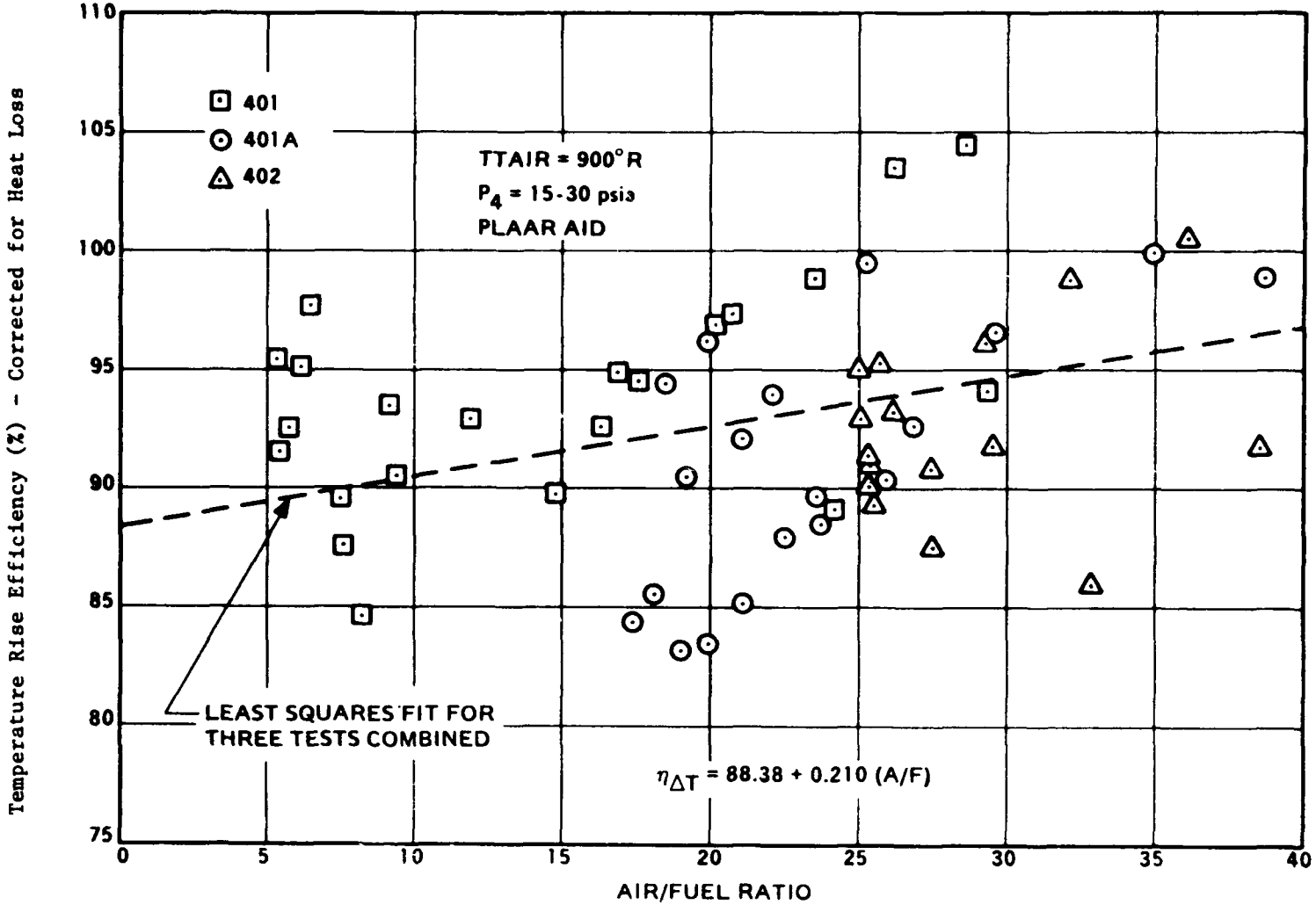

Figure 47. Efficiency Data - MK1 - Test 401, 401A and 402

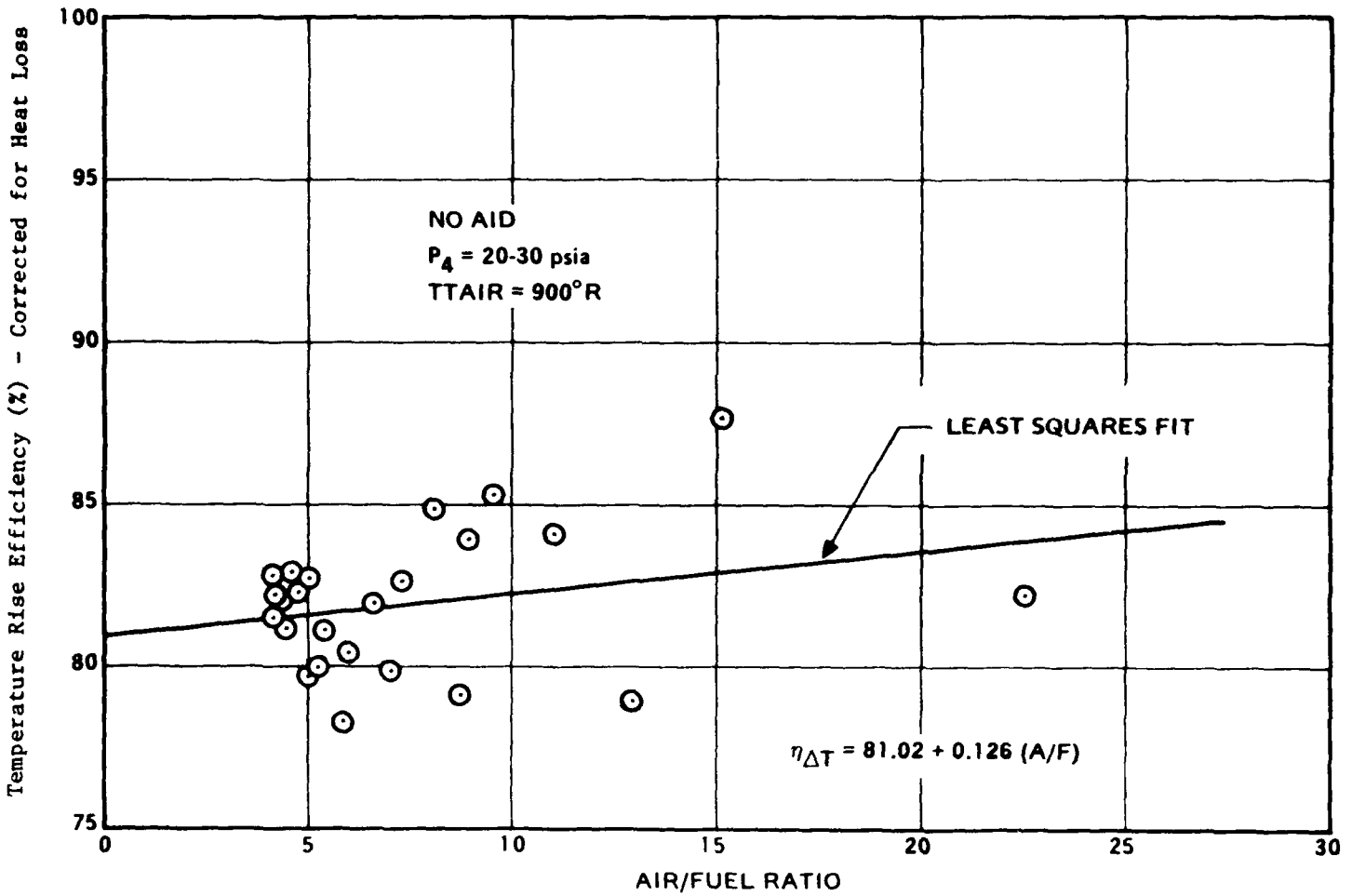

Figure 48. Efficiency Data - MK1 - Test 451

aid, no such flame was seen, indicating, in combination with high efficiency numbers, that mixing/combustion was complete.

If the efficiency increase observed in going from no aid to the PLAAR aid is indeed due simply to better mixing, rather than to recirculatory flameholding, this suggests that such performance increase might also be obtained simply through the use of multiple nozzles in cases where a single primary nozzle would lead to relatively low values of afterburner length/primary nozzle diameter ratio. Such use of multiple nozzles rather than the PLAAR aid should be considerably less detrimental in terms of primary stream momentum degradation and combustor drag.

Results of a single test with a second castable composition, MK12, are presented in Figure 49. Test conditions employed in this test were particularly severe (afterburner pressure of 16 to 18 psia, air/fuel ratio of 28/1 to 39/1) conditions under which state-of-the-art boron formulations yield temperature rise efficiences of 40 to 60 percent. As may be seen, this formulation, which has considerably higher theoretical performance than MK1 due to use of 2/1 magnesium/aluminum, rather than all magnesium as the metal additive, performed quite well, yielding temperature rise efficiencies in excess of 90 percent at air/fuel ratios below 30/1, although this efficiency did drop off to about 80 percent at an air/fuel ratio of 37/1.

The main conclusion from this test series is that the castable magnesium propellants formulated in this program generally afterburn well under adverse conditions (low pressure, high air/fuel ratio) even without a high drag mixing/flameholding aid. It appears that mixing limitations can cause some performance degradation at near stoichiometric conditions for relatively low values of afterburner length/primary motor nozzle diameter: a possible low-drag solution to this problem is the use of multiple nozzles under these conditions.

The probable reason for the excellent afterburning characteristics of these formulations, even under highly adverse conditions, has been alluded to earlier. These formulations have been shown through

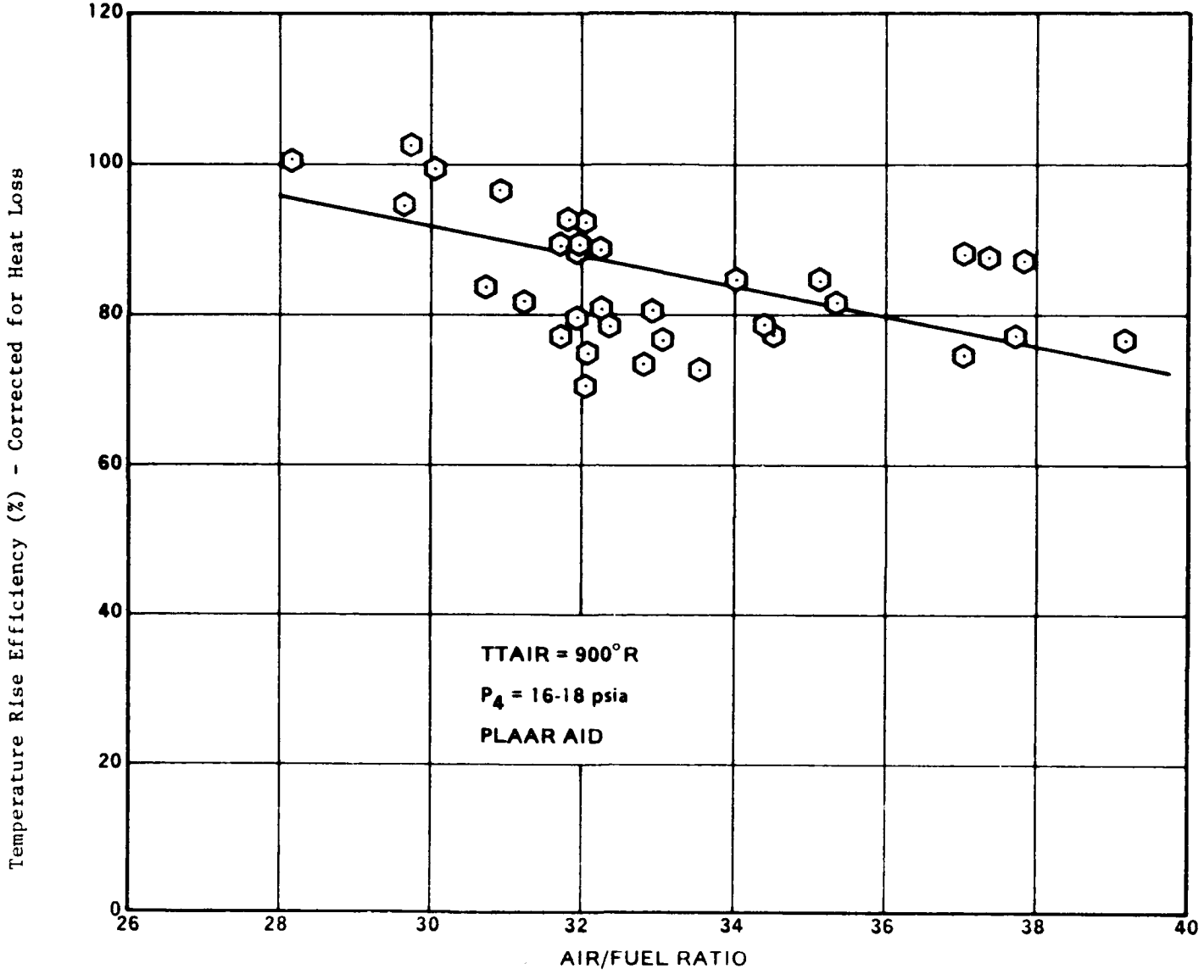

Figure 49. Efficiency Data - MK12 - Test 403

atomic absorption experiments to produce large amounts of magnesium vapor in the exhaust streams of the primary motors. This magnesium vapor, as shown in the theoretical analysis presented in Section III-F, reacts extremely rapidly with O_2 molecules to produce O atoms, which are violently reactive, promoting vigorous ignition and combustion with all fuel species which they contact. Thus, as rapidly as the fuel stream can be mixed with air, the Mg vapor reacts leading to vigorous combustion of the fuel stream and the system is essentially mixing limited.

The high afterburning efficiency of the MK12 formulation is particularly gratifying in that it has, by a considerable margin, the highest theoretical performance of the castable compositions examined (heating value of nearly 10,000 BTU/lb or 600 BTU/in^3) as shown in Table 7.

2. Pressed Compositions

As indicated earlier, one connected-pipe air-augmented rocket test (Test 460) was performed with the pressed composition, TK1. The same equipment and data reduction procedures as described above were used in analysis of this test. However, as a result of the unusual burning behavior of the primary motor (See Figure 44.), the afterburning performance data obtained with this test is somewhat suspect. The PLAAR mixing aid described previously was employed in this test. Air total temperature was again 900°R and the afterburner operating pressure was approximately 15 to 25 psia, again representing highly adverse conditions as regards efficient afterburning. Observation of the pressure-time trace of Figure 44 indicates that only efficiency data obtained in the first 0.5 to 0.6 seconds of the test are likely to have any validity, and that even these data points are open to question in that it is difficult to accurately calculate instantaneous fuel-flow rates from such a pressure-time curve, and also in that the heat losses to the hardware are likely to be larger than calculated by the data reduction procedure described above during this initial hardware heatsoak period. Nevertheless, efficiency data for the first 0.6 seconds of the test are presented in Figure 50. As may be seen, temperature rise efficiencies of 60 to 80% are calculated (even with the conservative assumptions

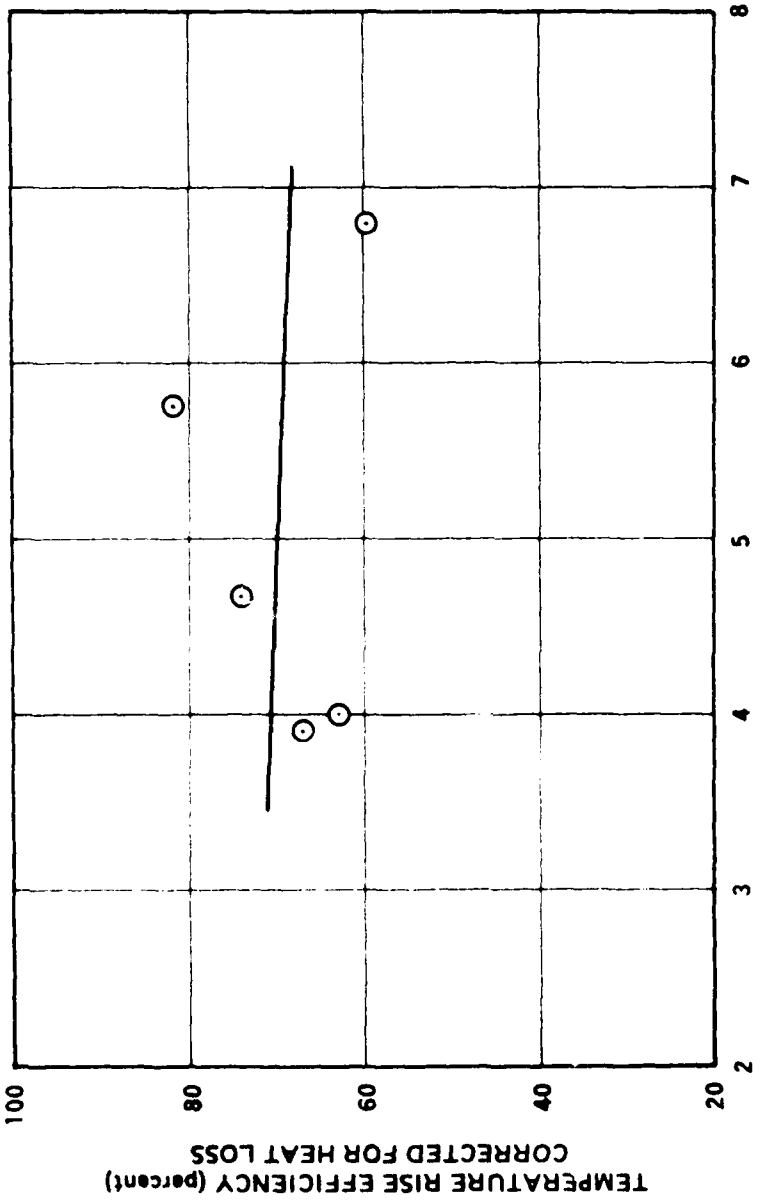

Figure 50. Efficiency Data — TK1 — Test 460.

regarding heat losses to the uninsulated ramburner).

In addition, one connected-pipe ramburner test was run with a formulation quite similar to TK1 (same ingredients, slightly different proportions, approximately 2% lower theoretical heating value) on an Internal Research and Development program. This test did not encounter the same primary motor interior ballistics problems and yielded meaningful data over an air/fuel ratio range of approximately 3/1 to 7/1. Air total temperature was approximately 900°R once again, but afterburner operating pressure was slightly higher (30 to 40 psia) and no mixing/flameholding aid was used (two factors which should tend to compensate). In this test, temperature rise efficiency, corrected for heat losses to the hardware, ranged from approximately 80% at air/fuel = 7/1 to 90 to 100% at air/fuel = 31.

Thus, it appears that pressed compositions in the TK1 class offer considerable potential for air-augmented rocket applications, having theoretical heating values in the range of 10,000 BTU/lb (750 BTU/in^3) and offering the promise of very high afterburning efficiencies under adverse conditions (relatively low air temperature, low afterburner pressure) typical of high altitude cruise applications where boron-loaded forumlations encounter afterburning difficulties.

REFERENCES

1. King, M.K., and Maček, A., "Studies of the Ignition and Combustion of Boron Particles for Air-Augmented Rocket Applications," Interim Report AFOSR-TR-75-0043, October, 1974.

2. Friedman, R., and Maček, A., "Ignition and Combustion of Aluminum Particles in Hot Ambient Gases," Combustion and Flame, 6, 1, pp. 9-19 (1961).

3. Friedman, R., and Maček, A., "Combustion Studies of Single Aluminum Particles," 9th Symposium (International) on Combustion, Academic Press, N.Y., pp. 703-712 (1963).

4. Friedman, R., Maček, A., and Semple, J., Heterogeneous Combustion, Academic Press, N.Y., p. 3 (1964).

5. Maček, A., "Fundamentals of Combustion of Single Aluminum and Beryllium Particles," 11th Symposium (International) on Combustion, The Combustion Institute, Pittsburgh, Pa., pp. 203-217, (1967)

6. Maček, A. and Semple, J., "Experimental Burning Rates and Combustion Mechanisms of Single Beryllium Particles," 12th Symposium (International) on Combustion, The Combustion Institute, Pittsburgh, Pa. pp. 71-81 (1969)

7. Maček, A., and Semple, J., "Combustion of Boron Particles at Atmospheric Pressure," Combustion Science and Technology, 1, pp. 181-191 (1969).

8. Maček, A., "Combustion of Boron Particles: Experiment and Theory," 14th Symposium (International) on Combustion, The Combustion Institute, Pittsburgh, Pa., pp. 1401-1411 (1973).

9. Prentice, J.L., et al., Metal Particle Combustion Progress Report, Naval Weapons Center Report TP4435, Appendix A, p. 106 (1968).

10. Mohan, G., and Williams, F., "Ignition and Combustion of Boron in O_2/Inert Atmospheres," AIAAJ, 10, 6, pp. 776-83, (1972).

11. King, M. K., "Boron Ignition and Combustion in Air-Augmented Rocket After-Burners," Comb. Science and Technology, 5, pp. 155-64 (1972).

12. King, M. K., "Boron Particle Ignition in Hot Gas Streams," Comb. Science and Technology, 8, 6, p. 255 (1974).

13. King, M. K., "Predictions of Laminar Flame Speeds in Boron-Oxygen-Nitrogen Dust Clouds," 15th Symposium (International) on Combustion, The Combustion Institute, Pittsburgh, Pa., 1975.

14. Maček, A., Goede, P., Scheffee, R.S., and Zukovich, P.P., Final Report, Contract No. F30602-73-C-0313 (ARPA through RADC), March, 1974.

15. Cassel, H., and Liebmann, I., "The Cooperative Mechanism in the Ignition of Dust Dispersion," Combustion and Flame, 3, 4, December 1959, pp 467-75.

16. Mikatarian, R.R, Kau, C.J., and Pergament, H.S., A Fast Computer Program for Nonequilibrium Rocket Plume Predictions, AFRPL-TR-72-94, August 1972.

17. Kashireninov, O., Oral presentation at AIAA 13th Aerospace Sciences Meeting, Pasadena, CA, January 1975.

CHRONOLOGICAL BIBLIOGRAPHY OF PAPERS AND REPORTS

RESULTING FROM CONTRACT F44620-71-C-0124

1 Maček, A., and Semple, J.M., "Composition and Combustion Characteristics of Condensed Exhaust From Boron-Containing Fuel-Rich Rocket Motors," 9th JANNAF Combustion Meeting, Monterey, Calif., Sept., 1972, CPIA Publication 231, Volume I, p. 359, Dec., 1972.

2. King, M.K., "Boron Particle Ignition in Hot Gas Streams," Combustion Science and Technology, 8, pp. 255-273, 1974.

3. King, M.K., Combustion Studies of Fuel-Rich Propellants, Progress Report (Jan. 1, 1974 - June 30, 1974), AFOSR Contract F44620-71-C-0124, August 21, 1974.

4. King, M.K., and Maček, A., "Studies of the Ignition and Combustion of Boron Particles for Air-Augmented Rocket Applications," Interim Report, AFOSR-TR-75-0043, October, 1974.

5. King, M.K., and Maček, A., "Combustion Studies of Magnesium-Loaded Fuel-Rich Propellants," 11th JANNAF Combustion Meeting, Pasadena, CA, Sept., 1974, CPIA Publication 261, Vol. III, p. 65, Dec., 1974.

6. King, M.K., "Predictions of Laminar Flame Speeds in Boron-Oxygen-Nitrogen Dust Clouds," 15th Symposium (International) on Combustion, The Combustion Institute, Pittsburgh, PA, 1975.

7. King, M.K., Combustion Studies of Fuel-Rich Propellants, Progress Report (July 1, 1974 - June 30, 1975). AFOSR Contract F44620-71-C-0124, August 8, 1975.

8. King, M.K., and Childs, L.B., "Development of Highly-Magnesium-Loaded Fuel-Rich Propellants," 12th JANNAF Combustion Meeting, Newport, Rhode Island, Aug., 1975, CPIA Publication 273, Vol. III, p. 201, December, 1975.

9. King, M.K., and Fields, J.L., "Combustion of Highly-Magnesium-Loaded Fuel-Rich Propellants," 13th JANNAF Combustion Meeting, Monterey, CA, Sept., 1976. To be published in CPIA Publication.